Electroencephalogram spindle detection from simultaneous Electroencephalogram (EEG) / functional Magnetic Resonance Imaging (fMRI) data for a sleep deprivation study

Aude Jegou

A Thesis

In

The Department

Of

Physics

Presented in Partial Fulfillment of the Requirements

For the Degree of Master of Science (Physics) at

Concordia University

Montreal, Quebec, Canada

April 2018

CONCORDIA UNIVERSITY

School of Graduate Studies

This is to certify that the thesis prepared

By: Aude Jegou

Entitled: Electroencephalogram spindle detection from simultaneous Electroencephalogram (EEG) / functional Magnetic Resonance Imaging (fMRI) data for a sleep deprivation study

And submitted in partial fulfillment of the requirements for the degree of

Master of Science (Physics)

Complies with the regulations of the University and meets the accepted standards with respect to originality and quality.

Signed by the final Examining Committee:

_____ Chair

Dr. Salzmann Ingo

_____ Examiner

Dr. Gauthier Claudine

_____ Examiner

Dr. Lina Jean-Marc

_____ Supervisor

Dr. Dang-Vu Thanh

_____ Supervisor

Dr. Grova Christophe

Approved by _____

Dr. Bianucci Pablo

_____2018 _____

Dean of Faculty

ABSTRACT

On Electroencephalogram spindle detection from simultaneous Electroencephalogram (EEG) / functional Magnetic Resonance Imaging (fMRI) data for a sleep deprivation study

Aude Jegou

Sleep deprivation is an important and common problem with many consequences for mental and physical health. A sleep deprivation study was conducted to better understand the effects of insufficient sleep on cognitive functions and recovery. Studying specific spontaneous sleep waves occurring during the recovery sleep after sleep deprivation allows us to better understand the brain mechanism during sleep and its importance. The focus of my Master project is the detection of these sleep waves on scalp Electro-EncephaloGraphy (EEG) data, especially spindles, using different automatic detection algorithms and comparing them to a visual detection. Automated detection of these typical EEG discharges is challenging because many artifacts occur when EEG data are recorded within the Magnetic Resonance Imaging (MRI) scanner, so in presence of a large magnetic field. EEG data should be carefully processed from MRI related artifacts before considering detection of sleep specific discharges. In the second section of the thesis, we investigated within the whole brain the Blood Oxygen Level Dependent (BOLD) responses, measured with functional MRI, to identify brain areas involved in the generation of sleep spindles detected from scalp EEG. Preliminary results showed that automated detection was not accurate enough, because of residual artifact and other consequences of preprocessing. Moreover, visual detection is limited by the complexity of the EEG data. Therefore, there are expected improvements in post-review of the automated detection or investigating the optimal parameters for automated methods. The first BOLD response maps showed similarity between automated and visual detection and also with a study conducted by (Manuel Schabus et al. 2007). To conclude, further investigation on automated methods must be performed to find the best compromise between visual detection, automated detection, and post-review of automated detection.

ABRÉGÉ

Sur Détection de fuseaux sur un Encéphalogramme venant de données Electroencéphalographie (EEG)/ Imagerie par Résonance Magnétique fonctionnel (IRMf) simultané pour une étude sur la privation de sommeil

Aude Jegou

La privation de sommeil est un problème important et commun impliquant de nombreuses conséquences pour la santé mentale et physique. Cette étude sur la privation de sommeil a été réalisée pour mieux comprendre les effets du manque de sommeil sur les fonctions cognitives et sur la récupération. Étudier les ondes spontanées spécifiques au sommeil apparaissant lors du sommeil de récupération qui suit une privation de sommeil, nous permet de mieux comprendre les mécanismes du cerveau se produisant lors du sommeil et l'importance de bien dormir. L'objectif principal de mon projet de Maîtrise est la détection des ondes de sommeil sur des données d'électro-encéphalographie (EEG) et plus particulièrement la détection des fuseaux du sommeil. Le but est d'étudier différents algorithmes de détection automatique et de les comparer à une détection visuelle. La détection automatique des fuseaux sur ce type de données EEG est difficile puisque beaucoup d'artefacts se produisent quand les données EEG sont acquises dans le scanner IRM, en raison du grand champ magnétique qui s'y produit. Les données EEG doivent donc être prétraitées avec attention pour enlever les artefacts associés à l'IRM avant de pouvoir effectuer la détection des fuseaux. La seconde étape de mon projet est de rechercher les réponses associées à ces fuseaux basées sur la concentration d'oxygène dans le sang (BOLD) du cerveau, mesurée grâce à l'IRM fonctionnelle, et d'identifier les régions du cerveau impliquées dans la génération des fuseaux détectés par l'EEG. Des résultats préliminaires ont montré que l'application des méthodes de détection automatique sur ce type de données n'était pas assez précise en raison de la présence de résidus d'artefacts dans l'EEG et du prétraitement des données. De plus, la détection visuelle est limitée par la complexité des données EEG. Pour améliorer ces détections, deux solutions peuvent être envisagées. La première est de vérifier à posteriori les éléments détectés par la détection

automatique, ce qui rend la détection semi-automatique. La deuxième est de rechercher les paramètres optimaux à appliquer aux détections automatiques pour ce type de données. Les premières cartes de réponse BOLD ont montré une similitude entre celle venant de la détection visuelle et celle venant de la détection automatique et son concordantes avec une étude conduite par (Manuel Schabus et al. 2007). Pour conclure, d'autres travaux sur les méthodes de détection automatique doivent être menées pour déterminer le meilleur compromis entre la détection automatique, la détection visuel, et la détection semi-automatique.

ACKNOWLEDGEMENTS

I would like to express my appreciation and gratitude to Dr. Christophe Grova and Dr. Thanh Dang-Vu, my supervisors, for providing me this research opportunity, guiding me through the sleep deprivation study, and for their useful critique of this research work.

This study has been founded by PERFORM centre and CSBN that I would like to thanks for their confidence and support.

I would like to thanks my committee, Dr. Claudine Gauthier, and Dr. Jean-Marc Lina, for their time and willingness.

I also would like to express my appreciation to all people who helped me to acquire the data, especially Antonys Melek MRI technician at PERFORM, the summer interns Mariève Cyr, Anca Ionescu, Robert Hovey, and Brian Hodhod, and also the volunteers of the sleep lab.

I would also like to thank my colleagues and friends Dr. Umit Aydin, Dr. Florence Pomares, Dr. Florian Chouchou, Dr, Chifaou Abdallah, Dr. Dylan Smith, Dr. Thomas Vincent, Tanguy Hedrich, Zhengchen Cai, Kangjoo Lee, Julia Huck, Fatemeh Razavipor, Amanda Spilkin, and Obai Ali for their help, their advice, and their moral support.

Finally, I wish to thanks my parents, my sister, and brother-in-law for their moral support.

Table of Contents

List of Figures

List of Tables

Chapter 1

Introduction:

Sleep is a period during which the body is relaxed and the reactivity to external stimuli is reduced. Sleep is generated by specific populations of neurons in hypothalamus and brainstem as well as through the interactions of thalamic and cortical neurons. Sleep is regulated by the need to sleep which increases with the awake time, the so-called homeostatic pressure which is defined as the internal timer that generates a pressure for sleep. Sleep is also regulated by circadian processes which consists in a rhythm following a cycle of 24 hours (i.e. our internal biological clock). Sleep architecture consists in several cycles, each of them lasting between 90 to 120min. Within each cycle, two broad sleep stages alternate. On the one hand, paradoxical sleep or Rapid Eye Movement (REM) sleep corresponds to 20% of our total sleep time during which vivid dreams take place. On the other hand, Non-Rapid Eye Movement (NREM) sleep corresponds to 80% of our total sleep time and is subdivided into three stages. Sleep stages are characterized by specific neuronal bioelectrical signals measured using scalp Electro-EncephaloGraphy (EEG). N1 of NREM sleep is a state of light sleep and drowsiness occurring when we fall asleep and during which the alpha rhythm (8-13Hz) decreases while theta rhythm (4-7Hz) appears. N2 is a stage during which other specific transient EEG discharges like spindles and the K-complexes appear. Spindles are oscillations with a frequency ranging between 11-16Hz, their role is to inhibit the transmission of the stimuli at cortical level in order to preserve sleep stability; moreover, they are also involved in memory consolidation (Dang-Vu, Schabus, et al. 2010b). Spindles are separated into two subtypes: fast and slow spindles. Fast spindles have a frequency range of 13-16Hz while slow spindles have a frequency range of 11-13Hz. Fast spindles are more often detected over parietal and central areas whereas slow spindles are more localized in frontal areas (M. Schabus et al. 2007). Slow waves appear during stage N2 but become more abundant during stage N3. They are characterized by a frequency range between 0.5-2Hz and a peak-to-peak amplitude equal or higher than 75 μV. They are predominantly detected over frontal areas and may have a role in plasticity (Massimini 2004). These different waves (e.g. spindles, slow waves, and K-complex) are specific to sleep because they do not appear while people are in a conscious state. They will be referred as “sleep waves” in this thesis. Stage N3, also denoted slow wave sleep, corresponds to deep sleep and is specifically

defined by the presence of slow waves and delta activity. In order to determine these different stages, we need to record the bioelectrical activity from the brain, but also from the muscle, and ocular region. To do so, the main modality to consider is the Electroencephalogram (EEG), which measures synchronized bioelectrical activity of the neurons using electrodes attached to the scalp. For sleep study, EEG is usually associated with the Electrooculogram (EOG), which monitors the eyes movements. Additionally, an Electromyogram (EMG) may be used to record muscle activity, as for instance to monitor legs movements but also chin movements. The combination of these modalities is denoted a Polysomnography (PSG) study. A PSG records the electrical activity of the brain and the muscles to determine the different sleep stages. PSG is also used to detect and diagnose sleep disorders, such as for instance sleep apnea or periodic leg movements during sleep. To detect sleep apnea, the standard PSG is completed with the recording of a respiratory belt, to monitor respiration. During NREM sleep, brain activity decreases when compared to wakefulness, especially within brain areas involved in arousal and vigilance. While associative cortical areas are the most active during wakefulness, NREM sleep allows to recover the homeostasis (i.e. stability) in these cortical areas (Dang-Vu 2014). Studies have demonstrated that NREM sleep also allows to recall events of the day and store them (memory consolidation), to improve the plasticity of the brain, and to reorganize the brain networks (Sejnowski and Destexhe 2000). This reorganization actually requires biological resources and time, so it cannot be processed during the awake state: this is the main reason why this is so important to sleep.

Sleep deprivation is an important and common problem, which affects an increasing number of people. In adulthood, a normal overnight sleep duration should last between 7.5 to 8.5h in average, in order to have a healthy sleep. However, the need for sleep varies between individuals (Bhopal and Khatwa 2014). Sleep deprivation can be total or partial and results in various effects on cognitive functions, behavior, and health; nevertheless, with a variation in intensity from one individual to the other. A partial sleep deprivation occurs when the person sleeps less than 6.5h per night, whereas a total sleep deprivation corresponds to no sleep during all night, which means that the person stays awake during 24h continuously (Short and Banks 2014). The common consequences of sleep deprivation are an increase of sleepiness, the deficit on vigilance, attention, and cognition, and a bad mood. Moreover, the effects of total sleep deprivation will be more extreme and will be instantly visible whereas the effects of partial sleep deprivation will appear after many sleep restriction nights (Short and Banks 2014).

Starting from the importance of the sleep and its characteristic, the purpose of our proposed study was to use neuroimaging techniques to investigate the effects of sleep deprivation on brain activity, especially how the brain recovers from a lack of sleep. In order to complete this project successfully, we acquired simultaneously two modalities: EEG and functional Magnetic Resonance Imaging (fMRI). EEG allows measuring the electrical activity of neurons from the scalp with excellent temporal resolution at the millisecond scale (Mulert Christoph and Lemieux Louis 2010). Functional magnetic resonance imaging (fMRI) allows monitoring the cerebral activity during a specific task or at rest by measuring the "Blood Oxygenation Level Dependent" (BOLD) signal which reflects oxygen consumption and related blood flow changes within the whole brain at a spatial resolution of few millimeters (Mulert Christoph and Lemieux Louis 2010). Combining both methods simultaneously allows taking benefit of the good spatial resolution of fMRI and together with the excellent temporal resolution of EEG (Daunizeau et al. 2007). We hypothesize that analyzing data obtained by these two complementary modalities will shed light on fundamental mechanisms involved in sleep-related cognitive functions.

Our research refers to a sleep deprivation study and involves three main objectives. The first one is to study the impact of sleep deprivation on cognitive function. To do so, data acquired during cognitive tasks following a normal night of sleep will be compared to data obtained when performing the same tasks after a sleep deprivation night in order to characterize the difference in brain activities in both conditions. The second objective is to study the impact of sleep deprivation on cerebral function during the so-called recovery sleep. Recovery sleep is the sleep time after a sleep deprivation night. In our study, it refers to the nap after the sleep deprivation night. Our third objective is to study the reorganization of resting-state functional connectivity pattern at different levels of consciousness in sleep when compared to wakefulness. With the present study, we expect to further understand the cerebral mechanisms underlying sleep homeostasis and the recovery of cognitive performance after sleep deprivation. My Master of Science project is more specifically related to the second objective of this sleep deprivation study. The goal of my project is to analyze the EEG/fMRI data from the recovery night (i.e. the nap) and notably brain regions involved during the generation of the spindles. Detecting spindles from EEG data acquired inside an MRI scanner is challenging because of the presence of several MR-related artifacts. In this study, we propose to carefully study and compare different spindle detection methods, whereas the best detection methods will identify the associated hemodynamic BOLD response from fMRI data. As a result, a

brain map exhibited brain regions involved during spindle generation will be provided. Studying spindles during the recovery sleep will allow us to understand the mechanism of the brain to recover the lack of cognitive function. Therefore, we hypothesize that the sleep spindles characteristics detected on EEG during recovery sleep will be different than during a normal night of sleep, and the brain responses associated with spindles will be enhanced during the nap when compared to a normal night. Moreover, these changes in brain responses during sleep will modulate the improvement of cognitive performance after the nap.

The project of my Master of Science in the Department of Physics focuses on the analyses of EEG data during the nap. The functions of spindles are diverse since they seem to be involved in the inhibition of exterior noise, memory consolidation, and processing information, and indexes the intellectual ability (Dang-Vu, McKinney, et al. 2010; Bergmann et al. 2012; Fogel and Smith 2011). Consequently, spindles should be the sleep waves the most involved in recovery function, so accurate spindles detection on EEG is the main challenge of this proposed study. Using EEG/fMRI simultaneous recordings adds another level of complication since EEG data acquired in the MRI scanner are contaminated by several large artifacts that need to be corrected for. However, removal of MRI induced EEG artifacts is far from perfect and might also remove some pertinent EEG information. The project consisted in assessing the performance of several algorithms proposed in the literature to detect automatically spindles when applied to artifacts EEG data acquired in the MRI scanner. We compared the performance of different automatic algorithms with a visual detection provided by an expert electroencephalographer. Then, the second objective of this thesis was to evaluate the influence of different spindle detection strategies when analyzing the fMRI data to estimate the brain hemodynamic responses associated with spindles generation.

Chapter 2

State of the art of sleep and EEG/fMRI modalities:

The purpose of this chapter is to provide a review of the literature to present the concept of sleep deprivation, together with its effects and characteristics on brain activity. We will then introduce how brain activity during sleep and sleep deprivation could be studied using neuroimaging techniques. In that context, spindles are highly involved in memory consolidation and play a key role in the recovery of cognitive function after sleep deprivation. Therefore, the proposed methodologies needed to improve EEG signal quality and methods dedicated to automatically spindle detection will be carefully reviewed, since their evaluation is central to this Master project.

2.1 – Physiology of sleep

It is important to review the physiological aspects of sleep deprivation and the associated EEG waves produced during sleep in order to analyze and interpret correctly the different results of our present study.

2.1.1 Sleep deprivation (SD)

Sleep is an important aspect of our life to maintain our body in a proper functioning. Sleep is notably involved in memory consolidation and brain plasticity processes (Sejnowski and Destexhe 2000). The numbers of sleep hours required decrease with age, and at adulthood, an average of 7.5h is usually required (Bhopal and Khatwa 2014). According to the National Health Interview Survey conducted from 2005 to 2007, 30% of adults in the US only get 6 hours (or less) of sleep per day (Bhopal and Khatwa 2014). Causes of sleep deprivation vary according to the age, but common causes in adulthood include sleep breathing disorders, circadian rhythm disorders, medical and psychiatric disorders. However, our modern society brought other causes to sleep deprivation, such as the use of electronic devices within the hour before bedtime. Furthermore, due to social or professional factors, people also have voluntary sleep insufficiency.

A survey from National Sleep Foundation showed that adult who sleeps less than 8 hours per night have more chance to develop obesity (Bhopal and Khatwa 2014). All kinds of sleep deprivation, whether they are considered as partial or total, have important consequences on health. Sleep deprivation can exacerbate medical conditions such as cardiovascular and metabolic disorders, or reinforce psychiatric disorders such as depression and anxiety (Bhopal and Khatwa 2014). In a study conducted by Dawson and Reid (Dawson and Reid 1997), they compared performance to specific task after sleep deprivation to the effects caused by alcohol. They found that after 17h of wakefulness, cognitive functions performance were similar to those of a person with 0.05% of blood alcohol concentration, whereas after 24h of SD it was equivalent to 0.10% of blood alcohol concentration.

For the present study, we focused on the effects of SD on cognitive functions. Many cognitive functions are altered after SD. Among them, alertness (i.e. fully aware), attention (i.e. concentration on something special) and vigilance (i.e. intensely watchful), which depend on structures such as the thalamus and prefrontal cortex, are involved in many aspects of our daily life and gradually decline after 16 hours of wakefulness (Killgore and Weber 2014). To better characterize what we will consider here as cognitive functions, we first need to further define the following concepts: (i) alertness consists in being fully aware, (ii) attention consists in being concentrated and mentally focused, and (iii) vigilance consists in carefully watching our environment. Several well-controlled paradigms have been proposed in psychology to study these cognitive functions. To assess the decline of vigilance, one task has been often proposed in SD studies: the Psychomotor Vigilance Test (PVT). PVT test consists in presenting a visual stimulation requiring a decision of the participant, while measuring the reaction time of participant, i.e. the time delay between stimuli presentation and the answer (Killgore and Weber 2014). In our sleep deprivation study, we considered a version of the Mackworth clock test for the PVT task. The Mackworth Clock Test of Psychomotor Vigilance involves a series of visual stimuli spatially similar to the ticking of a clock, presented sequentially on screen. Participants are instructed to press a button as quickly as possible in response to a skipped "tick" on the "clock", i.e. when the stimulus jumps ahead in sequence (Lichstein, Riedel, and Richman 2000). After SD, the response times tend to be slower, with an increase in the duration and frequency of the period of non-responsiveness, reflecting that people become less vigilant (Babkoff et al. 1991). Moreover, Babkoff et al. 1991 reported that sleep-deprived people made more omissions and also responded when no stimuli were presented. This

instability in performance is more likely related to a compensatory effort (Doran, Dongen, and Dinges 2001). To assess the attention level of participants, the so-called Attention Network Task (ANT) task has been proposed. The ANT task is a computerized stimulus-response based task. Participants are instructed to press one of two response buttons (left or right) in response to a specific stimulus (Killgore and Weber 2014). The visual stimulus consists of an array of 5 arrows, and the participant must respond by pressing the corresponding button in response to the direction presented by the center arrow. In order to assess the attention of participant, different cues such as valid, invalid or double (i.e. both boxes are flashing) are presented to disturb the participant. Cues are presented prior to the arrows in the form of two rectangular shapes on both sides of the screen. Stimulus presentations take the form of three different types: uncued, congruent cued, and incongruent cued, which yield three separate measures: alerting, orienting and executive control. Congruent means that the five arrows are presented in the same direction, whereas incongruent means that arrows have different directions. Alerting system corresponds to the vigilance of the person and involvement of thalamic, parietal and frontal regions have been reported during this task (J Fan et al. 2005). Orienting system is the attention to the specific information given by the arrow or the cue to the participant. This system is associated with the superior and inferior lobule, frontal eye fields and subcortical regions (Jin Fan et al. 2002). The executive control system aims at resolving a conflict between response which means the decision taken by the participant while he responds to the task and is associated with the anterior cingulate cortex and lateral prefrontal cortex (Jin Fan et al. 2002). After SD, inattention moments have been reported, which can be explained by the occurrence of micro-sleep (Alhola and Polo-Kantola 2007).

Sleep is highly involved in memory consolidation and sleep deprivation has been shown to affect memory. Memory is the information center of everything we learned in our life, and it allows to keep our experiments and to access them. Memory is divided into two main systems which are interconnected. Firstly, working memory is the short-term memory localized in the prefrontal cortex. Secondly, long-term memory which regroups three subtypes the semantical, the episodic, and procedural memory. Long-term memory is the knowledge of ourselves, the automatism, and the memories of our day. Long-term memory is mainly localized in the temporal lobe, the hippocampus, and the cerebellum. Episodic and semantic memory are merged to form the declarative memory which is the memory that we can consciously recall. Several studies suggested that after SD, the brain has difficulty to acquire and encode new information (Drummond et al.

2000; Yoo et al. 2007). To assess working memory functioning, studies used a memory task called N-Back. N-Back Task is a computerized version of a widely used working memory paradigm, in which a series of letters are presented in sequence (Chee and Choo 2004). Participants are then asked to press a response button if the current stimulus is the same as the stimulus that was present n-letters before it. For example, in a 2-Back, when presenting the sequence (C A C), the participant should respond to the second presentation of "C". The following brain regions have been shown to be involved during the N-back task: lateral premotor cortex; dorsal cingulate and medial premotor cortex; dorsolateral and ventrolateral prefrontal cortex; frontal poles; and medial and lateral posterior parietal cortex (Owen et al. 2005; Schmidt et al. 2009). Studying the effects of SD on working memory task showed that sleep is important to be able to acquire new information and facilitate the stabilization and the assimilation of new knowledge (Diekelmann and Born 2010; Walker 2008).

PVT, ANT, and N-back tasks are not the only tasks used to assess the attention ability, the learning condition or the deduction capabilities. Nevertheless, these three tasks have been chosen to study the impact of SD on cognitive functions in our study.

2.1.2 - The role of Spindles and Slow waves

Spindles and Slow waves are transient bioelectrical discharges measured using scalp EEG that are appearing during NREM sleep stages (Figure 1 and 2). Spindles are present during stage N2 and N3, whereas slow waves are more predominant in stage N3. In the following section, I will more describe spindles characteristics.

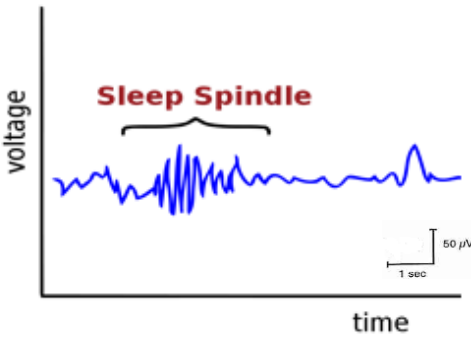

Figure 2: Sleep spindle shape
Source: Psychology Today

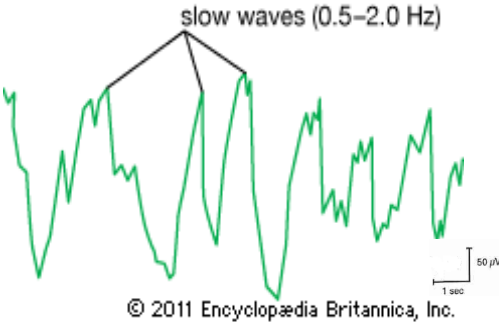

Figure 1: Slow waves shape
Source: Encyclopedia Britannica

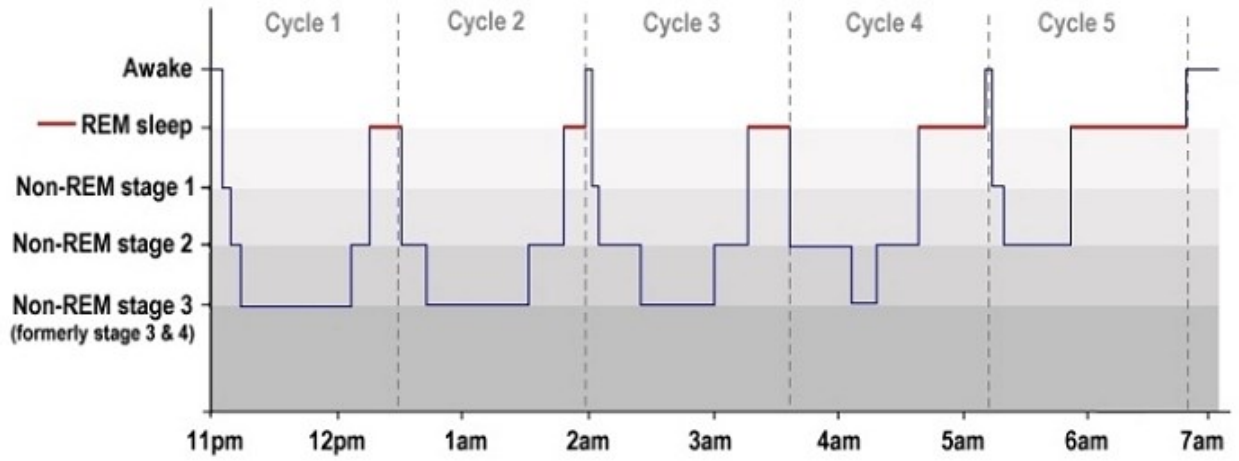

Figure 3: Sleep night cycles
Source: www.howsleepworks.com

A sleep night is divided into 4 to 5 cycles, and each cycle is a succession of NREM and REM stages. During a night, several sleep cycles and therefore several stage N2 periods do occur (Figure 3). Sleep researchers observed dynamic changes of spindle activity throughout the sleep episodes. Spindle density, which is defined as the number of spindles per minute, is usually higher in N2 than in N3 and increases across consecutive sleep cycles. Consequently, at the end of the night, EEG should show more spindles than at the beginning of the night (Knoblauch et al. 2003). On the other hand, slow waves are more abundant at the beginning of the night when compared to the end of the night (De Gennaro and Ferrara 2003b). According to a study conducted by Ueda et al. 2001b, spindles appear when slow waves activity decreased in the EEG background. Moreover, when spindles appear in one epoch, i.e. within a 30s window, then slow wave activities are usually increased in the following epoch (Ueda et al. 2001a).

Studies demonstrated that spindles are generated by GABAergic thalamic reticular neurons. According to a study conducted by Steriade, McCormick, and Sejnowski 1993, spindles are “the results of synaptic interactions and intrinsic membrane properties of inhibitory neurons of the reticular thalamic nucleus and excitatory thalamocortical, and their interaction with cortical pyramidal neurons.” (citation from Sejnowski and Destexhe 2000). Not only is the thalamus involved in the generation of spindles, but also the brainstem. Brainstem would generate the time course of power (i.e. the envelope) in the spindle frequency band and imposes it to the thalamus (De Gennaro and Ferrara 2003b).

In 1935, spindles were characterized by a frequency range of 12-14Hz (Loomis, Harvey, and Hobart 1935; D.-J. Dijk, Hayes, and Czeisler 1993). Since 1935, studies demonstrated that spindle should be classified into two categories fast and slow spindles. On the one hand, fast spindles are in the frequency range of 13-16Hz, and more located in centro-parietal areas(Manuel Schabus et al. 2007). On the other hand, slow spindles present a frequency range of 11-13Hz and are more located in frontal areas. The classification of spindle into subtype comes from a visual scoring observed by Gibbs and Gibbs in 1962. They observed a difference in spindle frequency according to the EEG channels. The majority of spindles with a frequency of 14Hz were visible at the vertex (i.e. parietal and central areas) while spindles with a frequency at 12Hz were visible in frontal areas. This hypothesis has been confirmed by analyzing the topography of spindle and by using automatic detectors (De Gennaro and Ferrara 2003a). The presence of two spindle types could be explained by two different source generators. One spindle generator, for slow spindles, seems located in the prefrontal cortex, while the second generator, for fast spindles, seems located in the precuneus (Anderer et al. 2001). Moreover, different studies demonstrated a functional dissociation of the spindles type with maturation, circadian factors or menstrual cycle phase (D. J. Dijk and Czeisler 1995; Driver et al. 1996; Landolt et al. 1996). Although the classification into two subtypes has been demonstrated by different studies, it is still not unequivocal. According to De Gennaro (De Gennaro and Ferrara 2003a), this doubt comes from the fact that alpha band and spindles share a frequency range. It has been suggested that that the frequency range of the spindles should be only 12-14Hz, whereas the other frequencies usually classifying slow and fast spindles actually consist of alpha band oscillations (Rechtschaffen and Kales 1968). Conversely, another MEG study conducted by Zerouali et al. 2014 suggested that there are two type of spindle and demonstrated that the beginning of the spindle has a higher frequency while the end has a lower frequency. These results suggest that all spindles are showing an evolution of the frequency from fast to slow along the time course of the spindle. To conclude, sleep community mainly agreed that spindle is classified into two subtypes, but controversial results have been reported and a doubt persists.

According to the literature, spindles are involved in different functions. One of their function is to keep the sleeper in a quiet environment. Spindles are able to reduce the influence of external noise (Dang-Vu, McKinney, et al. 2010). A recent study from Bergmann et al. 2012 demonstrated that spindles are also involved in memory consolidation and information processing. In this study, they analyzed EEG/fMRI data from healthy participants who were asked to perform some learning

and visuomotor tasks, then sleep and recall (i.e. performing the tasks again) in the evening. Their results showed that spindles activity were present in the hippocampus and adjacent Parahippocampal lateral gyrus. Moreover, the BOLD (Blood Oxygen Level Dependent) response increased when the spindles were of larger amplitude (Bergmann et al., 2012). Since the hippocampus is related to memory, their results suggested that spindles are associated with memory consolidation. The role of fast versus slow spindles is not well-understood. However, it seems that slow spindles are involved in rotary pursuit learning (i.e. motor performance), whereas fast spindles seem more involved in sequence learning. Moreover, spindle density can also predict the performance of learning in individuals (Fogel and Smith, 2011; Bergmann et al. 2012a). In fact, spindles can be an index of intellectual ability. Some studies showed that children with mental disability or below normal IQ had a low spindle density, whereas people with a high score IQ had a higher number of spindles (Gibbs and Gibbs 1962; Shibagaki and Kiyono 1983; Fogel and Smith 2011).

Spindle characteristics such as density and amplitude vary depending on several factors such as age, menstrual cycle and sleep cycle (Nicolas et al. 2001; Fogel and Smith 2011). Generally, spindles are characterized by a frequency range of 11-16Hz, an amplitude between 8-14μV and a duration between 0.5-3s; however, sleep deprivation can vary these values (M. Schabus et al. 2007; Knoblauch et al. 2003). By studying spindles during a recovery night after SD, researchers demonstrated differences when compared to a normal night. Dr. Knoblauch discovered that the spindle density and the spindle frequency significantly decreased during a recovery night when compared to a normal night (Knoblauch et al. 2003). On the other hand, they demonstrated that spindle amplitude significantly increases during a recovery night. They also showed that spindle duration is longer during a recovery night but these results were not statistically significant. These results are shown in figure 4.

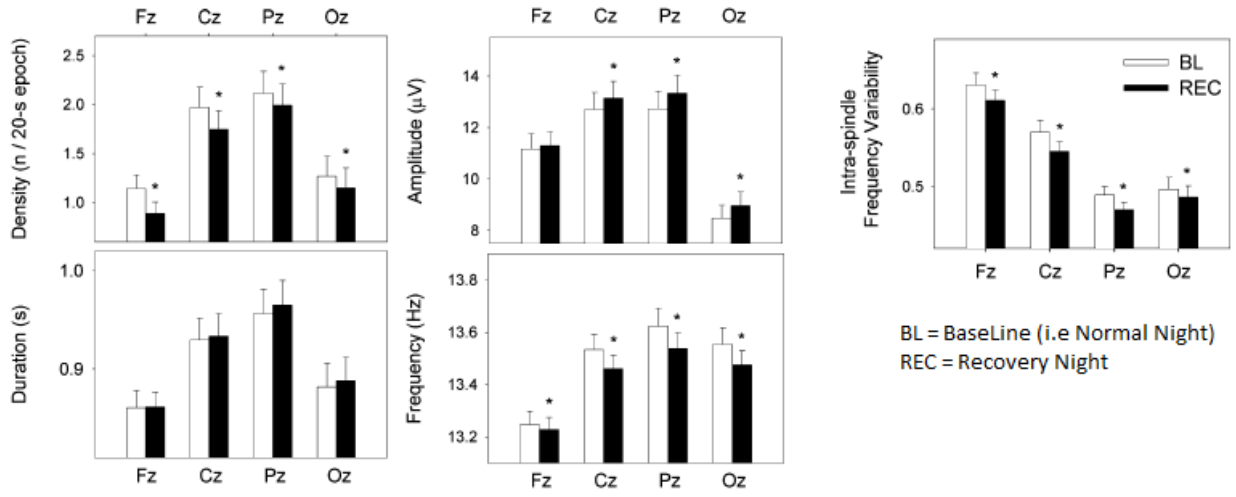

Figure 4: Spindle characteristics affected by SD
Source: Knoblauch et al., 2003

During a recovery night, the spindle density follows the same pattern that during a normal night, i.e. the spindle density increases after several NREM epochs. It seems that anterior and posterior brain regions are not affected in the same way by SD. For example, spindles detected in Pz, in the parietal lobe have a lower amplitude during recovery night when compared to a normal night, whereas spindles detected in Fz, in the frontal lobe keep the same amplitude during normal and recovery nights (Knoblauch et al. 2003).

To conclude, many factors can influence spindle characteristics, including the effects of sleep deprivation. As a result, the change in the spindle characteristics should be taken into account while performing spindle detection.

2.1.3 - Studying sleep deprivation and sleep patterns using neuroimaging

To localize and further understand which brain regions are involved during sleep patterns, researchers have used neuroimaging techniques such as PET and simultaneous EEG/fMRI acquisitions. EEG is a modality with an excellent temporal resolution but only records neuronal activity from the scalp surface, therefore offering a limited spatial resolution. On the other hand, fMRI data allows exploring the whole brain at an excellent spatial resolution of few millimeters. However, fMRI only measures indirectly neuronal activity through elicited blood flow and oxygenation variations. Combining EEG/fMRI modalities provides an excellent trade-off between temporal and spatial resolution and may allow localizing patterns of spatio-temporal neuronal activity that would not be detectable by considering only single modalities (Gotman and Pittau

2011; Huster et al. 2012). As described by Herrmann and Debener, "EEG measures the direct consequence of neuronal activity and feature the same timescale as the underlying cognitive processes, while hemodynamic signals (fMRI) are related to the energy consumption of neuronal populations". (Herrmann and Debener 2008). A typical application of simultaneous EEG/fMRI is in the domain of epilepsy, where EEG is used to detect spontaneous transient epileptic discharges, while fMRI is considered to identify the brain regions involved in the generation of those discharges (Gotman and Pittau 2011). Similarly, using EEG/fMRI in sleep allows specifying the sleep patterns of different sleep stages and assessing what brain regions are involved in the generation of spindles and slow waves, as spontaneous discharges detected from scalp EEG. In EEG/fMRI, typical spontaneous discharges detected on scalp EEG are considered to build an event-related design convolved by a hemodynamic response function, in order to analyze fMRI data within the whole brain, using a general linear model approach (Herrmann and Debener 2008; Gotman and Pittau 2011). Simultaneous EEG/fMRI could also be considered to analyze what brain regions are involved during specific EEG rhythms, such as alpha band activity (Tyvaert et al. 2008).

Brain activity is not only different during wakefulness and sleep, but also between NREM and REM. A PET study comparing glucose metabolism between sleep and wakefulness showed that brain activity decreases during NREM, particularly during N3, where a 40% decrease of glucose brain metabolism was found in sleep when compared to wakefulness (Maquet et al. 1990). Such decrease was located in subcortical (brainstem and thalamus) and cortical (prefrontal cortex, anterior cingulate cortex, and precuneus) regions. Brain glucose metabolism during REM sleep is similar to wakefulness. While higher activity was observed in the thalamus, amygdala, and hippocampus, there appeared to be lower activity in the prefrontal cortex, precuneus, inferior parietal cortex. As a result, brain activity during NREM and REM sleep was drastically different. (Dang-Vu, Schabus, et al. 2010a).

Using EEG/fMRI to investigate brain regions specifically involved during the generation of spindles and slow waves, within N2 and N3 of NREM sleep, Dang-Vu et al (2010a) demonstrated that brain activities related to spindles are associated with the thalamus, the paralimbic, and cortical areas. Furthermore, some changes in the BOLD signal during the generation of slow waves demonstrated their links with the frontal gyrus, the parahippocampal gyrus, the precuneus, the posterior cingulate cortex, and the cerebellum. (Dang-Vu, Schabus, et al. 2010a).

During REM sleep, a global level of brain metabolism similar to wakefulness was suggested in a PET study conducted by Maquet et al. 1990. However, at the regional level, some structures such as the thalamus, amygdala, and hippocampus showed increased blood flow or brain metabolism while others such as precuneus, inferior parietal cortex, and dorsolateral prefrontal cortex showed decreased activities, when compared to wakefulness (Dang-Vu, Schabus, et al. 2010a). An EEG/fMRI study conducted by Kaufmann et al. 2006 investigated the specific pattern of different sleep stages after sleep deprivation, and compared brain responses between sleep stages and wakefulness. However, this paper did not study the brain activity of the spindles particularly but all brain activities during the different stages. Stage N1 showed a deactivation on the thalamic and cingulate structures compared to the wakefulness state, whereas slight increases of brain activity were found in occipital and temporal regions. During stage N2, cingulate and temporal structures were deactivated, and activity in thalamic and hypothalamic areas decreased, while activity increases were suggested in the left inferior frontal gyrus. In stage N3, frontal areas, cingulate cortex, and subcortical areas were no longer activated; however, a higher activity was observed in the temporal and parahippocampal regions (Kaufmann et al. 2006). The paper sought to differentiate brain activities between the different stages. Stage N2 showed higher activities in the cerebellum, the parahippocampal and the hippocampus than stage N1 which could be explained by the presence of spindles. This paper demonstrated a correlation between deeper states of sleep and deactivation of brain regions and different brain activation between sleep stages (Kaufmann et al. 2006). By comparing Dang-Vu et al. and Kaufman et al. paper, there is an apparent difference in brain activation compared to the wakefulness state. Dang-Vu et al. demonstrated increase brain activities in the thalamus and hippocampus while the brain activities of these areas decreased in stage N2 of Kaufmann et al. paper. The difference in patterns can be explained by the fact that participants in the study of Kaufmann were sleep-deprived.

Recent simultaneous EEG/fMRI studies showed brain regions exhibiting a hemodynamic response associated with the generation of spindles. Fast and slow spindles were found to involve similar brain areas such as the thalamus, the anterior cingulate cortex, and the left insula. However, the generation of slow spindles was also more specifically involving the floor of the third ventricle (i.e. basal forebrain/hypothalamus), the midbrain tegmentum and the right superior frontal gyrus. On the other hand, the generation of fast spindles was more involving the middle frontal areas, the precentral and postcentral gyri and the supplementary motor area (M. Schabus et al. 2007).

fMRI also allows investigating brain hemodynamic responses elicited during tasks after a night of sleep deprivation (Chee and Choo 2004; Drummond and Brown 2001). Sleep deprivation was associated with decrease activity in the visual cortex related to the lapse in attention during the ANT tasks (Chee et al, 2008). In a PET study, they demonstrated a decreased activity in the thalamus, the prefrontal, and posterior parietal cortices during alertness for a serial addition/subtraction task (Maria at al, 2000). SD studies demonstrated a decrease of brain activity in temporal lobes during working memory N-back task, together with an increase in brain activity in prefrontal and parietal cortex regions. Increased activity in parietal regions might actually reflect some compensatory mechanisms (Chee and Choo 2004; Drummond and Brown 2001).Combining EEG/fMRI modalities is an efficient method in detecting spontaneous events and identifying the brain areas involved. This technique has been used in epilepsy but also in sleep to identify the different sleep patterns related to the different stages and to the sleep waves. By comparing two papers studying the sleep patterns of the sleep stages by using EEG/fMRI, brain activities seem to be affected by sleep deprivation. Therefore, our study used EEG/fMRI to analyze the effects of sleep deprivation on spindles and brain activity during a recovery nap.

Now we will present the methodological approaches and challenges associated with simultaneous EEG/fMRI analysis since they are central in our proposed study.

2.2 - Methodology to analyze EEG

2.2.1- Artifacts occurring on EEG

Despite their clear potential for promising neuroimaging technique to study sleep and sleep deprivation, simultaneous EEG/fMRI acquisitions are challenging. Indeed, an MRI scanner is more likely the worse environment to record an EEG signal. Indeed, recording EEG data inside an MR scanner induces several types of very large artifacts on EEG traces. It is, therefore, crucial to pre-process appropriately EEG data acquired inside the MRI, to remove those artifacts before allowing any analysis of EEG data. The rest of the section will describe the origins of these artifacts and the strategies we considered to clean our EEG data.

2.2.1.1 Gradient artifact

The first MRI-related EEG artifact is called the gradient artifact (Figure 5). To understand the origin of this artifact, one needs to review briefly how MRI data are being acquired.

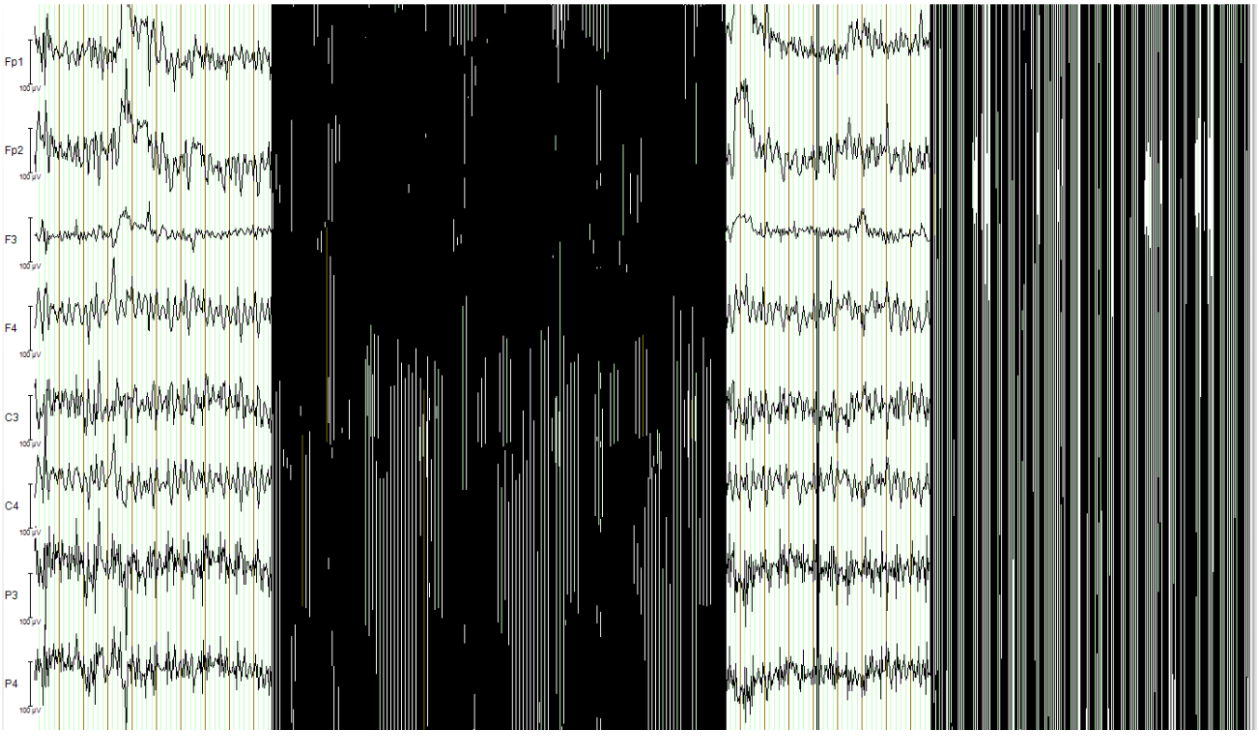

Figure 5: Gradient artifact occuring on an EEG

The overall principle of MRI it to measure the nuclear magnetic resonance of the hydrogen atom, and notably it nucleus, which is a single proton. Since Hydrogen is mainly present in water and our body is mainly composed of water, MRI is a unique technique to image the soft tissues of the body.

Each Hydrogen atom owns a nucleus composed of a single proton, which possesses a specific physical property: the spin. The spin is characterized by a magnetic dipole moment, with the property of rotates around itself such as a spinning top. When placed in a large uniform magnetic field, two phenomena appear: (i) the spins are getting aligned with the magnetic field, either in parallel or antiparallel manner, (ii) the spins start rotating around the axis of the field at a specific frequency that depends on the nucleus of the atom and the strength of the magnetic field, the so-called Larmor Frequency. Depending on the level of energy of the system, within a population of hydrogen atoms, there are not the same number of spin aligned in a parallel and in an antiparallel manner, resulting in a non-null magnetization, aligned with the external magnetic field created by the scanner. It is possible to excite the system by sending a radio-frequency (RF) pulse, i.e. a rotating magnetic field at the exact Larmor frequency. Such excitation will allow rotating the magnetization in the plane transverse to the static magnetic field. Once the excitation is done, spins will follow a relaxation process to get realigned to their original position, a signal can be measured in the transverse plane during this relaxation process. Since time constant of the relaxation processes in the transverse plane and in the axial plane are tissue dependent, it allows MRI acquisition to explore different contrast to image soft tissues. In order to obtain 3D images, three spatial gradients of the magnetic field are used to amplify the intensity of the signal in a specific x, y, and z-direction. First of all, a radiofrequency (RF) pulse is sent to tilt the magnetization along the transverse plane, then the gradients are switched on, but not at the same time. Gradient x (Gx) is the read gradient, which means the signal will be read only when Gx is on. Gradient y (Gy) is the phase gradient because the y-coordinate will be deduced from the phase signal. Gradient z (Gz) is the slice-selective gradient. Gz is switched on at the same time of RF pulse to excite only a specific slice (the excitation plane could actually be obtained along any direction, which is a specificity of MRI scanners). Consequently, only the protons belonging to this slice will be excited and will emit an MR signal. Gy is switched on after Gz, and depending on the position of the proton in the y-direction, the Larmor frequency of the protons will not be the same. However, this effect last only when Gy is on. Then, Gx is switched on and the signal can be recorded (Figure 6). The frequency of the signal given by the proton will give the x-coordinates, while the phase of the signal will give the y-coordinate. In order to have the exact y-coordinate and to construct a full image, Gy should be switched on several times (Mulert Christoph and Lemieux Louis 2010).

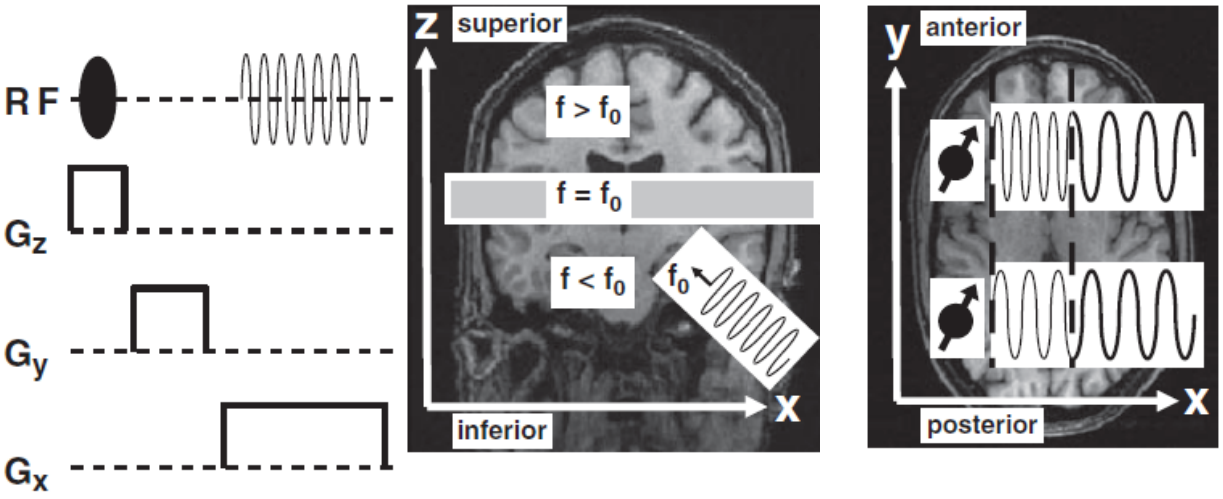

Figure 6: Gradient of MRI image (Mulert et al, 2010)
The pulse sequence diagram is shown on the left, and the right represent the signal

More specifically, Echo Planar Imaging (EPI) has been proposed to allow fMRI data acquisition. EPI sequences produce T2* weighted images and T2* is mainly affected by the inhomogeneity in the magnetic field. Unlike oxyhemoglobin, deoxyhemoglobin (hemoglobin without oxygen) is paramagnetic and introduces inhomogeneity to the local magnetic field. Therefore, EPI sequences allow inferring local deoxyhemoglobin concentrations. Activation of brain regions cause increased blood flow and decreased deoxyhemoglobin level which reduces the inhomogeneity and the T2* relaxation time. Thus, the T2* weighted data measured with EPI sequences allows to measure deoxyhemoglobin levels and to infer on neuronal activity. This phenomenon is called Blood Oxygenation Level Dependent (BOLD) (Chavhan et al. 2009). Protons at different positions will have a different frequency due to the magnetic field's gradient x (some have weak frequencies when other have high frequencies), so some signal is lost due to the dephasing of the spin, mainly caused by local inhomogeneity of the magnetic field, called the T2* effect. To solve this issue, Gx is inversed which re-phase the spins and allows recovering most of the signal, it's called Gradient Echo (GE). EPI images acquire a series of gradient echo and a Gy switching on between each GE, as a result, a full image can be reconstructed with these data (Figure 7) extremely rapidly, therefore, allowing functional imaging. However, image quality is reduced due to the acquisition time (Mulert Christoph and Lemieux Louis 2010).

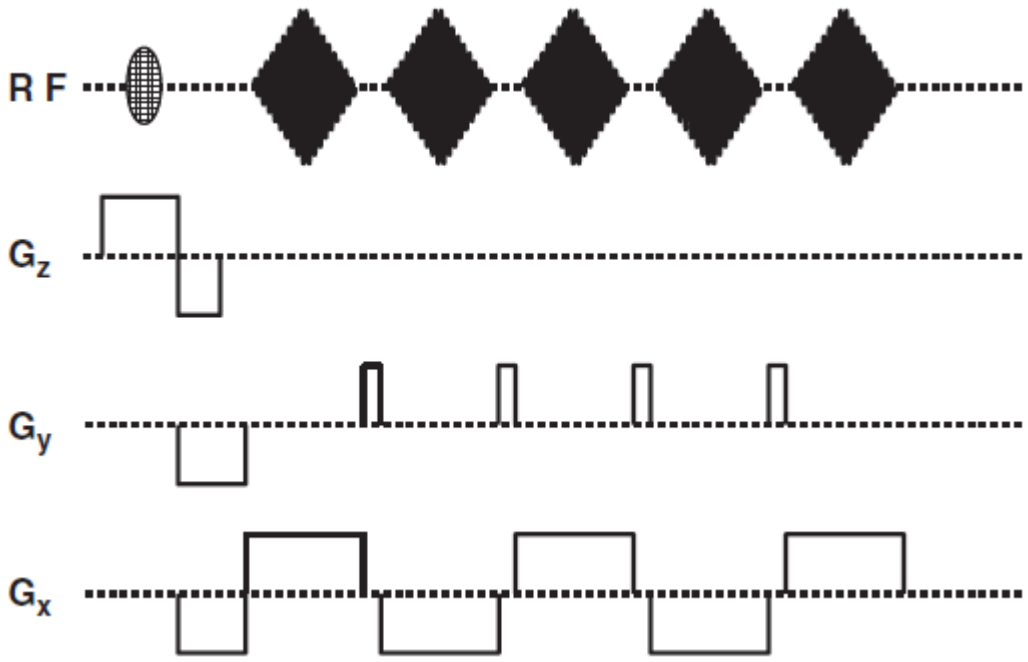

Figure 7: Description of EPI (Mulert et al, 2010)

The so-called gradient artifact recorded on EEG is caused by rapid changes of Magnetic gradients during MRI sequence. Consequently, magnetic fields varying with time will result in electric currents of very large intensity on electrode wires, and consequently on the EEG signals: the origin of this artifact is, therefore, magnetic induction caused by the variations of the gradients of the magnetic field. This artifact appears after each RF pulse and each gradient switching (Gx, Gy, or Gz). Consequently, this artifact is highly predictable and following a similar pattern all along the EPI sequence notably (Jose L. Ferreira, Aarts, and Cluitmans 2014). The amplitude of the artifact is larger than the EEG amplitude (10000µ V versus 100µV for EEG signal), therefore it completely obscures all the EEG data (Figure 5). To be able to record accurately such an artifact, one needs to EEG amplifier systems allowing excellent sampling rate (1000Hz quite larger than usual EEG acquisitions) and detectors with a large dynamic range in order to avoid any saturation of the system. Once we can make sure the artifact signal could be recorded accurately over different sequences, the signal is averaged to build an artifact template and subtract from the EEG channels to retrieve the underlying EEG signals, following the method proposed by Allen et al. (Allen et al. 1998a).

2.2.1.2 Ballistocardiogram artifact

Ballistocardiogram artifact (BCG) is a physiological artifact because it is linked to the heartbeat. This artifact appears on all electrodes of the EEG cap (Figure 8). The exact origin of this artifact is not clear and several hypotheses were considered in the literature. In 1993, Ives et al. made the hypothesis that the BCG artifact was caused by small motions of the head inside the MRI because of the acceleration of the blood flow in the aortic arch (Debener et al. 2008; Ives et al. 1993). The physical principle behind the BCG artifact is that the "movements of electrically conductive material in a static magnetic field result in electromagnetic induction" (cited by Debener et al. 2008). Even if overall the community agreed to say that BCG should result from motion, there is still a disagreement on what kind of motion exactly. Some studies suggested that the head rotation is caused by axial body motion (Allen et al. 1998, Huang-Hellinger et al, 1996), whereas other suggested that this movement might be caused by the dilatation of the blood vessels at each heartbeat which would induce a small pulsation under the electrodes (Bonmassar et al, 2002).

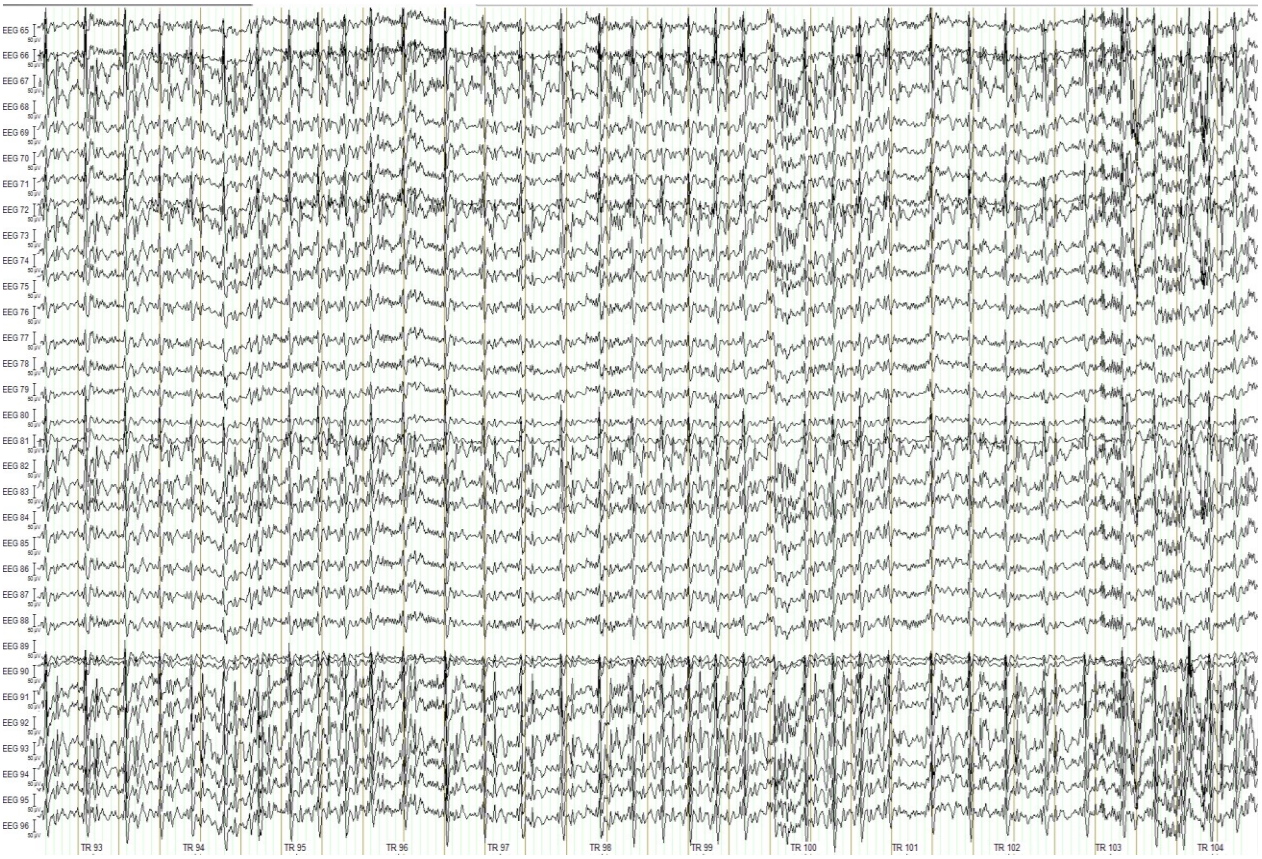

Figure 8: Ballistocardiogram artifact

As the BCG artifact is therefore related to the heartbeat, the electrocardiogram (ECC or EKG) is used to detect the bioelectricity of the heartbeat signal. Figure 9 shows three EEG channels and one ECG channels. From the EEG signal, the green lines correspond to the R-peaks in the ECG that were automatically detected by thresholding. Note that after each R-peak, a BCG artifact appears on most of the EEG channel 210ms later (see Figure 8 and 9). The BCG being of physiological origin is, therefore, more variable from one heartbeat to the other and therefore more difficult to correct.

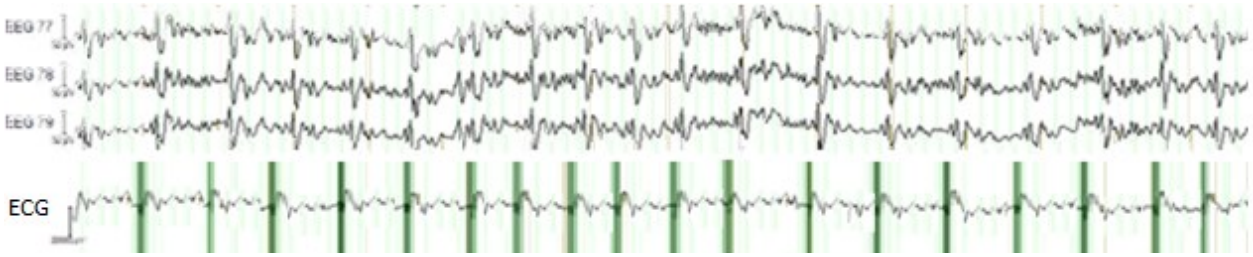

Figure 9: BCG artifact and R-peaks detection on ECG

2.2.1.3 EEG preprocessing: MR artifacts removal

In the context of simultaneous EEG/fMRI studies, the first step is to preprocess EEG data in order to remove those MR-related artifacts. Several methods have been proposed for this purpose (José L. Ferreira, Cluitmans, and Aarts 2012; Niazy et al. 2005; Sun and Hinrichs 2009), two of them will be presented in this section.

Average Artifact Subtraction:

One of the first method developed to remove the gradient artifact is denoted the "Average Artifact Subtraction" (AAS) method. It has been developed by Dr. Allen (Allen et al. 1998a). The first hypothesis made by this method was that the artifact should be constant, stable and reproducible. AAS is therefore particularly adapted to remove the MR related gradient artifact. The AAS method consists in the following steps:

- On one channel, the EEG signal is divided into segments of 10s each
- On each segment, the artifact is detected. The gradient artifact is detected thanks to the TR trigger send by the MRI machine on the EEG. For the BCG artifact, it is explained below.
- A template of the artifact is creating by averaging different segments
- The template artifact is subtracted from each channel on each segment

- A low-pass filter at 50Hz is applied to remove the remaining residuals

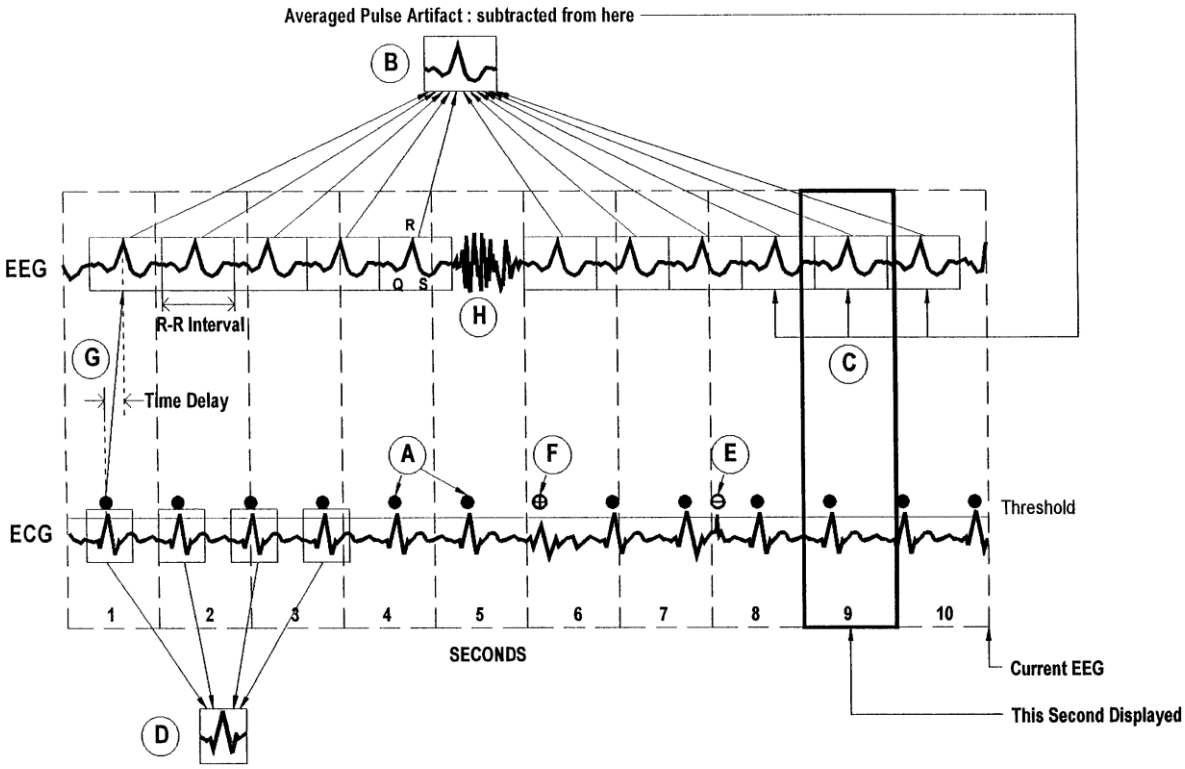

Figure 10: AAS method by Allen et al

The method can therefore be summarized as:

$$EEG_{corr,i} = EEG_{raw,i} - \Gamma_{i_s}$$

With i: segment corr: EEG cleaned of artifact

Γ_{i_s}: Template of the artifact raw: EEG with artifact

As the BCG artifact is not a constant artifact due to its shape and time variation in each segment, the steps of the AAS method are a little bit different than for gradient artifact. The application of AAS to remove the BCG artifact is summarized in Figure 10.

The first step is to divide the EEG signal into segments of 10s..., as for the gradient artifact. The second step consists of detecting the R-peaks on the electrocardiogram (ECG). The BCG artifact is then assumed to appear on scalp EEG channels, 210ms after the R-peak detected on ECG (Figure 10G). A template of all BCG artifact is created by averaging all the segments (figure 10B) and then subtracted from each EEG channel on every segment (Figure 10C).

AAS method is overall really efficient to correct for the gradient artifact since the artifact template is stable and highly reproducible all along the EEG signal. However, the efficiency of AAS method for BCG artifact removal highly depends on the accuracy of the R-peak detection on ECG. Therefore, to ensure efficient R-peaks detection on our data, we considered a semi-automatic approach. Automatic R-peak detection was carefully evaluated visually by an expert who had the possibility to accept, modify or reject an R-peak detection. This expert-guided intervention was important to improve the overall accuracy of AAS method, especially because the ECG itself can be quite noisy when recorded in the MR environment (Allen et al. 1998b).

Independent Component Analysis (ICA):

This method decomposes the EEG signal into statistically independent temporal components. ICA is a standard data driven exploration technique, allowing to decompose a multivariate signal into a series of temporal components, time courses that are mutually statistically independent. Each temporal component is actually associate to a spatial topography reporting what are the contributions of every EEG channel to that specific temporal component. ICA has been proposed as an extremely efficient data-driven de-noising technique (Mantini et al. 2007).

The mathematical equation of ICA decomposition is given by (Langlois, Chartier, and Gosselin 2010):

$$\boldsymbol{x_{c,t}} = \boldsymbol{A}.\boldsymbol{s_{cs,t}} + \mathrm{n}$$

With

x: Channel of EEG with c the number of channels and t the time sample

A: Coefficient which determines the components distribution

s: independent Components of the signal with cs the number of components and t the time sample

n: Noise Gaussian

The user has to choose the total number of components expected to describe the signal, then the components are calculated. To remove MR related artifact, an expert should then review every temporal component and associated spatial topography to identify the BCG artifact (Figure 11). Once the components are labeled as an artifact, one can reconstruct the overall EEG signal, by removing the influence of those components.

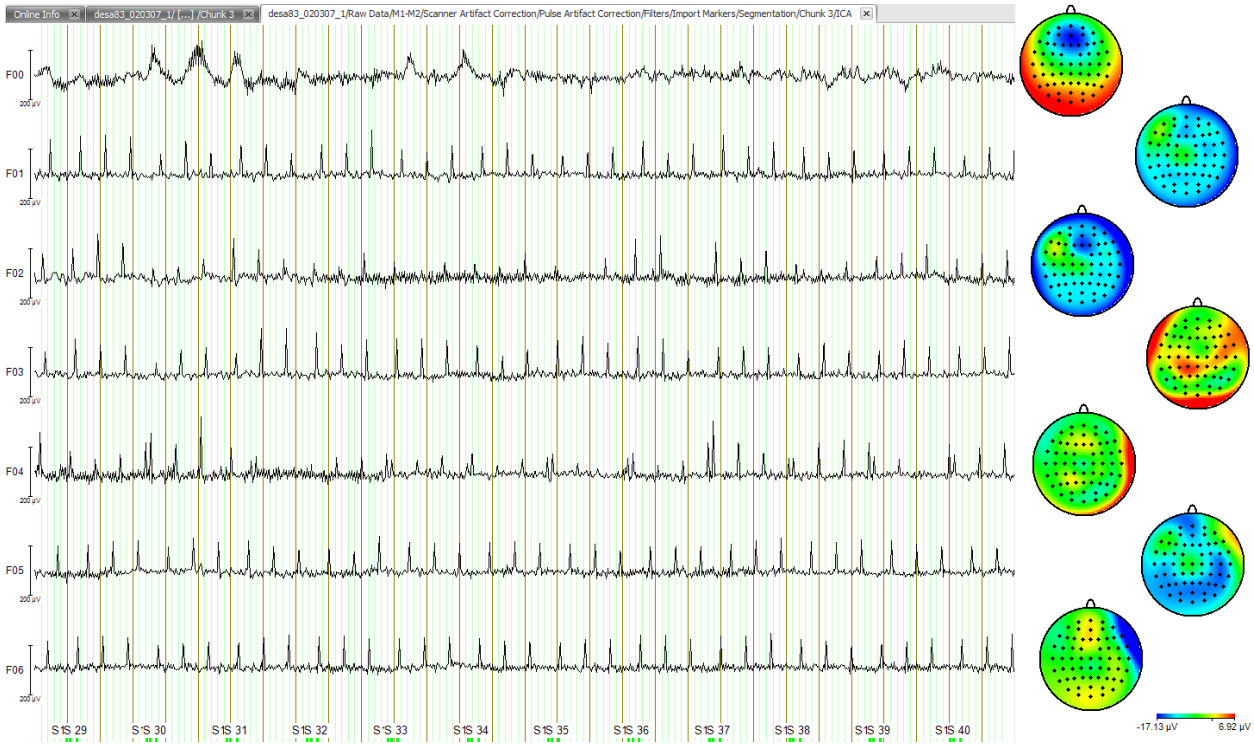

Figure 11: Describe signal and topography of some components

In Figure 11, seven temporal components are displayed with their topographies. In this figure, at least four components (F01, F03, F05, and F06) have been labeled as an artifact due to the repetitive template each second. It looks like these components are a residual artifact from Gradient or BCG artifact.

This method does not hypothesize that the artifact is stable in time. ICA is therefore very efficient to extract noisy components of large amplitude which are variable in time. However, it might be sometimes difficult to identify what are the components corresponding to the artifacts. However, as a purely data-driven technique, ICA is difficult to control and if a component was wrongly classified as an artifact component, some important physiological information could be lost.

Once artifacts are removed from the EEG data, the EEG analyses can start. Now, we will present you the different methods to detect the spindle on EEG. Spindle detection on EEG data acquired in the scanner has been applied only few times.

2.2.2 - Automatic methods for spindle detection

In the nineties, spindles were mainly detected visually by an expert Electroencephalographer, but this was time-consuming and the accuracy of the detection depended on the experts. Therefore, the team of Schimicek decided to develop an automated method for spindle detections (Schimicek et al. 1994). Spindles were detected by amplitude thresholding while rejecting contributions from the muscle activity and the alpha band, which may contaminate the spindles. This method was validated by comparing the results of the automated detection with a visual detection made by an expert. On 10 young healthy subjects, the automated method found the spindles correctly at 89.7%, they had a false positive rate at 6.5% and false negative events at 3.8% (Schimicek et al. 1994). The method was successfully validated, even if the validation can be discussed due to the small sample size used. Afterward, many researchers developed new algorithms to detect automatically the spindles on EEG data. Those methods have been validated on specific datasets, involving mainly limited sample of data, thus question the validity of such validation procedures. The very important study proposed by Warby et al. aimed at comparing the performance of several of these automatic detection methods on the same sample of normal EEG data (Warby et al. 2014a). They compared six automatic algorithms with a visual spindle detection of experts and non-experts. Experts were Registered Polysomnographic Technologists (RPSGTs), while non-experts were random person with no a priori knowledge in sleep and EEG. For their study, they used a sample of 110 healthy subjects with a mean age of 57 years old. Twenty-four experts from sleep clinics

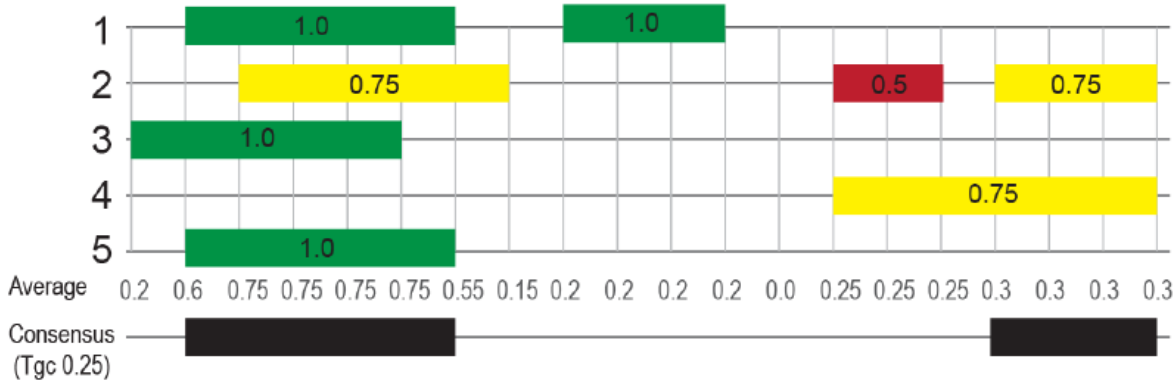

Figure 12: Spindles Consensus (Warby et al)

in USA and Canada were hired to detect spindles on 2 000 epochs of N2 sleep. At least 5 experts viewed each epoch, so a consensus could be created in order to accept the spindles detected by the experts or not. For each spindle, experts provided a satisfaction score (1.0 = definitely, 0.75 = probably, 0.5 = Maybe, 0 = No spindle). When the average of all weighted scores was superior or equal to $T_{egc} = 0.25$, the spindle was labeled as detected (Figure 12). This consensus detection made by the experts was considered as the gold standard in that study, whereas the visual detection made by the non-experts and the results of the detection algorithms were compared and validated against this gold standard. The group of non-experts was made of 114 individuals without any experience in sleep and EEG, although a brief training was delivered to each of them. A spindle consensus was computed for the non-expert group (Figure 11), but instead of 0.25, the threshold of the weighted average was set at $T_{ngc} = 0.4$. The automated detection methods consisted in different methodological approaches. Two automated methods were based on Mölle (Mölle et al. 2011) and Martin (Martin et al. 2013) methods, which were directly inspired by the Schimicek algorithm (Schimicek et al. 1994). These methods consisted in first band-pass filtering the EEG signal within the spindle frequency range (10-16 Hz) (Figure 13B), followed by a root mean square (RMS) of the signal estimated over a moving window (Figure 13C). A threshold was calculated based on the

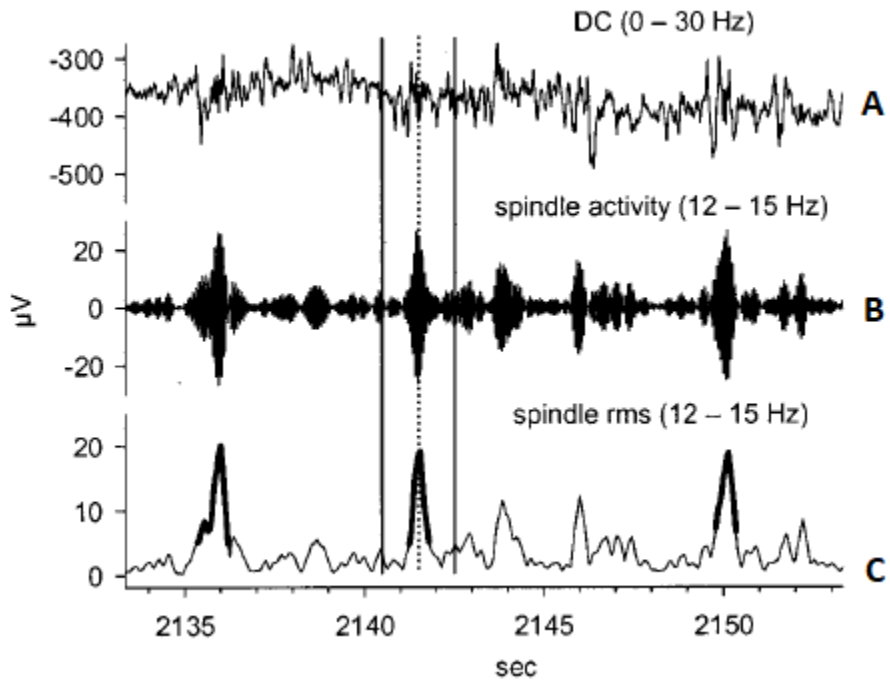

Figure 13: Mölle method (Mölle et al, 2002)

amplitude of the RMS signal (the tuning of this threshold varied depending on the authors). If the amplitude of the RMS was superior to this threshold then a spindle was marked as detected.

Another algorithm evaluated in Warby et al (Warby et al. 2014a) was the method proposed by Wamsley et al (Wamsley et al. 2012), which is considering a Wavelet time-frequency decomposition of the EEG signal. They applied a wavelet transform, consisting in an 8 parameters complex Morlet wavelet. The EEG signal was first filtered within the band 0.5-35Hz to remove residual artifact before applying the wavelet transform. The wavelet transform was applied on the EEG filtered signal of the N2 epochs to calculate the threshold. The signal mean was calculated by sliding window (100ms) averaging of the wavelet coefficient for the scale between 10-16Hz. The threshold was 4.5 times this signal mean. Finally, the wavelet transform was applied to the filtered EEG signals, and when the wavelet coefficient of the scale portion (10-16Hz) exceeded the threshold, it was marked as a spindle. Wamsley et al. (Wamsley et al. 2012) validated their algorithm by comparing the spindle density (i.e. Number of spindles per min) found when using automated and visual detections, on schizophrenia EEG data obtained from 10 patients and 10 healthy participants. The ratio between manual and automated detection was not found significantly different, suggesting that automated methods were as good as the visual method (Wamsley et al. 2012). A third method was based on Bodizs (Bódizs et al. 2009) and used spindle

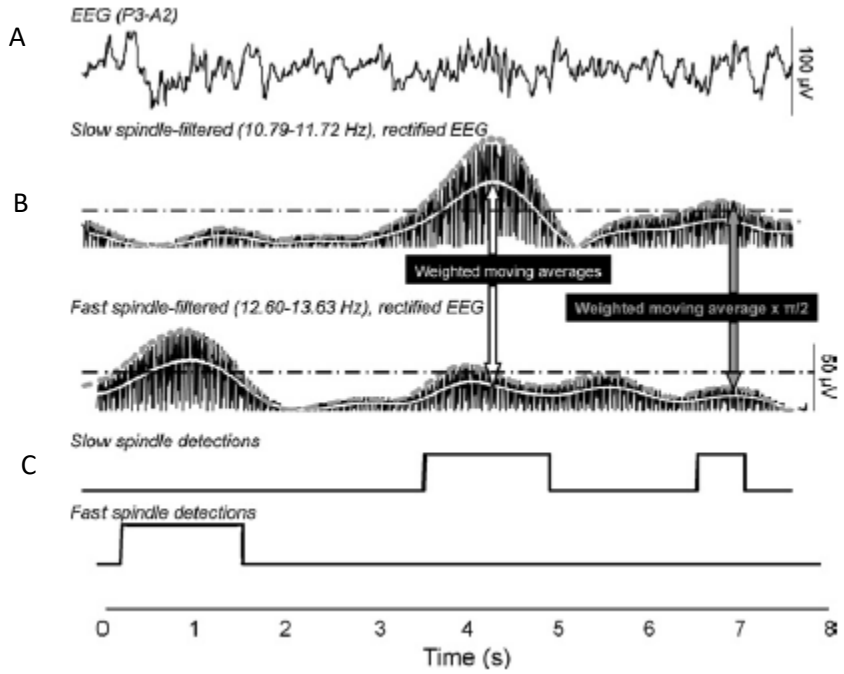

Figure 14: Bodizs method (Bódizs et al. 2009)

characteristics. First, the EEG was bandpass filtered at the peak frequency band of slow (10.8-11.7Hz) and fast (12.6-13.6Hz) spindles, separating the two types. Secondly, the filtered signal was rectified which means smoothed by a 22-point Hanning-weighted moving average, and then multiplied by the inverse of the mean of a rectified sinewave ($\pi/2$). As a result, an envelope of the filtered signals for the slow and the fast spindles were obtained. (Figure 14B). Finally, a spindle was detected when the envelope exceeded a predefined threshold (Figure 14C).

The two last methods evaluated in Warby et al considered an estimation of the spindle envelope, i.e. methods proposed by Ferrarelli et al (Ferrarelli et al. 2007) and Wendt et al (Wendt et al. 2012). These methods first performed a band-pass filter in the frequency range of spindle (12-15Hz) (Figure 15B). Then, the absolute amplitude of the filtered was applied to extract the envelope called "Absolute Amplitude" (Figure 15C). Two thresholds were estimated, an upper threshold corresponding to 8 times the average of the absolute amplitude and a lower threshold corresponding to twice the average of the absolute amplitude. Spindles were detected if the absolute amplitude

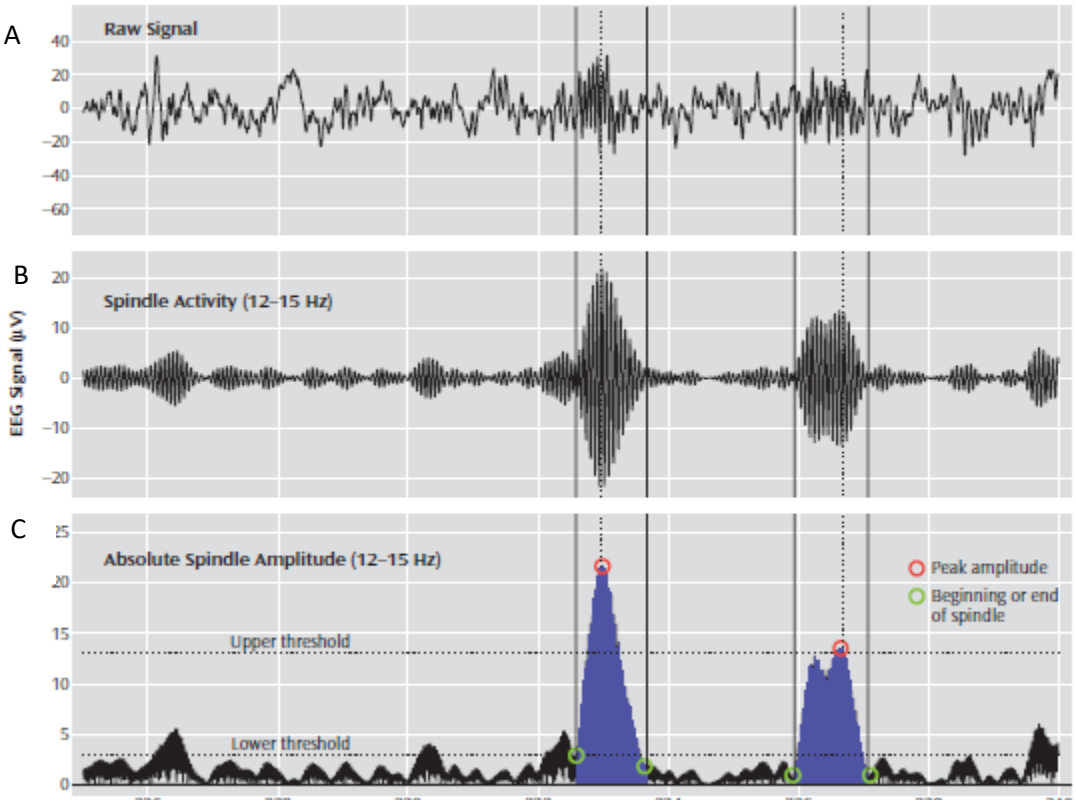

Figure 15: Ferrarelli method (Ferrarelli et al)

exceeded the upper threshold, whereas the beginning and the ending of the spindles were defined when the signal exceeded and fell behind the lower threshold (Figure 15C).

To evaluate the performances of each visual or automated detection, they estimated two parameters: the sensitivity and the precision, considering the consensus detection of the experts as the Gold Standard. The sensitivity was defined as the proportion of spindles that were correctly identified, whereas the precision was defined as the proportion of correct detections provided by the algorithm or non-experts. They also estimated a parameter denoted as the F1-score, summarizing the balance between sensitivity and precision. They reported the precision of the non-expert group to be 73% and 62% for the sensitivity, with an F1-score of 0.67. For the automated methods, they demonstrated that the algorithm exhibiting the best performance was Wamsley algorithm with a precision of 55% and a sensitivity of 50% for an F1-score 0.52. The other algorithms presented a lower F1-score, three of them being 0.21. However, when considering all automated detections together with a consensus rate to accept or not the spindles detected by all methods, a better F1-score was obtained. Indeed, the spindles detection of all methods was taken into account and when at least three methods found a spindle at the same location, this spindle was accepted. Using this automated method consensus, they obtained an F1-score at 0.54 better than the F1-score of the best automated method.

They concluded that overall the non-expert group performed well because their detection performance was close to the expert detection. As the automated methods did not have the same parameters, it was difficult to compare them. However, in this case, Wamsley algorithm was closer to the expert detection than others, even if the difference was not statistically significant. The most interesting message of this study was that the combination of several automated methods provided detection performance closer to the gold standard obtained from expert marking.

The originality of our proposed study was to evaluate automated methods for spindle detection, in the context of a nap following sleep deprivation and for high-density EEG data acquired simultaneously in an MRI scanner. Sleep deprivation (SD) has a huge effect on cognitive function and brain functioning. During recovery sleep, in order to compensate the issues cause by SD, brain activity pattern should be different than during a normal night. As spindles are involved in memory consolidation and memory processing, spindles should play a major role in the recovery of cognitive functions. However, studies demonstrated that spindle characteristics are slightly different after SD. Moreover, studying EEG data recorded in the MRI scanner requires additional preprocessing and artifact removal, therefore automated spindle detections methods have not been

evaluated in this context. One study conducted by Schabus et al. (Manuel Schabus et al. 2007) detected spindle on EEG data acquired inside the scanner via automated detection based on Mölle method. However, they did a post-review of their automated detection which becomes a semi-automatic detection to ensure the quality of spindle detection.

The focus of this MSc project was to evaluate and identify the best method to detect spindle on EEG data acquired inside the scanner since those marking will then be considered to assess brain map activity of the spindle generation by analyzing fMRI data. Inspired by the study of Warby et al (Warby et al. 2014a), we evaluated four automated spindle detection methods on our EEG data and compared to the visual detection made by an expert. According to the literature review, we hypothesize that spindle criteria (i.e. density, amplitude, duration, and frequency) should be different during the recovery night than during a normal night.

Chapter 3

Study Protocol: Neural correlates of sleep deprivation using simultaneous ElectroEncephaloGraphy (EEG) / functional Magnetic Resonance Imaging (fMRI)

In this section, the overall protocol for this sleep deprivation study will be presented, i.e. subjects recruitment, study design and data acquisition and data analysis. This study was completed at PERFORM centre and has been approved by "Comité Centrale d'éthique de la Recherche" (CCER).

3.1 – Subjects Recruitment

After obtaining CCER approbation for our study, recruitment flyers were posted in different places such as within the University, at PERFORM Centre, as well as on corresponding Facebook and Twitter accounts to find volunteers for our study. Then, to assess the eligibility of the volunteers to participate in our study, a semi-structured interview was first performed. According to our inclusion criteria, participants should be aged between 18 to 30 years, healthy and good sleeper. The exclusion criteria were the following:

- Pregnant woman
- Claustrophobic person because the MRI is a confined space
- Person with metallic objects into the body: vascular clip, prosthetic valve, metal prosthesis, metal fragment, pacemaker
- Sleep disorders: obstructive sleep apnea, narcolepsy, insomnia, etc.
- Neurological disorders such as epilepsy, migraine, and stroke
- Medical conditions such as chronic pain and chronic respiratory diseases
- Individuals with psychiatric conditions (e.g., major depression, anxiety disorder, psychotic disorder)
- Individuals taking psychotropic medications (e.g., hypnotics, antidepressants)

In total, fifty-one participants were considered for the screening phase, and twenty-eight volunteers were selected as eligible. After the first night of polysomnography, three participants were excluded because they had sleep disorders. Two of them had periodic legs movements during their

sleep and the other one had sleep apnea. Moreover, three participants have been later excluded because of equipment problems occurring after the second night. Finally, six participants withdrew before the end of the experiment. Consequently, sixteen participants completed this sleep deprivation study, including ten females and six males.

3.2 - Materials

The whole study took place in the sleep lab and in the neuroimaging unit of PERFORM centre. Two data acquisition systems were considered, one for the whole night monitoring and one for the EEG/fMRI acquisition the next morning.

Whole night monitoring:

A polysomnography (PSG) equipment combining EEG, an Electrooculogram (EOG), an Electromyogram (EMG), nasal-oral thermocouple airflow, transcutaneous finger pulse oximeter and a respiratory belt was used for the first selection night, in order to assess whether participants had no sleep disorders; whereas only the EEG, the EOG, and the EMG were used for the normal night (Figure 16). The EEG for the first night consisted of 12 electrodes following the 10-20 system. For the normal night, the EEG consisted of 18 electrodes (Figure 17).

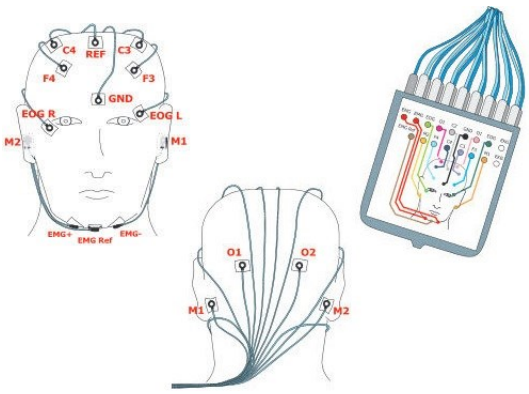

Figure 17: EEG equipment
Source: http://www.medicalexpo.fr/prod/somnomedics/

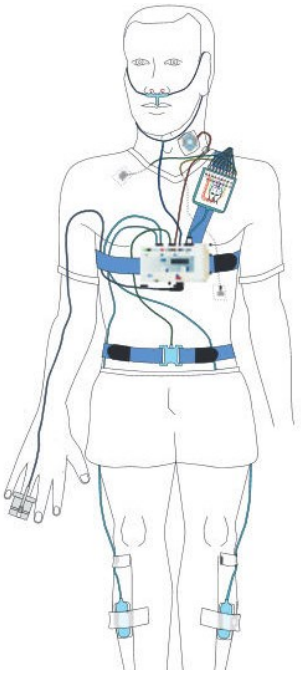

Figure 16: PSG equipment
Source: http://www.medicalexpo.fr/prod/somnomedics/

To ensure that participants had regular sleep before the normal night and follow their daily activities, participants were asked to wear an actiwatch during 7 days before the normal night acquisition. This actiwatch allowed recording the movements and had a light sensor to record the light sensitivity, in order to ensure that the participant slept normally few days before the study.

The system used for simultaneous EEG/fMRI acquisition:

The acquisitions have been done at PERFORM Centre (Concordia University). The MRI system is a 3T General Electric (GE) scanner and 8 channels coil was used. In order to measure EEG/fMRI simultaneously, we needed an EEG system compatible with MR.

The EEG system we used is Electrical Geodesics Inc. (EGI) system with a cap of 256 electrodes. Before installation, the cap was soaked in a saline solution (i.e. baby shampoo + potassium chloride) to ensure good electrical conductivity between the sponges attached to each electrode and the head. The impedance of each electrode was kept inferior to 100 kΩ, and the head of the participant was wrapped to keep the electrodes wet in order to maintain good quality EEG recording during the whole imaging study.

Figure 18: Participant with EEG cap inside MRI room

The data acquisition set-up further detailed in Appendix A.

3.3 – Study design

Once the participants were recruited for the project, they were instructed to come for three visits separated by one or two weeks at PERFORM Centre. The first visit consisted in a control

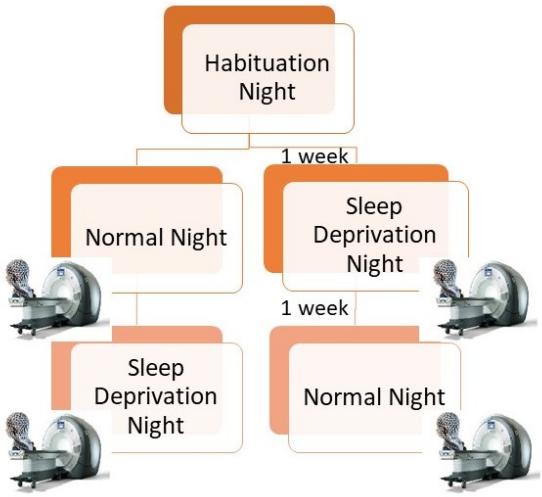

Figure 19: Nights protocol procedure

night monitored using the PSG equipment, in order to ensure that participants did not present any sleep disorders. If the PSG result showed a disorder, the participant was excluded from the study. For the two other nights, the order of the visits was randomly assigned (Figure 19). One of the visits consisted in a normal night at the PERFORM Centre, monitored with the PSG equipment, followed by an EEG/fMRI acquisition in the next morning. Participants were asked to sleep a minimum of 6 hours during normal the night in the sleep lab. The other visit consisted in a sleep deprivation night followed by an EEG/fMRI acquisition in the morning. During the sleep deprivation night, a member of the study stayed overnight with the participant and ensured that he or she did not fall asleep by offering to talk, watch movies or play games.

EEG/fMRI acquisitions were very similar for both visits. A first part was dedicated to study cognitive functions. The first task was the N-back task with 3 difficulty level (0, 1, and 2). N-back is a memory task where a series of letter is presented to the participant, and he or she has to press the button if the letter presented is the same that the letter presented N times before (Figure 20).

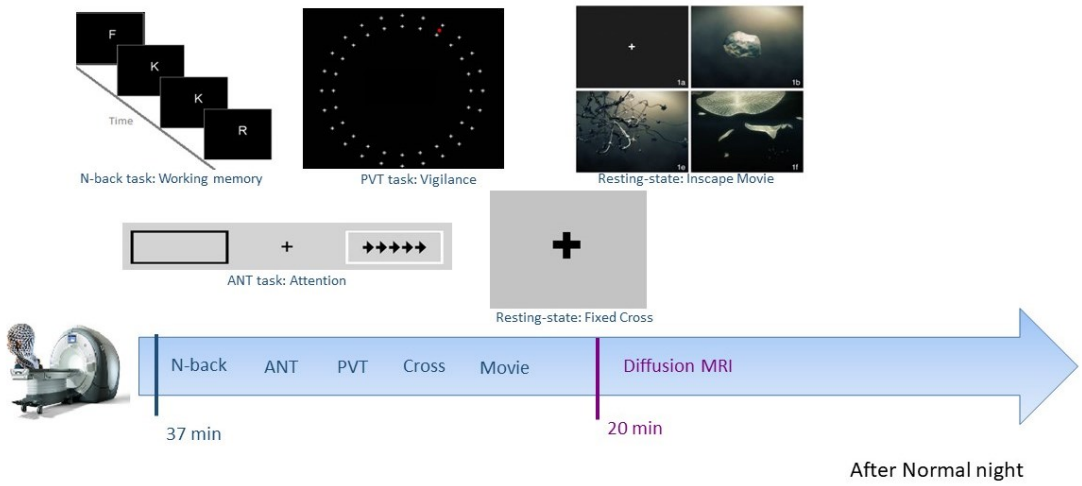

Figure 20: EEG/fMRI acquisition protocol after Normal night

The second task was the ANT task. ANT is an attention task where the participant has to give the direction of the arrow in the middle of an array of 5 arrows. Different cues were sent before the apparition of the arrows to distract the participant and to ensure maintaining his level of attention (Figure 20). The third task was the PVT task. PVT is a vigilance task, which involves a series of stimuli presented sequentially on screen spatially similar to the ticking of the clock. The participant had to press the button when the stimuli skip a sequence (Figure 20). After these three tasks, resting state data were acquired, divided into two blocks. During the first block, the participant had to fix a cross, while during the second block he had to watch a small movie (Figure 20) (Vanderwal et al. 2015). For these two blocks, the participant was asked to focus on the screen (cross or movie), while remaining relaxed limiting his motions as best as possible. Note that the movie we presented has been shown to limit the amount of motion during resting state fMRI acquisition, as demonstrated in Vanderwal et al. (Vanderwal et al. 2015). Finally after the normal night only, we performed a diffusion MRI acquisition to assess underlying anatomical connectivity (Figure 20).

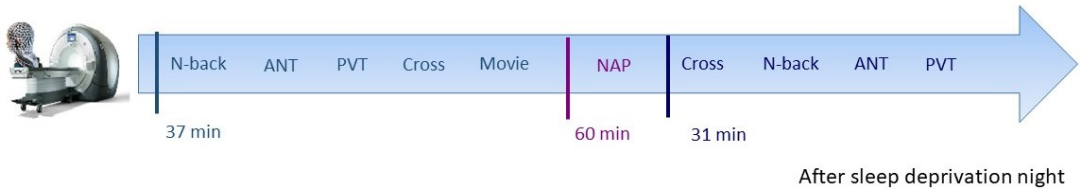

Figure 21: EEG/fMRI acquisition protocol after sleep deprivation night

EEG/fMRI acquisition after sleep deprivation night was similar to the acquisition described above, except for diffusion MRI acquisition. Indeed, after the three task and resting state data acquisition (in two blocks), the participant was allowed to take a nap to sleep for a maximum of one hour. After one hour of nap, we woke up the participant before performing the same tasks and resting state data acquisition again (Figure 21).

As acquisitions were long, a total of 1h45 for the normal night and 3h for the sleep deprivation, the most important point was to make sure that the participant was comfortable inside MRI. Therefore, we offered to the participant the possibility to get out of the scanner before or after the nap in order to stretch his/her legs or to go to the bathroom.

During my Master, I took part in every process of the study. I participated in the ethics application, subjects' recruitment, screenings, data acquisition and the analysis. Next, I will present the different analyses performed on EEG data.

Chapter 4

Methods to analyze the data:

The objective of my Master project was to optimize automated spindle detection on EEG data acquired simultaneously with fMRI. The first step was to perform EEG preprocessing to remove artifacts and improve the quality of EEG. The second step was to use automatic and visual (manual) spindle detection and evaluate their performances. The last step was to do a BOLD correlation with the spindle detection (two methods) and compared the brain activity map obtained.

In this section, I will present the methodology and the analysis I did on the data to detect the spindles. The first section will be on EEG preprocessing, the second section will present spindle detection methods and statistical evaluation of automated methods. Finally, the last section will cover fMRI data analysis.

4.1 – Spindle detection from scalp EEG data

We are considering EEG data that have been recorded inside the MRI using an MR compatible EGI system. Therefore, before considering spindle detection, EEG data should be carefully preprocessed and notably MR related artifacts should be removed.

4.1.1. EEG preprocessing: MR artifacts removal

To have an optimal cleaning scheme for our EEG, EEG data were pre-processed using BrainVision Analyzer 2. First of all, EGI data were exported in edf format, since Brainvision software is not compatible with raw EGI file format. However, before exporting the signals, a high-pass filter at 0.1Hz was used to avoid signal saturation during the exportation. The first step was to clean the gradient artifact. Brainvision analyzer uses AAS algorithm by using the trigger TR as a marker to detect the artifact and to create the artifact's template. In our case, the fMRI acquisition was continuous so the artifact was also continuous, and the TR happened every 2.5 seconds. At the same time, we decided to downsample the data at 500Hz and to apply a low pass filter at 50Hz in order to remove remaining high-frequency activity that can appear as a result of noise. The second step was to clean the BCG artifact. Brainvision Analyzer used AAS method with R-peaks semi-

automatic detection. Firstly, R-peaks were detected from the ECG signals. R-peak detections were then carefully reviewed by an expert user, who could accept, modify or refuse every detection. Then, the template of the BCG artifact was created by averaging EEG signals following each R-peaks. BCG artifact removal was finally obtained by subtracting the BCG template to all EEG channels at the time of each R-peak. Following BCG artifact correction, we applied a band-pass filter at 0.3-20 Hz to remove the residual artifact and the artifact due to sweat. The filter was a zero phase shift Butterworth filter order 8 (Figure 22). The choice of an order 8 was to have the ideal response because it covered the defined frequency well. Choosing a frequency between 0.3-20 Hz can be perceived as too restrictive, but as we are interested in detecting sleep waves, it allowed us to focus only on the frequency band of interest.

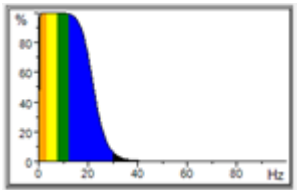

Figure 22: Butterworth filter order 8

Corrected EEG signals were carefully reviewed visually. For some subjects, when this correction was evaluated as not sufficiently accurate, we also applied an Independent Component Analysis (ICA) to remove any occurring residuals artifacts. To calculate the components, we used all the electrodes except the ECG electrodes and the electrodes located on the face. Indeed those electrodes tended to dry very rapidly, resulting in very noisy recordings, they were then discarded from our analysis. The number of total ICA components was set 32, the components were estimated using a 150s window of the signal. Once the "noisy" artefacted components were visually identified, a projector was built in order to remove the contribution from such a component on the whole duration signal. Therefore, this 150s window of EEG signal should be carefully selected and should not present any movements artifacts. Once the artefacted components were identified, the user decided which components should be removed from the signal. Then, the signal was recomposed with the source components accepted by the user. Finally, the EEG signal was re-referenced using the Mastoid M1-M2 as a reference electrode, in order to remove the impact of signal fluctuations occurring in those channels.

Following this pre-processing procedure, EEG data became readable and spindle detection could then be considered. However, it is important to keep in mind that cleaning the data, notably the ICA, might have removed some physiological signal of interest, which could therefore disturb

spindle detection. As a result, the spindle detection criteria might be different from the one proposed for good quality EEG data acquired outside the MRI scanner.

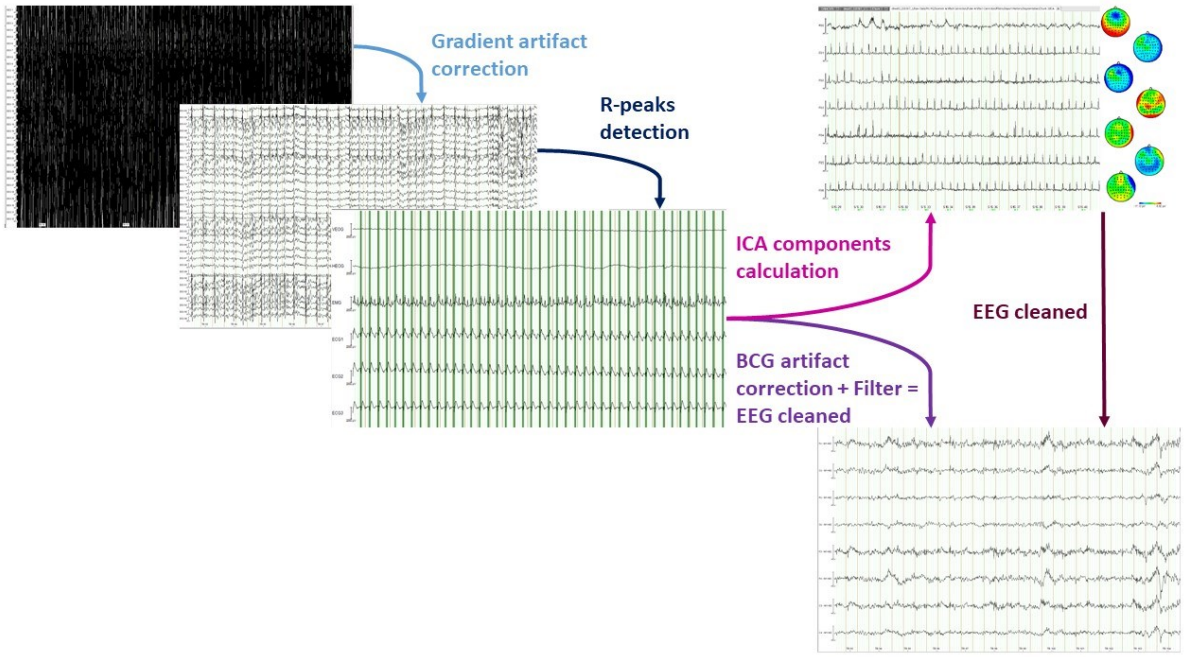

Figure 23: Method to preprocess the EEG data

4.1.2. Spindle detection methods

For this project, two types of spindle detections have been considered. On one hand, the spindle detection was made by a neurologist, expert Electroencephalographer, who will be denoted as the expert in this thesis. On the other hand, different automated algorithms have been considered for spindle detection and compared with the expert detection.

4.1.2.1- Expert detection:

The expert performed a visual detection; this detection was considered the reference for comparison with the automated detection methods. Before performing the detection, all data have been scored according to the American Academy of Sleep Medicine (AASM). The spindle criteria for the detection were a frequency ranging between 10-16Hz by separating fast (13-16Hz) and slow spindles (10-13Hz) and a duration of 0.3-3s. The detection was made on EEG channels Fz, Cz, F3, F4, C3, and C4, during stage N2 and N3. The expert used a Python toolbox named Wonambi, created by Gio Piantoni and Jordan O'Byrne for the detection. Wonambi is a toolbox created to perform scoring, and automated spindle and slow waves detection in our sleep lab at PERFORM Centre at Concordia University.

4.1.2.2 - Automated spindle detection:

Several automated spindle detection algorithms have been developed during the last 20 years. Four methods were selected for this comparison study. The first method was implemented in FASST (fMRI Artifact rejection and Sleep Scoring Toolbox) a Matlab toolbox developed by Cyclotron Research Centre (CRC), University of Liège (ULg), Belgium. This algorithm actually uses Mölle method (Mölle et al. 2002), however, I implemented some modifications based on Schimicek method (Schimicek et al. 1994). The second method was Wamsley method (Wamsley et al. 2012), and the algorithm implemented by Warby (Warby et al. 2014a) in Matlab was considered. The third method was Mölle method, but following their second published in 2011 (Mölle et al. 2011), and the algorithm implemented in Wonambi was considered. The last method was Nir method (Nir et al. 2011), as implemented in Wonambi. I selected Wamsley method because it provided the best performances in Warby's paper. Moreover, it is the only method that considered a wavelet transform analysis. FASST has been selected because it is the automated method that I applied during a previous summer internship (summer 2015) on similar data analysis (article in

preparation). I have selected Mölle method because it is based on a similar algorithm than the one implemented in FASST, therefore providing an opportunity to compare performance and to validate my personal modifications implemented in FASST method. Nir method was selected as the second method provided best performances on sleep EEG data acquired in our sleep lab for other studies (after Mölle method).

The spindle criteria provided to all detection methods was a frequency range of 10-16Hz, a duration of 0.3-3s, separated by at least 1s, and a detection performed by considering Fz, Cz, F3, F4, C3, and C4 electrodes.

FASST algorithm (Schrouff et al. 2013):

Data were first converted in Matlab, then the scoring of sleep stages was applied because it was required for the spindle detection. Several parameters can be chosen by the user, such as the frequency range of the spindle, the percentile for the threshold calculation, and the channel for the detection. I will explain the different steps involved in this detection and clarified the modifications that I made specifically for the purpose of this study.

Firstly, the user selected the required channels for the detection. The channels were selected according to the location of spindles in the literature. Then, a band-pass filter was applied. The band-pass filter was a Butterworth order 4 and used the frequency range specified by the user. In our study, the 10-16Hz the frequency range was considered. Secondly, a threshold was determined for each channel. The calculation of the threshold was made only on the data scored as stage N2. The threshold was an amplitude value corresponding to the "percentile" of the stage N2 data. For example, if the user chooses a percentile value at 95, the threshold was an amplitude value where 95% of the amplitude of stage N2 EEG data were inferior or equal to this value. Thirdly, the root mean square (RMS) was estimated from the filtered data. Root mean square (RMS) is defined as the square root of the mean square, the mathematical equation for a continuous signal is given by:

$$f_{\mathrm{rms}} = \sqrt{\frac{1}{T_2 - T_1}\int_{T_1}^{T_2} [f(t)]^2\, dt},$$

In the interval $T_1 \leq t \leq T_2$

To be more explicit, the mean square was estimated using a moving window of 5s duration and the RMS was the square root of this mean. Fourthly, the selected threshold value was applied to the RMS (Figure 24C). When the RMS was above this threshold, a spindle was detected.

I also implemented few modifications within FASST methods. These modifications were based on Schimicek paper, in order to take into account the alpha band and the muscle activity to discriminate these activities from the spindle. As spindles and alpha rhythm share a similar frequency range, taking into account the alpha band to accept spindle detection allows avoiding false detection. To do so, two additional conditions to accept the spindle were added in FASST software. From raw EEG data, we applied band-pass filters in the frequency range of the alpha band (8-12Hz), and in the frequency range of muscle activity 30-40Hz. Then, RMS was also calculated on these filtered data named RMS-alpha for the data filtered in the alpha band (Figure 24D), and RMS-muscle for the data filtered in muscle activity frequency (Figure 24E). When a spindle was detected on RMS, the ratio RMS-alpha / RMS had to be inferior or equal to 1.2 and the RMS-muscle had to be inferior to 5µV to be accepted as a spindle. Moreover, the duration of the spindle had to fit the criteria given by the user and spindles had to be separated by at least 1s.

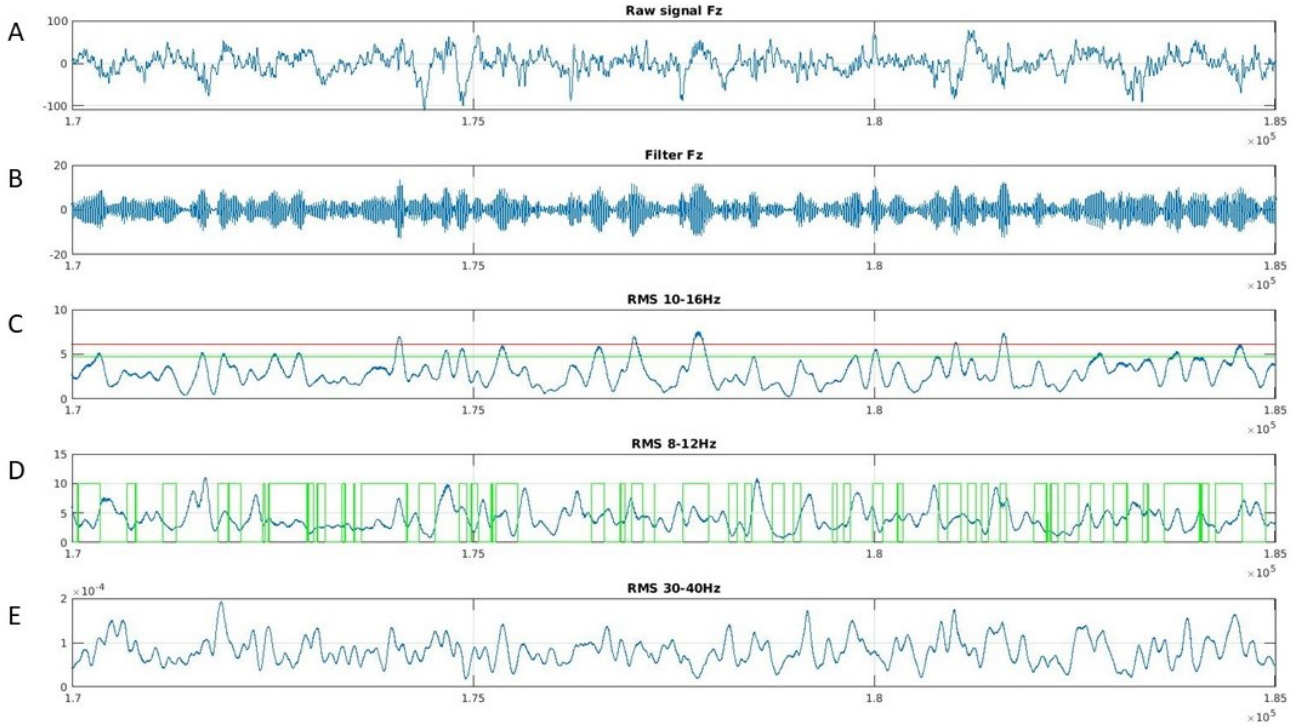

Figure 24: Description of Fasst method
(A) Raw signal of Fz, (B) Filtered signal in 10-16Hz of Fz, (C) RMS of B signal with the thresholds (95% in red, 90% in green), (D) RMS of filtered signal in alpha band with the ratio (green), (E) RMS of filtered signal in muscle activity band

This algorithm also allowed further classifying detected spindles in the two subtypes Slow and Fast spindles. The algorithm got the spindle frequency and classified it either as slow if the frequency is below 13Hz or as fast if the frequency is superior or equal to 13Hz.

Figure 24 describes the methodology of FASST, including my own modifications, for a signal window of 30s. On figure 24C, there are two thresholds, the red one is with a percentile at 95%, whereas the green one is with a percentile at 90%. We are reporting the two thresholds in order to illustrate the influence the tuning of this threshold could have on spindle detection. Indeed, lowering the threshold could lead to more false spindles detections. On figure 24D, when the green signal was set at a value 10, it meant that the ratio RMS-alpha / RMS was inferior to 1.2. On figure 24E, we can see that RMS-muscle was always inferior to 5µV, this was more likely the case because of the low pass filtering considered during EEG preprocessing, so it was not possible to detect a spindle with RMS-muscle > 5 µV in our case.

Mölle algorithm (Mölle et al. 2011):

We used a version of the Mölle algorithm (Mölle et al. 2011) implemented in the Wonambi toolbox developed by Jordan O'Byrne in the lab of Dr. Dang-Vu. Before detecting any spindles, the user had to evaluate the scoring of sleep stages of the data, then one could choose some parameters such as spindles frequency, spindles duration and the value used to estimate the threshold. The first step described by Mölle et al (Mölle et al. 2011) was to filter the EEG signal in order to differentiate the two subtypes of spindles. The goal was to find the peak frequency of fast versus slow spindles that were specific for each subject. The algorithm allowed specifying a spindle frequency range specifically for each subject in order to be more accurate. The peak frequency was determined using the power spectra of the raw data, then a band-pass filter was applied. For fast spindles, the frequency range of the band-pass filter depended on the chosen subject specific peak frequency ±1.5Hz around this peak. However, for slow spindles, due to the difficulty to find the peak frequency for each subject, a mean peak frequency was calculated on the remaining subjects (i.e. only considered subjects who demonstrated identifiable peaks) and a band-pass filter ±1.5H around this average peak was applied to all subjects. However, Jordan O'Byrne, the developer of Wonambi toolbox decided to not implement this approach. Instead of determining the peak frequency for each subtype, a zero-phase 4th order Butterworth filter in a frequency range chosen by the user was considered. In our case, the band-pass filter was set to 10-16Hz. The second step

was to calculate the RMS of the filtered data at each sample point, by using a moving window of 0.2s duration. Spindles were detected when the RMS signal was found above a threshold (Figure 25C). The threshold was set as the mean plus one standard deviation of the filtered signal multiplied by a fixed value of 1.5. This threshold is represented in red on the figure 25C.

In our case, the frequency range of the filtered signal was set to 10-16Hz and the spindle duration to 0.3-3s. So the RMS signal needed to be above the threshold for at least 0.3s and less than 3s to label a detection as a spindle detected. The main differences between this version of the algorithm and the one implemented in FASST was the method chosen to estimate the threshold as well as my additional modifications to take into account alpha band and muscle activity implemented in FASST. By investigating the performances of these two similar algorithms, we will be able to assess the relevance of my proposed modifications and to evaluate whether combining these two algorithms could be more efficient than using only one of those.

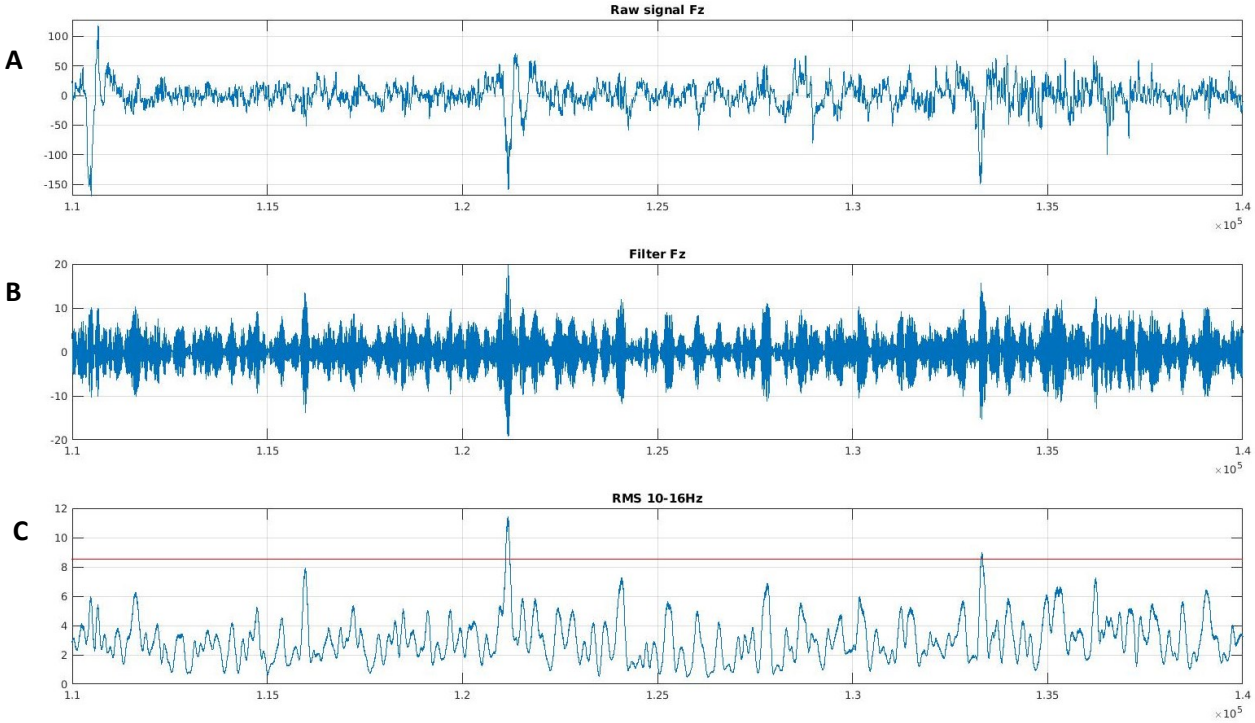

Figure 25: Mölle method
(A) Raw signal on Fz channel, (B) Filtered signal in 10-16Hz, (C) RMS of the filtered signal with the threshold in red

Nir algorithm (Nir et al. 2011):

Nir method has been developed in 2011 to optimize spindle detection (Nir et al. 2011). The algorithm considered here is the one implemented in Wonambi toolbox. Data were first converted to edf format. Before detecting any spindles, the user had to provide the scoring of the sleep stages of the data, then he could choose some parameters such as spindles frequency, spindles duration and the value of the threshold.

Here again, there were few differences between the method reported in Nir et al (2011) and the implementation of the method in Wonambi toolbox. In Nir et al (2001), the authors first selected the channels exhibiting better spindle activity in order to perform the detection on this one. In order to select this channel, the spectral power of EEG was calculated, and a 1/f model was fitted on the spectra of each channel. The spectral power and the 1/f model were compared. When the spectral power was larger than the frequency predicted by the 1/f model in the frequency range of spindle, this channel was selected. In Wonambi, the user had the opportunity to select himself the channels considered for the detection. The second step was to apply a band-pass filter between 10-16Hz to the raw EEG data. The filter used was a zero-phase 4^{th} order Butterworth within a frequency range chosen by the user. Instantaneous amplitude, which corresponds to the envelope of the signal within a specific frequency band, was calculated on the filtered signal via a Hilbert transform (Figure 26C). Two thresholds were then calculated, the largest one was used to detect the occurrence of a spindle, while a smaller one was considered to determine the beginning and the ending of the spindle (Figure 26E). The detection threshold was chosen as the mean amplitude of the envelope signal plus 3 standard deviations, whereas the start/end threshold was set as the mean envelope amplitude plus one standard deviation of the signal. Spindles were detected if the instantaneous amplitude was above the detection threshold and above the start/end threshold while respecting the spindle duration criterion of 0.3-3s.

Figure 26 illustrates Nir algorithm. In the Figure 26C, Hilbert transform was applied to the filtered signal. The resulting envelope is the red curve connecting the positive peaks of the signal. In Figure 26E, the two thresholds for spindle detection are represented. The grey one is the detection threshold. Since the envelope of the signal is crossing this red curve, a spindle is detected there.

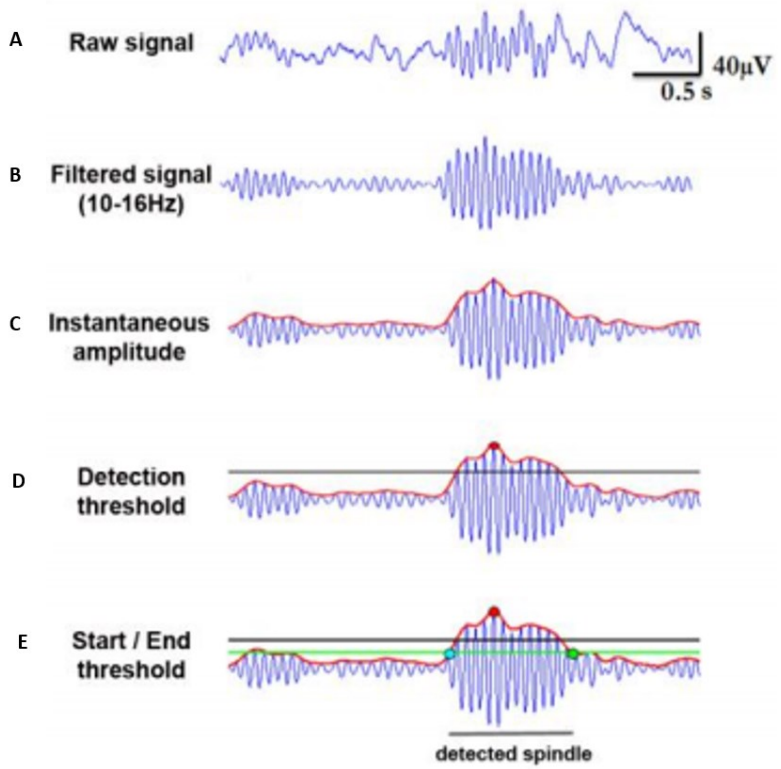

Figure 26: Nir method (Nir et al, 2011)

Finally, the green line corresponds to the start/end threshold: the cyan dot represents the beginning of the spindle whereas the green dot represents the end of the spindle. In my project, to be accepted as a spindle, these two dots had to be distant at least from 0.3s and a maximum 3s.

Wamsley algorithm (Wamsley et al. 2012):

The version of Wamsley algorithm used in our study is the one implemented by Warby (Wamsley et al. 2012), freely available in Matlab environment (https://www.nature.com/articles/nmeth.2855#supplementary-information). The format of the data was the same as the one used for FASST. Wamsley detection algorithm is based on a wavelet transform. The wavelet has been developed to overcome the default of Fourier transform. The wavelet allows giving a simultaneous representation in frequency and time of the signal. A wavelet transform means that the signal is convolved by a window including the wavelet. During the transformation, this window will change in time (translation) and in scale (1/frequency). As a result, for each scale and time, a wavelet coefficient summarizing the contribution to the signal for this specific time-scale box is estimated (Figure 28).

Wamsley algorithm uses a Morlet wavelet represented in figure 27. The equation of Morlet wavelet is the following: $\psi(t) = \frac{1}{\sqrt{\sigma}}\, e^{-\frac{1}{2}(\frac{t-a}{\sigma})^2} \cos(2\pi k t)$

With "a", the modulation parameter, "σ" the scaling parameter, and "k" the number of periods (i.e.$\sigma = \frac{k}{f}$).

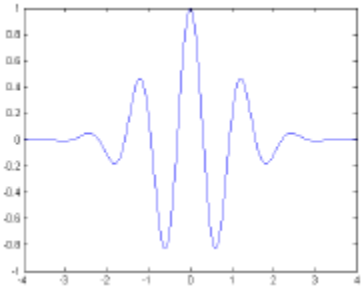

Figure 27: Real-valued Morlet wavelet (ESIEE Paris)

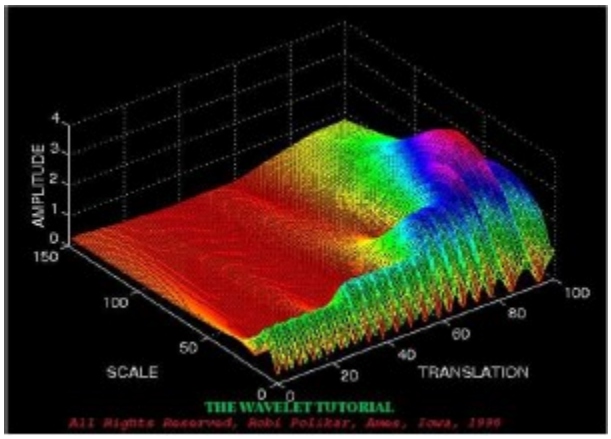

Figure 28: Wavelet transform (ESIEE Paris)
Present the signal in time-frequency domain after wavelet transform

In this algorithm, two wavelet transforms were considered. The first was to calculate the threshold for the detection and the second was to detect the spindle on the signal. The threshold is normally calculated on all N2 epochs of the signal, but in our case, only a small N2 epoch of a duration of 7-12min was considered. Choosing smaller epochs allowed us to ensure to select epochs that were free of artifact, movement or arousal, so an overall better quality and more stable signal. The continuous Morlet wavelet transformation was then applied to the signal N2 filtered within the band 0.5-30Hz, then the average of the wavelet coefficient in the scale corresponding to 10-16Hz was calculated with a sliding window of 100ms. This average was named the mean signal. The threshold was set the mean signal multiply by a fixed value. In the paper, the fixed value was set to 4.5. However, in our case, since our EEG data recorded in the MR scanner were noisier, we chose to tune this fixed value to 1.5.

The second wavelet transform was applied on all the filtered signal (N1, N2, and N3 epochs included). The wavelet was a Morlet wavelet (Figure 27) with 8-parameters complex. Afterward, the wavelet coefficients in the scale corresponding to 10-16Hz were extracted and smoothed by using a moving window of 100ms. Then, the threshold calculated in the first step was applied to the signal (Figure 29B). The threshold is presented in green on figure 29B. If the signal exceeded the threshold, a spindle was detected.

Normally, detected spindles should be kept only if their duration ranges were 0.3 to 3s. However, when applied to our data, we noticed that several spindles were actually split into two

spindles, with a duration of 0.2s each. Therefore, to overcome this problem, if the time delay between two detected spindles was inferior to 0.3s, they were merged. This slight modification of Wamsley method when applied to our data, allowed us detecting more spindles. Therefore, spindles detected had a frequency of 10-16Hz, a duration between 0.3-3s, and being distant of 1s minimum.

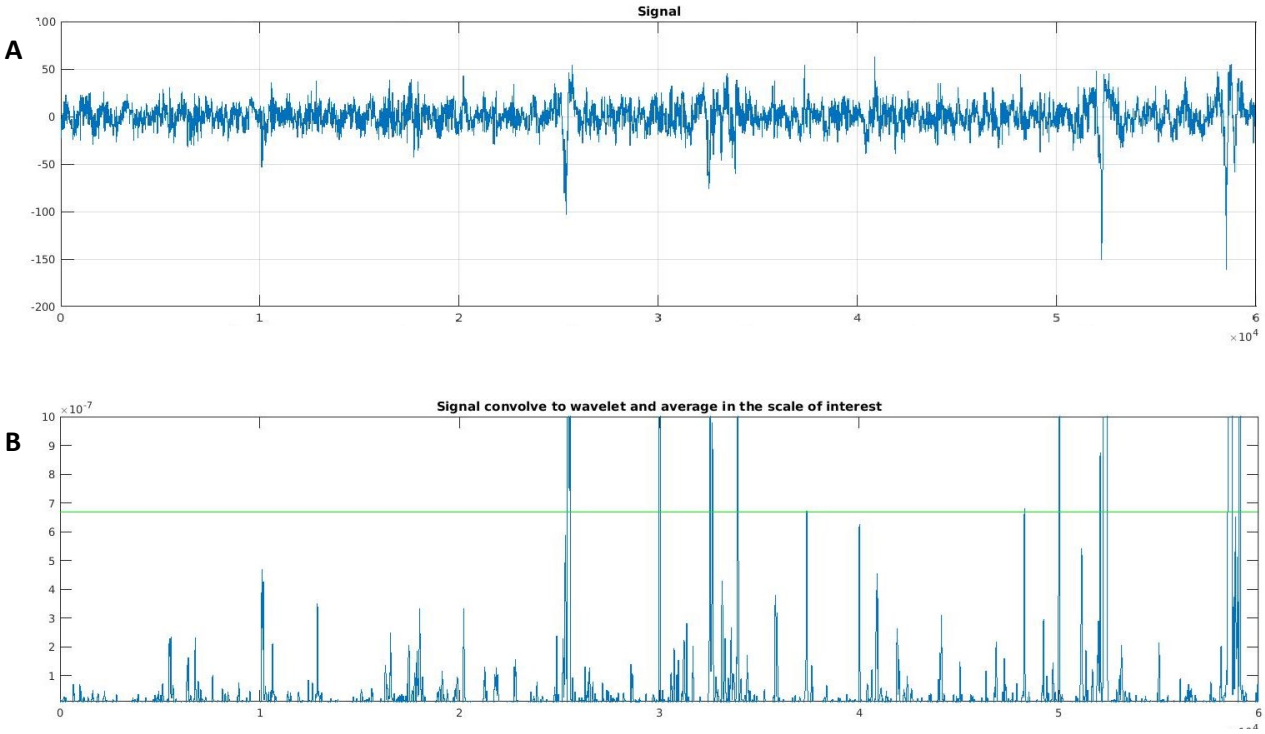

Figure 29: Wamsley method

(A) Raw signal on Fz channel, (B) wavelet coefficients (10-16Hz) after wavelet transformation of the signal with the threshold in green

4.1.2.3 - Statistical evaluation of automated detection methods

Once visual detection and automated detection were performed on 15 subjects by considering the N2 and N3 epochs, a statistical evaluation of the performance of each method was considered. The first step consisted in obtaining all the detection results in the same data format. To do so, a vector of zeros with the length of the signal was created for each method, therefore considering now the time in samples rather than in seconds. Since our sampling rate was 500Hz, every time sample was associated with a duration of 0.002s. Then, the spindle detection provided by each method (visual and automated detections) was converted into a binary vector, where a one indicated the occurrence of a spindle at that specific time sample. Figure 30 illustrates the spindle detection for each method: when values were set at one, a spindle was detected. In figure 30, the last binary vector refers to the consensus obtained by comparing all automated methods. This consensus vector was calculated by comparing the spindle detection between the four methods, and if a spindle was found at the same location by at least two methods, it was accepted as a spindle for the consensus. The second step was to assess the similarity of the detection between each method and the gold standard, which was actually the visual detection of the expert.

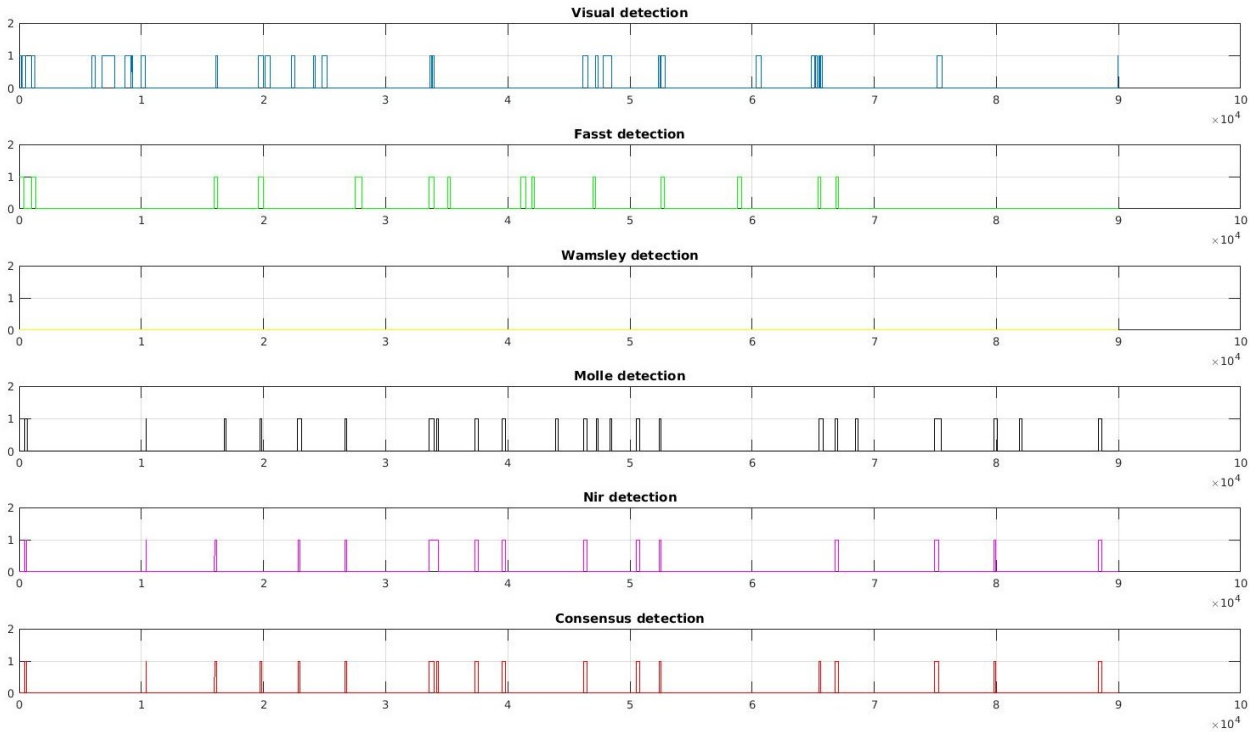

Figure 30: Transposing of the different detection in binary signal

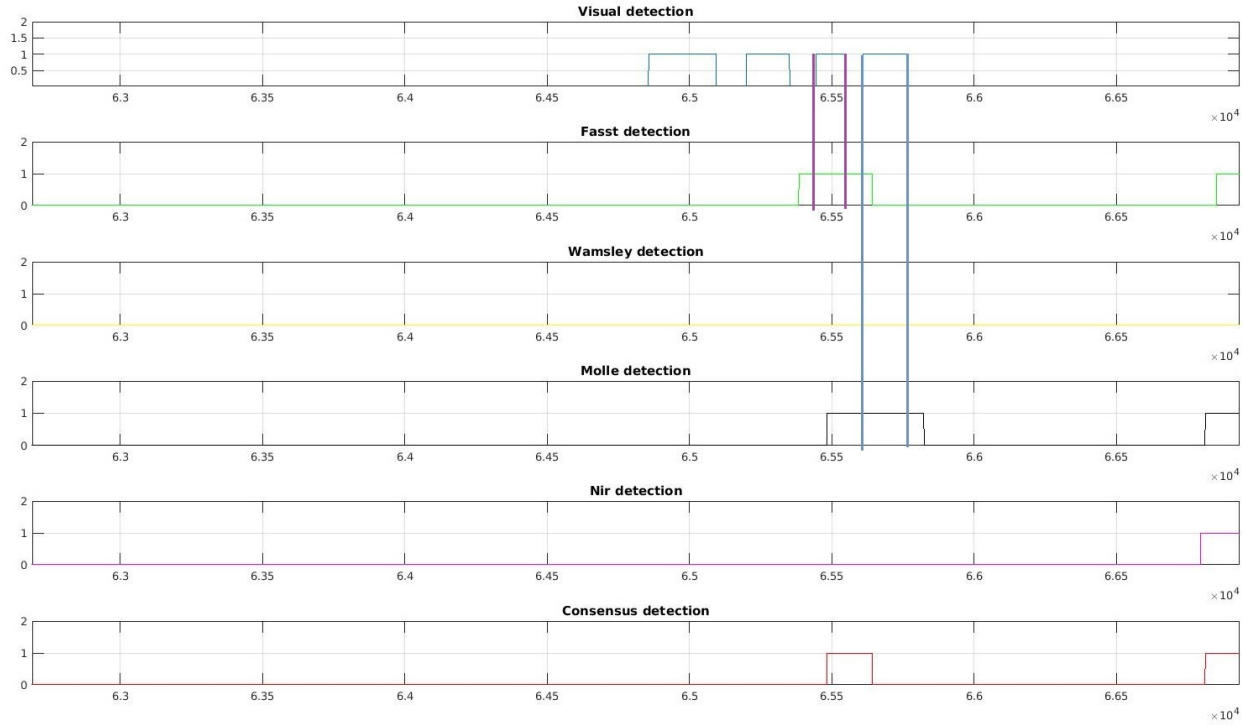

Figure 31: Similar events between the automated methods and the visual detection

Figure 31 is presenting a zoomed version of figure 30. Considering the two first lines, one can see a good correspondence between one spindle visually detected and the same one found by FASST.

The matching spindle is represented by the purple lines, whereas the blue lines represent a matching event between Mölle method and the gold standard. These matching events were therefore considered as true positive. The third step was to calculate the statistical metric evaluating the detection performances of every method. To do so, every detected event was first classified according to the following definitions:

- True Positive (TP): Match events between the automated method and the visual detection reference (Gold Standard)
- False Positive (FP): Events detected as spindle by the automated method but not by the visual detection reference
- True Negative (TN): Events which were not detected as spindle with both the automated method and the visual reference. Note that since our expert did not mark “negative events” where no spindles were present, while the whole signal was analyzed, it was impossible for this study to assess the rate of TN.

- False Negative (FN): Events that were not detected by the automated method but were detected as spindle by the visual detection reference

Table 1 summarizes the different classifications of the spindles by comparing the spindles detected using automated methods with the visual detection reference.

		Automated method detection	
		Spindle	**No Spindle**
Visual detection	**Spindle**	True Positive (TP)	False Negative (FN)
	No Spindle	False Positive (FP)	True Negative (TN)

Table 1: Summary of statistical parameters

To compare the performance of all detection method, the following summary statistics were estimated for each method: the sensitivity, the precision, the false detection rate (FDR), and the F1-score. The sensitivity measured the proportion of spindle correctly identified by the automated method. The precision measured the percentage of correct detection for the automated method. The FDR measured the proportion of false detection. F1-score consisted in computing the harmonic average between sensitivity and precision. The specificity assesses the proportion of negative events that are correctly identified. Note that it was not possible to estimate the specificity at the spindle detection level since the expert did not identify True Negative events. However, as suggested in Warby et al (Warby et al. 2014a), we had to calculate the statistic by sample to be able to estimate the specificity. Each sample of the signal was discriminated individually and was classified as a spindle, or not a spindle, which provided the number of true negative events. To clarify, by events, the spindle was considered as true positive if, on his duration, a spindle was also detected on visual detection. The start, the end, or the duration could be different. Nonetheless, only a number of spindles was given at the very end. However, by sample, each sample was compared and classified as TP, FP, FN, or TN. Therefore, the statistical comparison is more

accurate and strict. At the end, all the other statistical criteria were estimated either at the event level or at the sample level.

$$Sensitivity = \frac{TP}{TP + FN}$$

$$Precision = \frac{TP}{TP + FP}$$

$$FDR = \frac{FP}{FP + TP}$$

$$Specificity = \frac{TN}{TN + FP}$$

$$F1 - score = 2 \times \frac{Precision \times Sensitivity}{Precision + Sensitivity}$$

To conclude, the automated method exhibiting the best sensitivity and precision together with a lower FDR was considered as the best detection method and considered for fMRI data analysis.

4.2– Analysis of the hemodynamic BOLD response to sleep spindles

Once the spindle detection was completed according to the method exhibiting the best performance, detected spindles were correlated to the Blood Oxygen Level Dependent (BOLD) signal in order to identify the brain regions involved during the generation of the spindles. The software package used for fMRI analysis was Statistical Parametric Mapping (SPM12) (Penny et al. 2006). SPM12 is a Matlab toolbox developed by the "Trust Centre for Neuroimaging" in London, created and widely used for statistical analysis of brain neuroimaging data. In this section, I will present the fMRI analysis. The first sub-section is the preprocessing applied on the fMRI data to have the fMRI images in the same spatial domain. The second sub-section is the statistical analysis to find BOLD response areas.

4.2.1- fMRI preprocessing:

Before considering fMRI statistical analysis to localize brain regions involved in spindle generation, raw fMRI images must be carefully preprocessed to correct for movement artifacts and

to co-register all the data within the same spatial domain. This standard fMRI pre-processing pipeline is divided into the five following steps:

4.2.1.1. Slice timing correction:

Slice timing allows correcting for the time lag between the different MRI axial slices. In our case, acquiring one complete head volume took 2.5s for 41 slices. One slice was acquired every 6ms in descending mode (from the top to the bottom). Consequently, the last slice was acquired 2.44 seconds after the first one. The goal of this preprocessing was to realign all the slices to the same time frame, using interpolation techniques. In figure 32, the grey boxes represent the slices of a volume and the purple boxes show the interpolation made at the end of slice timing.

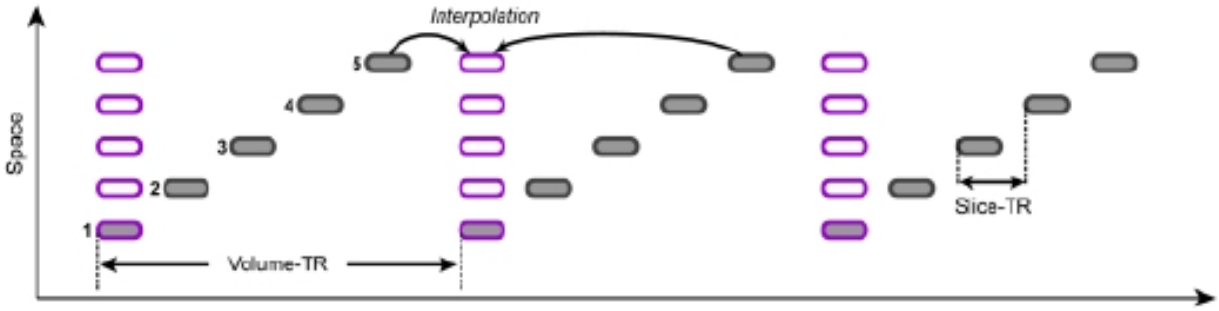

Figure 32: Slice Timing
Source: Dr. Habib Benali Concordia course

4.2.1.2. Spatial realignment:

Spatial realignment aims at correcting for the head movements occurring during the acquisition. A reference image was calculated as the mean of fMRI images of the run (duration varied between subjects because it was depending on their sleep duration), then each image (i.e. each volume) was realigned to this reference image by considering a rigid-body motion of the head (3 rotations, 3 translations). Rigid body transformation means that no deformation of the head was considered during this transformation. To do so, the correlation coefficient between every volume and the reference volume was maximized (K.J Friston et al. 1995).

In figure 33, the translation is represented on the axis x, y, and z whereas the rotation was referred to as pitch, roll, and yaw.

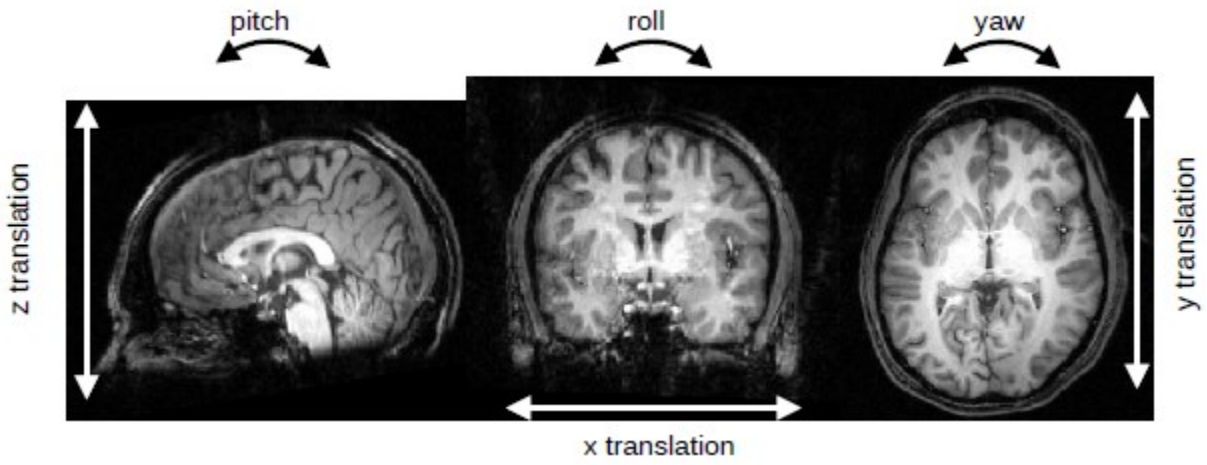

Figure 33: Rotation and translation of the images
Source: Dr. Habib Benali Concordia course

4.2.1.3. Registration with anatomical data:

It was important to carefully coregister anatomical high-resolution T1 data to functional MRI EPI data from the same subject, in order to provide an anatomical substrate for every analysis at the single subject level. To do so, a rigid body transformation model was considered, whereas the coregistration was obtained by maximizing Normalized Mutual Information between T1 data and the average reference EPI scan.

After this step, the voxel-to-voxel affine transformation matrix was stored in the header of the fMRI images. This matrix had the parameter s to transform the fMRI images in "final" orientation which orients the fMRI images in the same spatial domain as the anatomical images.

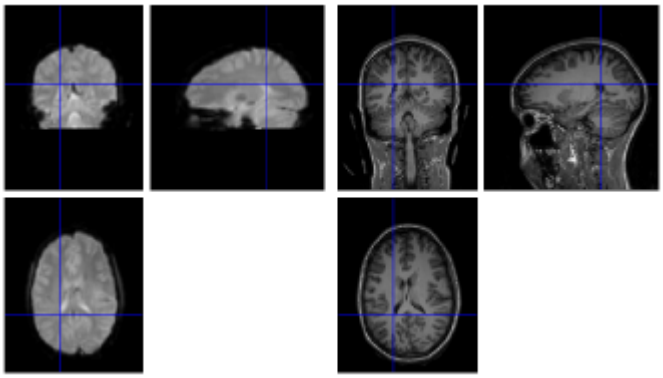

Figure 34: Coregistration of the fMRI image with the anatomical

4.2.1.4. Spatial Normalization:

EPI images were also co-registered to a template anatomical image considered as a common referential. The template referential image was created at the "Montreal Neurological Institute" and consists in the average of anatomical images from more than 150 subjects after non-linear coregistration (Collins et al. 1994). This spatial normalization step is essential to allow statistical group analysis (inter-subjects) because all images from the different subjects should be the same referential to allow such an analysis. The first step was to estimate a non-linear transformation to warp the anatomical images of each subject to the template (i.e. referential image). The second step was to apply this transformation to the fMRI images. At the end of this step, the anatomical image and the fMRI images were in the same spatial domain as the MNI template.

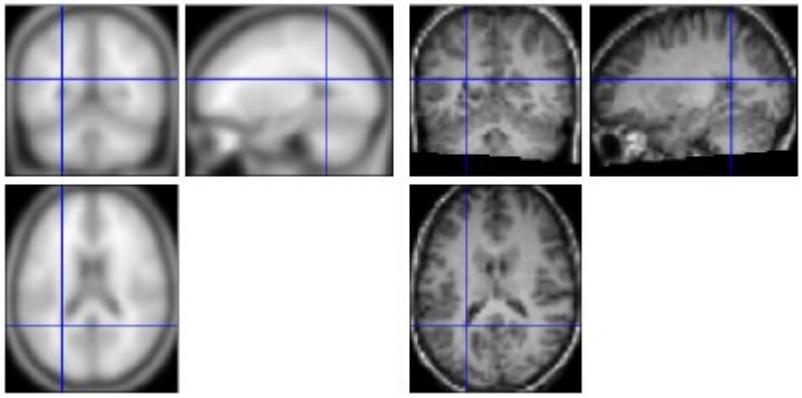

Figure 35: Anatomical image normalized to MNI template

4.2.1.5. Spatial Smoothing:

Spatial smoothing was applied to 3D fMRI data by applying a Gaussian kernel. Smoothing means that every voxel of the images was averaged with the ones in their close neighborhood. Spatial smoothing was needed to decrease the residual noise, ensuring more optimal between

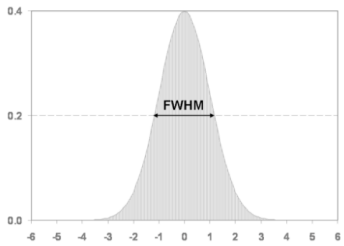

Figure 36: Gaussian filter
Source : Dr. Christophe Grova
Concordia course

subject spatial correspondences, and to fit with the hypothesis made by random field theory for statistical detection. Spatial smoothing was performed by applying a spatial Gaussian kernel filter of 8mm.

The size of the Gaussian kernel was defined by its Full Width at Half Maximum (FWHM) (Figure 36), i.e. it determined how many voxels were taken into account to apply smoothing. In our case, FWHM was equal to 8mm. Figure 37 shows a fMRI image after normalization on the left, and after spatial smoothing on the right.

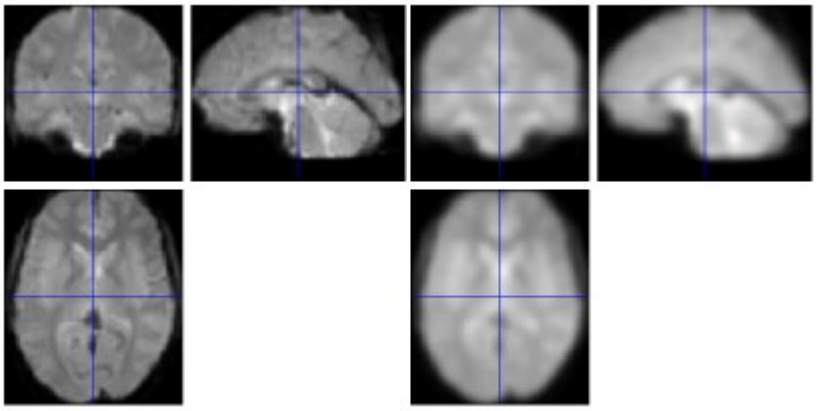

Figure 37: fMRI image smoothed

4.2.2 – First level statistical analysis

The first-level statistical analysis was subject-specific and allows estimating the hemodynamic brain response associated with the specific condition. This analysis is based on the "General Linear Model" (GLM) framework (K.J Friston et al. 1995). The GLM is applied to the signal of every voxel, therefore resulting in a massive univariate approach and is formalized as follows:

$$Y = X.b + \varepsilon$$

With Y: Time course of one voxel

X: Design Matrix

B: Estimated parameter

ε: Error

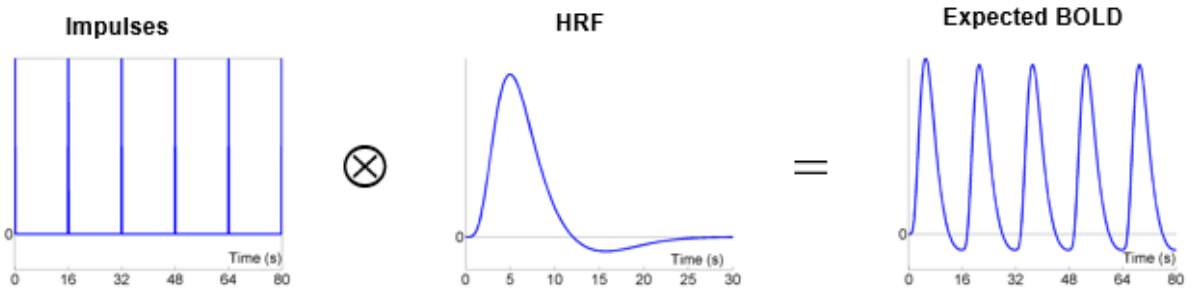

Figure 38: Convolution of events with Hemodynamic Response function to have the expected BOLD response
Source: Dr. Habib Benali Concordia course

The time course of the voxel corresponds to the BOLD signal during the fMRI acquisition. The design matrix is obtained by convolving the study paradigm with a model of expected Hemodynamic Response Function of the condition that we want to see activated (Lindquist et al. 2009). Since the BOLD signal associated to a particular brain activation is delayed and dispersed, the specific conditions of the paradigm should be convolved with the hemodynamic response function (HRF) to build the expected BOLD signal, the design matrix (Figure 38). Note that in our study, the protocol paradigm was either defined by the timing of the task (N-back, PVT, and ANT) or by the spontaneous occurrence of a spindle detected from scalp EEG.

Then, the BOLD signal measured at each voxel is compared to this expected BOLD signal, and a scale parameter b is estimated. The b value will then provide the intensity of the activation. If this parameter is evaluated as significantly different from zero within the GLM framework, this voxel will be denoted as activated. Finally, a statistical parametric map is obtained by deriving a statistical map of assessing the significance of the parameter b for all voxels. In my analysis, I did not only want to map neural activity but also the variation in time of onsets and shape of the HRF model associated with the generation of spindles. Therefore, instead of considering one HRF

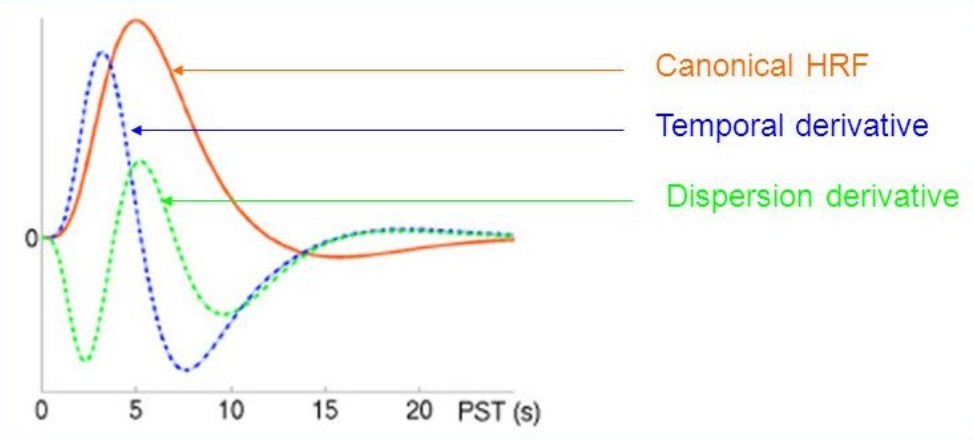

Figure 39: Canonical HRF and its derivatives
Source: SPM courses online

response model, we considered a linear combination of three responses: the canonical HRF, its temporal derivative and its dispersion derivative (Karl J. Friston et al. 1998). The temporal derivative captures the differences in latency of the peak response, whereas the dispersion derivative captures the difference in the duration of the peak. Having the effect of the canonical HRF response and its variations provided us a more complete description of the hemodynamic response associated to spindles.

To minimize the influence of some confounding factors on the GLM analysis, additional regressors were considered. Those additional regressors are included in the design matrix and their effect was modeled, but they were not convolved with the hemodynamic response. For example, the movements' parameter provided by the coregistration algorithm can be thus be added to take into account their effects, so while the effect of the HRF is estimated, this effect is not confounded with the movement effect. Three regressors were used in this study. The first regressor was the spectral power of the slow waves for each scan, the second regressor was the average of the R-peaks for each scan, and the last one was the motion parameters.

Afterward, Student t-tests, resulting in t-contrasts were generated to obtain a statistical parametric map of all brain activity in a specific condition (reporting the response to the task, to the occurrence of a spindle). t-contrast consist in Student t-test applied to each voxel to assess whether a significant increase or decrease of activity was found for the specific condition. The p-value, probability of making an error, must be provided to display the BOLD responses. According to this p-value, a threshold is calculated and compared to the t-value of each voxel. Next, the voxels are considered as showing a significant BOLD response or not. To compare different brain maps, the p-value has to be the same. This is challenging because one may have to increase the p-value so that the BOLD response can be observed (i.e. increased the chance to have false-positive voxels). In our study, in order to compensate for multiple comparisons, we first selected an uncorrected p-value of 0.001. However, due to unstable results obtained with this p-value (probably because of the small sample size of participants), we decided to use a p-value of 0.01 and the results should be interpreted accordingly. In our case, we wanted to generate the brain map associated with the generation of spindles, using either the visual spindle detection made by the expert or the best-automated spindle detection, and compared their characteristics.

Once the analysis has been performed on each subject, a group analysis is estimated (i.e. Second-level analysis).

4.2.3 - Second level statistical analysis

This second level of statistical analysis allowed comparing the first level analysis of every subject to infer statistics at the inter-subject group level. Group analysis was also considered within a general linear model framework. To do so, I considered a full factorial model which testes all main effects and interactions within a three ways ANOVAs. I created one factor with three levels. The first level consisted in the HRF response (t-contrast), the second level in its temporal derivative (t-contrast), and the third level in its dispersion derivative (t-contrast). The model tested, at the inter-subject group level, the effects of each HRF response for each voxel of the brain and provided the probability that each voxel was activated. Full factorial does not only study the effect of the main factors, but also the effects of the interaction between them. In our project, full factorial gave us the main effect of spindle occurrence, and the effect by taking into account spindles with unusual hemodynamic response. Afterward, F-contrast was generated by using an F-test to give the significant effects of HRF + derivatives for a specific condition.

4.2.4 – Contrasts

For my project, we wanted to see the brain activation for different conditions. Firstly, we wanted to assess brain activation when a spindle was generated, so all spindles (slow and fast) were taken into account. In this context, the effects of fast and slow spindle conditions were displayed. This contrast was denoted as “all spindles” analysis. Secondly, we wanted to localize brain activity for only Fast spindle, so only the Fast spindle condition was considered in building the design matrix for the second level analysis. This contrast was denoted as “Fast spindles”. Thirdly, we wanted to localize brain activity associated with only Slow spindles, so only the effect of Slow spindle condition was displayed. This contrast was denoted as “Slow spindles”. Lastly, we wanted to compare the brain activity elicited by Fast spindles versus Slow spindles. In that case, the effect size of fast spindles condition was “one” whereas the effect size of slow spindle condition was “-1”, therefore creating a contrast denoted “Fast-Slow spindles”. The different contrasts allowed to generate a brain mapping of the different spindles and assessed their roles by studying their location.

Chapter 5

Results

In this chapter, I will then present the first results obtained for the sleep deprivation project, involving EEG/fMRI acquisitions on 15 subjects. While other analyses are handled by collaborators on the project (fMRI task analysis (Pomares F. et al., Post-nap performance and brain activation recovery after total sleep deprivation. [abstract), OHBM 2018)) and fMRI functional connectivity), I will present results obtained in the context of my MSc project. The first section will then report our analysis on spindle detection and comparison between methods, while the second section will report the results of the BOLD hemodynamic responses measured in fMRI at the time of spontaneous spindles detected on scalp EEG. These results can still be considered as preliminary and will allow us to determine the future perspectives of the project.

5.1 – Comparison of spindle detection methods

The expert, Dr. Chifaou Abdallah, neurologist postdoctoral fellow in the lab of Dr. Grova, made a first detection on the channels Fz, Cz, F3, F4, C3, and C4. For this detection, the expert marked only the spindle exhibiting a very good Signal Noise Ratio (SNR), which means that only the most obvious spindles were detected. Indeed, this is the usual procedure considered in the case in EEG when the overall objective is to perform EEG source localization of transient discharges such as spindles or epileptic discharges (Abdallah et al. 2017). However, in the context of EEG/fMRI analysis, the strategy is different, since all discharges, even the ones that are more difficult to detect, should be considered, otherwise they will wrongly be considered as a baseline for subsequent fMRI analysis. For this reason, we asked the expert to perform a second detection, based on this new criteria, i.e. aiming at all the spindles that could be detected visually. This second marking was done on four channels F3, C3, F4, and C4. The general observation made when comparing the two set of events in visual detection, the second set displayed many more spindles and only overlapped 40% with the first set. This was probably due to the fact that the second analysis considered also less electrodes. Consequently, we decided to merge these two detections and to consider all spindles marked as our reference “gold standard” for automated methods comparisons.

The four automated methods, FASST, Mölle, Wamsley, and Nir, were performed using the six following channels Fz, Cz, F3, C3, F4, and C4. The density of detected spindles varied between subjects and methods. As you can notice in table 2, the two automated methods that found a maximum number of spindles were usually FASST and Mölle. Comparing detection provided by every automated method with the visual expert detection, performance statistics could be evaluated. Table 3 shows the number of True Positive spindles obtained for each method. The values reported in bold font correspond to the method providing the maximum of TP spindles for each subject. According to those results, we can conclude that FASST and Mölle were the methods exhibiting the best performance in term of TP.

To further confirm these trends, I estimated the sensitivity, precision, and the false detection rate (FDR) of each method by events and also the specificity, sensitivity, FDR and precision for each method by samples.

Subjects	*Time of sleep (min)*	*Gold standard*	*FASST*	*Wamsley*	*Mölle*	*Nir*
SDEP01	58	700	250	280	349	150
SDEP02	58	662	411	324	527	245
SDEP03	55	850	660	46	473	236
SDEP06	49.5	178	362	13	177	101
SDEP10	22.5	133	325	72	335	147
SDEP12	53	442	455	417	545	262
SDEP13	55	360	640	60	525	265
SDEP16	47.5	353	367	394	308	144
SDEP19	51	240	344	87	370	193
SDEP21	28	152	234	419	447	218
SDEP22	59	458	445	476	730	424
SDEP24	55	509	425	172	545	272
SDEP25	58.5	354	288	54	491	312
SDEP27	50	484	447	50	261	140
SDEP28	22.5	382	235	28	115	69

Table 2: Number of spindles by methods

Subjects	*FASST*	*Wamsley*	*Mölle*	*Nir*
SDEP01	**148**	81	117	58
SDEP02	178	115	**206**	130
SDEP03	**389**	19	210	141
SDEP06	**26**	2	4	3
SDEP10	43	9	**66**	51
SDEP12	168	**174**	167	108
SDEP13	101	15	**204**	123
SDEP16	**139**	124	94	68
SDEP19	**64**	12	63	45
SDEP21	35	**81**	64	39
SDEP22	134	134	**215**	144
SDEP24	122	33	**273**	163
SDEP25	**66**	8	27	16
SDEP27	**126**	0	69	39
SDEP28	**108**	3	44	23

Table 3: Number of True positive by methods

	By events				By sample				
	Sensitivity	**FDR**	**Precision**	**F1**	**Sensitivity**	**FDR**	**Precision**	**Specificity**	**F1**
FASST	**28.427**	69.269	30.731	**28.212**	16.192	**77.378**	**22.622**	94.177	**17.794**
Wamsley	14.425	78.500	21.500	16.278	5.845	91.251	8.749	**95.943**	6.362
Mölle	28.105	73.029	26.971	27.007	**17.822**	80.755	19.245	93.742	17.778
Nir	18.130	**66.453**	**33.547**	23.399	12.946	80.618	19.382	95.385	15.114

Table 4: Statistical values

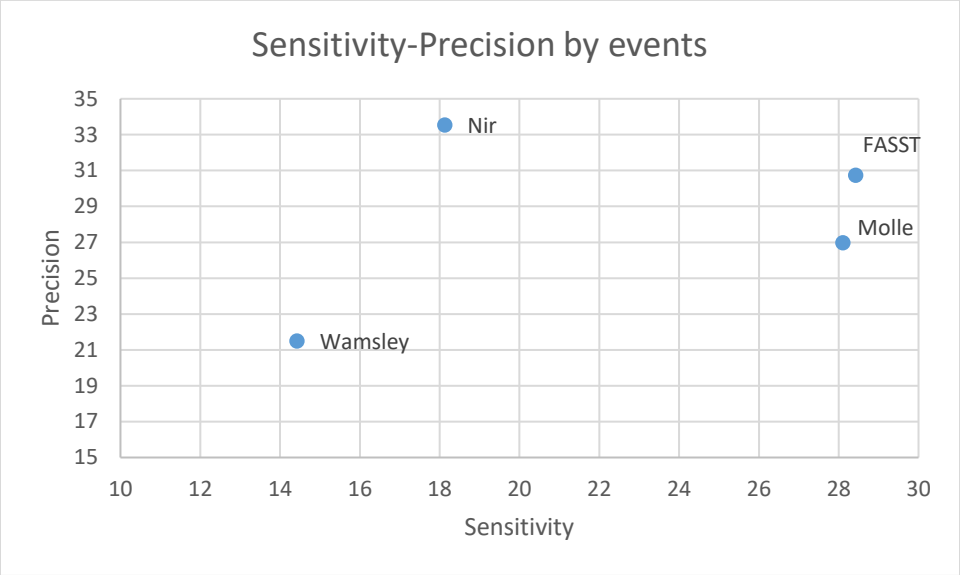

Figure 40: Sensitivity-Precision by events

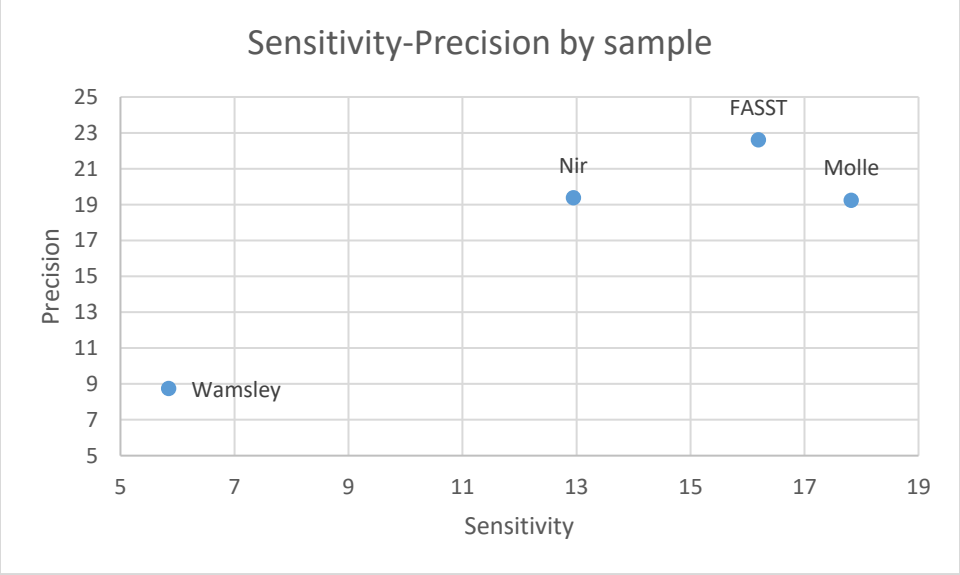

Figure 41: Sensitivity-Precision by sample

Overall FASST method provided the best sensitivity and precision and consequently the best F1-score in the analysis at the event level (Table 4). Mölle method was close to FASST in performance, but Wamsley and Nir were not efficient. The False Detection Rate (FDR) was lower for FASST than for Mölle, suggesting a better performance for FASST. However, the sensitivity and the precision changed when the calculation was made by sample due to the difference in spindles duration. The problem with the analyses by sample was that even when a spindle was labeled as TP, his duration might not exactly similar to the reference event detected, so it resulted in decreased sensitivity and precision of the methods. On the other hand, the estimation at the sample level was needed to provide an estimate of the specificity of the methods. Note that the specificity of the best methods was actually lower than the specificity of Wamsley and Nir because they detected more false positive (FP) events but it was still larger than 90%. Our results showed a low sensitivity and precision while FDR is high because a large number of spindles were detected by the automated methods and most of them were FP.

To conclude, the method we selected for the BOLD correlation was FASST because it was exhibiting the best sensitivity and precision and the lowest FDR.

5.2 – BOLD correlation of spindle detection

fMRI analysis of BOLD response associated with the generation of spindles was conducted using either the reference visual spindle detection made by the expert of the automated detection provided by FASST method. For the first level analysis, and for the two spindle detections methods, the paradigm model was built for each subject, by setting as “one” the conditions of the onsets of fast spindles and slow spindles, as well as their duration. The analysis was made taking into account the HRF response but also its temporal derivative and dispersion derivative. We estimated four different contrasts, i.e. the hemodynamic response to “all spindles”, “Fast spindles”, “Slow spindles” and “Fast-Slow spindles”. For the group level analysis, a full factorial analysis was performed using the canonical HRF contrast, the temporal derivative contrast, and the dispersion derivative contrast of each subject as dependent variable. As a result, our analysis provided the main effects of the canonical HRF (Figure 43) and the effect of the interaction between canonical HRF and its variation in time and dispersion (F-contrast) (Figure 44).

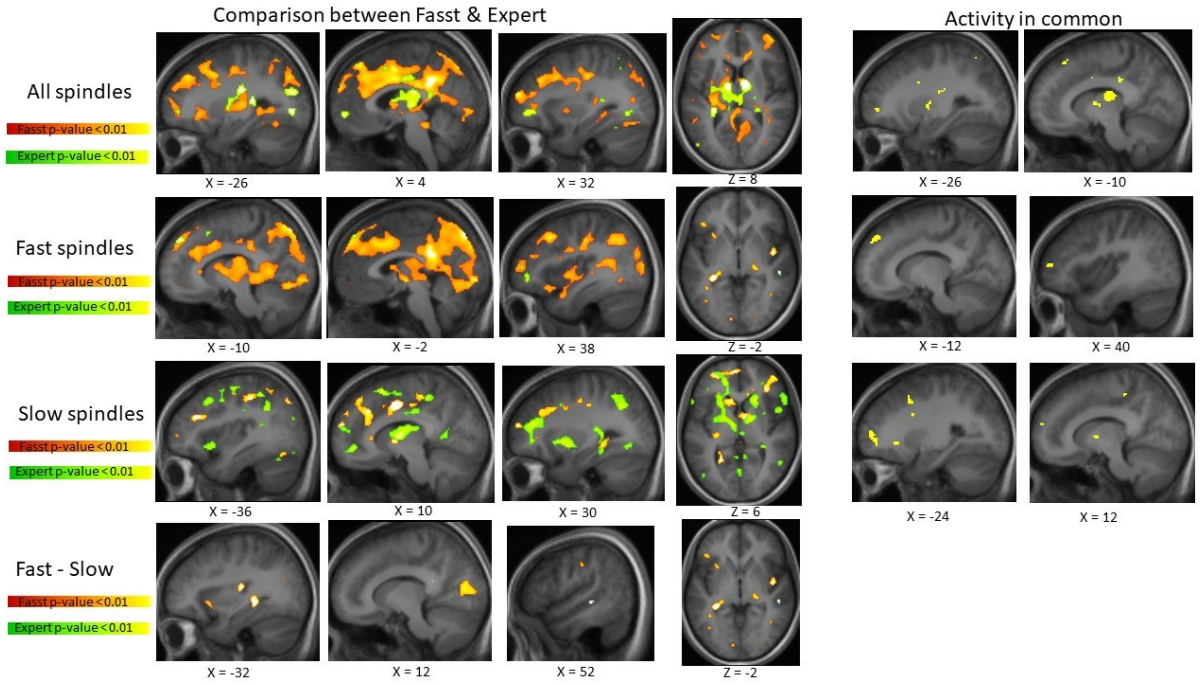

Figure 42: BOLD response of HRF

Figure 43 presents the BOLD responses when considering only the canonical HRF in the model, using spindles detected by the expert spindle in green versus the automated detection provided by FASST in orange. The p-value threshold was uncorrected and set at $p < 0.01$ for both detections. The hemodynamic responses to spindles were significant at an uncorrected threshold of p-value < 0.001 for the automated method (FASST) but not for the visual detection method. The right part of the figure presents the brain regions exhibiting a significant BOLD response for the two spindle detection approaches. The BOLD response of FASST detection is in orange while the BOLD response of visual detection is in green. As BOLD response of visual detection has been displayed in second, it is possible that the "green activity" overlap the "orange activity". The brain regions involved at the time of spindles found for the different contrasts are summarized in tables 5 and 6.

	Conjunction					Fast spindles					Slow spindles					Fast-Slow spindles				
	x	y	z	Z score	p-value	x	y	z	Z score	p-value	x	y	z	Z score	p-value	x	y	z	Z score	p-value
Precuneus	-4	-80	46	4.2	< 0.001	10	-66	42	3.47	< 0.001	-2	-78	48	3.43	< 0.001	-12	-70	48	2.95	0.002
Anterior Cingulate Cortex	2	-42	30	4.15	< 0.001	6	6	30	3.76	< 0.001	-2	30	16	3.36	< 0.001					
Superior Frontal Gyrus	16	56	28	3.85	< 0.001	18	58	28	4.04	< 0.001										
Mid-cingulate Cortex	14	-6	42	3.79	< 0.001	4	-42	32	4.56	< 0.001	0	-12	32	3.72	< 0.001					
Fusiform	-38	-68	-18	3.73	< 0.001	-38	-68	-20	3.91	< 0.001	-40	-68	-18	3.18	0.001					
						22	-42	-16	3.32	< 0.001										
Mid-frontal Gyrus	-42	22	40	3.13	0.001	-28	52	24	3.62	< 0.001	4	62	20	3.47	< 0.001					
Thalamus	-10	-20	18	3.09	0.001	24	-30	6	3.53	< 0.001	12	2	2	2.96	0.002	-10	-32	2	2.64	0.004
	-8	-8	-4	2.81	0.002	-6	-20	16	3.39	< 0.001										
Superior parietal lobe						-4	-78	50	3.95	< 0.001										
Inferior Frontal Gyrus											-24	26	-6	3.14	0.001	30	28	-12	3.25	0.001
ParaHippocampal											34	-38	-8	3.09	0.001					
Hippocampal																-30	-36	-2	3.29	< 0.001
PostCentral Gyrus																42	-22	42	3.1	0.001
Insula	34	2	-2	2.72	0.003	42	-6	-6	2.71	0.003	36	-16	-2	2.36	0.009	44	-6	0	3.04	0.001
Mid-Temporal Gyrus																-62	-8	-6	2.81	0.003
Cerebellum																-10	-72	-12	2.71	0.003

Table 5: Activated areas for HRF, Fasst method

	Conjunction					Fast spindles					Slow spindles					Fast-Slow spindles				
	x	y	z	Z score	p-value	x	y	z	Z score	p-value	x	y	z	Z score	p-value	x	y	z	Z score	p-value
Superior Frontal Gyrus	-20	12	46	3.3	< 0.001	16	46	40	3	0.001	8	14	58	3.77	< 0.001					
Mid-cingulate Cortex	8	-12	30	3.05	0.001															
Anterior Cingulate Cortex											4	24	24	2.62	0.004					
Fusiform	-38	-48	-14	2.76	0.003															
Mid-frontal Gyrus	32	46	-2	2.76	0.003	52	36	22	3.98	< 0.001										
Thalamus	10	-4	8	3.52	< 0.001						-8	-14	14	3.86	< 0.001					
Inferior Frontal Gyrus						-56	6	38	2.87	0.002	-60	20	6	2.91	0.002					
ParaHippocampal						-26	-28	-18	2.46	0.007	26	-36	-12	2.9	0.002					
PostCentral Gyrus											-48	-32	48	3.63	< 0.001					
Mid-Temporal Gyrus	50	-58	2	2.85	0.002															
Cerebellum						-18	-54	-32	2.62	0.004						84	-58	28	2.47	0.007
Superior Temporal Gyrus																52	-28	-2	2.51	0.006
Insula											48	8	2	2.88	0.002					

Table 6: Activated areas for HRF, Visual method

The fMRI responses to spindles obtained by the two spindle detection methods exhibiting some activated brain regions in the different contrast except for the "fast-slow spindle" contrast. For the generation of all spindles, both approaches identified the postcentral gyrus, the thalamus, the post cingulate cortex, the mid-frontal gyrus, and the superior temporal gyrus. During the generation of fast spindles, both approaches identified the medial frontal gyrus and the superior temporal gyrus. For the generation of slow spindles, the postcentral gyrus, cingulate cortex, as well as the cerebellum and parahippocampal, were found by both approaches.

Considering the BOLD response when taking into account the canonical HRF model with its variation in time and dispersion was then considered to allow for more flexibility in the expected BOLD response to spindles.

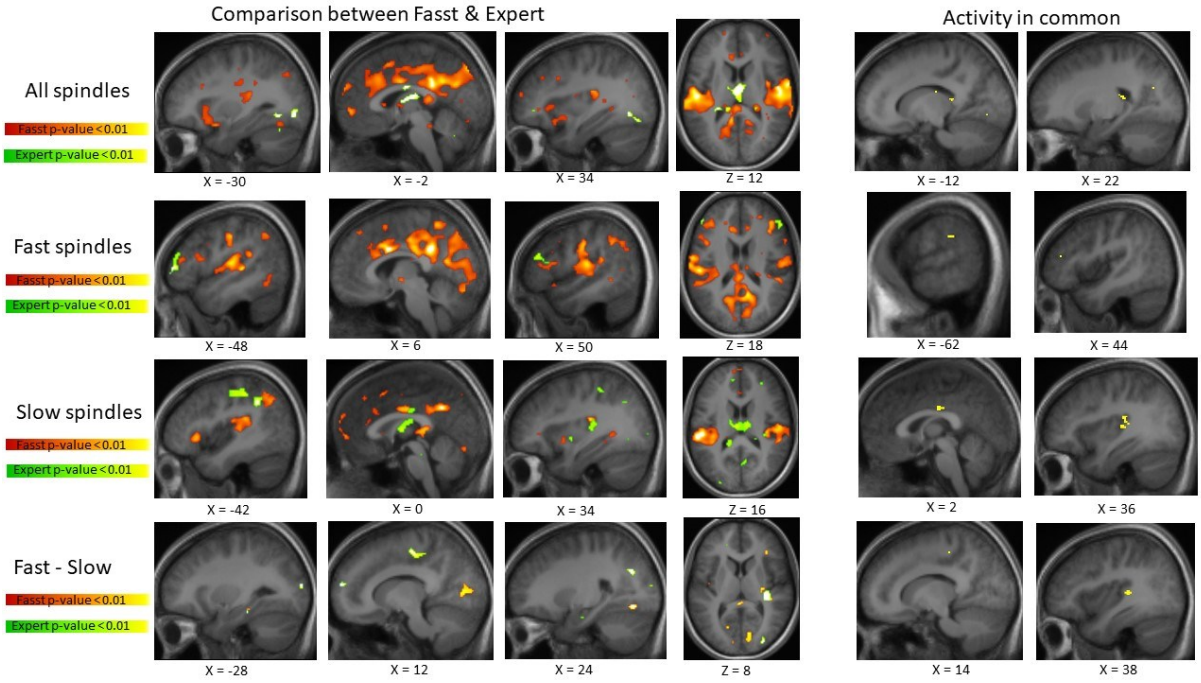

Figure 43: BOLD response of HRF and his variation

Figure 44 is presenting those results, using the same layout as figure 43 when considering the canonical HRF only (uncorrected threshold at $p<0.01$). The different brain regions exhibiting a significant BOLD response to this more flexible model are reported tables 7 and 8.

	Conjunction					Fast spindles					Slow spindles					Fast-Slow spindles				
	x	y	z	Z score	p-value	x	y	z	Z score	p-value	x	y	z	Z score	p-value	x	y	z	Z score	p-value
Precuneus	-8	-52	8	3.86	< 0.001	10	-68	42	3.18	0.001	-2	-52	34	4.27	< 0.001	-12	-70	46	2.74	0.003
Anterior Cingulate Cortex	-14	32	22	3.5	< 0.001	4	18	24	3.03	0.001	-10	30	24	3.22	0.001					
Superior Frontal Gyrus																-8	54	36	2.76	0.003
Mid-cingulate Cortex	12	-20	42	4.12	< 0.001	10	-20	40	4.31	< 0.001	-2	-12	32	3.45	< 0.001					
						6	6	30	4.05	< 0.001										
Fusiform	-38	-68	-18	3.39	< 0.001	-38	-68	-20	3.81	< 0.001						24	-70	-10	2.94	0.002
Mid-Frontal Gyrus	-8	54	-2	3.87	< 0.001	38	38	14	3.57	< 0.001	-8	56	0	3.25	0.001					
Inferior Frontal Gyrus																28	30	-12	2.83	0.002
PostCentral Gyrus	-52	-24	-18	4.42	< 0.001	-52	-18	40	3.54	< 0.001	-58	-28	10	4.27	< 0.001	50	-20	40	2.81	0.002
Insula	52	-6	8	4.08	< 0.001	-30	18	-14	2.88	0.002	-30	14	-8	3.12	0.001	44	-6	0	2.37	0.009
Superior Temporal Gyrus	54	-22	2	4.24	< 0.001	-50	-18	10	3.62	< 0.001	56	-22	8	4.29	< 0.001	36	-30	8	3.15	0.001
Hippocampal	24	-34	12	2.86	0.002											-28	-32	-14	2.43	0.008
Thalamus	-18	-22	22	2.77	0.003	-6	-20	18	2.70	0.003	6	-6	4	2.51	0.006	-16	-22	22	3.02	0.001

Table 7: Activated areas for HRF+variations, Fasst method

	Conjunction					Fast spindles					Slow spindles					Fast-Slow spindles				
	x	y	z	Z score	p-value	x	y	z	Z score	p-value	x	y	z	Z score	p-value	x	y	z	Z score	p-value
Precuneus																				
Anterior Cingulate Cortex																				
Superior Frontal Gyrus	-2	10	46	3.19	0.001															
Mid-cingulate Cortex											0	-20	30	2.53	0.006					
Mid-frontal Gyrus	30	46	-4	2.62	0.004	52	36	22	3.52	< 0.001						-10	16	42	3.02	0.001
Thalamus	4	-6	10	3.26	0.001						-6	-16	16	3.15	0.001					
Inferior Frontal Gyrus						-48	44	6	3.72	< 0.001	58	20	0	2.94	0.002					
ParaHippocampal																-26	-28	-18	3.11	0.001
Hippocampal	22	-30	18	2.67	0.004															
PostCentral Gyrus	-48	-28	42	2.9	0.002						-46	-30	50	3.61	< 0.001	-40	-20	48	2.85	0.002
Insula											32	-28	12	2.97	0.001	34	-28	8	3.26	0.001
Mid-Temporal Gyrus											6	-64	-38	2.63	0.004	-58	-58	0	2.9	0.002
Cerebellum						30	-56	-30	2.92	0.002										
Superior Temporal Gyrus											32	-28	12	2.97	0.001	46	14	-28	2.82	0.002

Table 8: Activated areas for HRF+variations, Visual method

The brain response exhibiting a significant BOLD response when considering both spindle detection methods were actually different than the regions found when considering only the canonical HRF in the model. During the generation of all spindles, the common areas were hippocampal, thalamus, and the lingual gyrus. However, for fast spindle generation, the areas were mid-frontal gyrus and inferior parietal lobe. The common areas during slow spindles generation were thalamus, superior temporal lobe, insula, postcentral gyrus, and the cerebellum. This time, the generation of the contrast "fast-slow spindles" showed significant brain responses found by both approaches, in superior temporal gyrus and the frontal lobe.

To conclude, the results were preliminary but it gave us an idea of the limits of the spindle detection methods, and what areas are involved in spindles generation.

Chapter 6

Discussion

6.1 – Performance of the spindle detection methods

6.1.1. Visual detection

Having two different visual detections made by the same expert demonstrated that visual detection on these data is not trivial, especially when dealing with noisy EEG data recorded inside an MRI scanner. The non-reproducibility of some events during the second detection can be explained by the fact that the overall marking strategy (marking discharges with largest SNR versus marking all discharges) and that different channels were considered for both markings. Reviewing the marking with the expert, it seemed that some of the most obvious spindles were actually more visible in Fz and Cz electrodes, and were not distributed in the others channels. However, another explanation to consider is that visual detection has its limitations, especially when considering poor quality EEG data. Neurologists are not used to read this type of EEG data (i.e. artefacted because being acquired in the scanner) and the marking can be influenced by the presence of residual artifacts. To overcome this issue, the expert should be trained to read this type of EEG data before performing the visual detection.

To address this issue, one of our future goals will be obtained visual marking from several raters, involving notably a neurologist who has more experience in reading EEG data acquired in the MRI scanner. In search of improvement, as suggested by Warby et al in their study (Warby et al. 2014b), a consensus between the different visual detection should be taken as described in figure 6 (chapter 2.2.2) (Warby et al. 2014a). Combining visual markers from several experts, our reference visual detection could be considered as a more accurate and reliable Gold Standard.

6.1.2. Automated spindle detection methods

Our preliminary results demonstrated overall poor performances of the different methods. In our case, FASST and Mölle were considered as the best methods but it is important to note that the sensitivity and the precision were lower than 50%, therefore suggesting the weakness of these methods. In Warby et al. 2014, six automated spindle detection methods were compared to visual detection. The detections were made on normal EEG that can be qualified as good quality data.

Two of their automated methods were actually similar to the methods we evaluated in our study: Wamsley and Mölle. In their case, the best method was Wamsley, exhibiting a sensitivity of 52% and a precision of 51%, which could still be considered as relatively low-performance scores. Moreover, the main discrepancy between our two studies was found for Wamsley method, since according to our study Wamsley was poorly performing, exhibiting the worst evaluation scores. These differences can be explained by the quality of the EEG data in both studies. Indeed, Wamsley method seems not to be efficient when dealing with noisy data. On the other hand Warby et al (Warby et al. 2014b) reported for Mölle method a sensitivity of 83% but with a precision of only 12%, suggesting that Mölle method was really good to detect similar spindles than the gold standard, but it detected too many spindles resulting in a large false detection rate. In our study, Mölle was found more precise (26.971%) and less sensitive (28.105 %). Therefore we concluded that Mölle method seemed to be more robust to handle more noisy data. To confirm the hypothesis, we further reanalyzed our results in regards of the overall quality of our EEG data acquired in the MRI scanner. To do so, we compared the sensitivity and precision of the methods by taking into account whether an ICA had to be considered during data preprocessing. In some case, an ICA was performed to remove all the residual artifacts and to increase overall signal quality. However, some EEG data still presented some noise after the normal preprocessing, but we decided not to proceed with an additional ICA preprocessing, in order to make sure we would not distort some components of interest of the signal by removing too much information. ICA is indeed a "black box" data-driven approach and it is not trivial to evaluate whether we are removing only noisy components or possible physiological components of interest.

	ICA (# of subjects = 7)		**No ICA (# of subjects = 8)**	
	Sensitivity	**Precision**	**Sensitivity**	**Precision**
Fasst	**31.969**	**40.681**	25.947	23.766
Wamsley	17.020	30.854	12.609	14.952
Mölle	26.568	30.001	**29.181**	24.849
Nir	17.491	40.422	18.578	**28.735**

Table 9: Sensitivity and precision classified by ICA or not

Table 9 summarizes the performance of the automated methods by classifying subject data whether ICA was used or not. FASST and Wamsley methods actually exhibited even better performances when an ICA was applied during the preprocessing of the data. However, since this effect involved only a small number of subjects (# of subject with ICA = 7 out of 15 subjects), no statistical

significance was found. This issue is actually complex. Indeed, applying ICA to our data does not mean that the data end up with a better quality. Indeed, for other subjects, EEG data quality was qualified as better for data not preprocessed with ICA. So, the most important aspect was to classify our EEG data after preprocessing as overall good or poor quality. However, data quality is a subjective factor and different expert might not qualify the quality of the date in the same way. Therefore, the performance of the methods for the different subjects should be investigated according to the quality of the data. However, the same metric should be considered to assess the signal quality of all subjects in the same way and the quality signal should be assessed by two experts.

Because of the large changes in performance between Wamsley method when applied to normal EEG data (Warby et al. 2014b) and on our noisy EEG data, we assume that the parameters of the method, and in particular the choice of the thresholds, were not optimal for EEG data acquired inside the scanner. One of our future perspectives will indeed be to investigate whether we can infer most the optimal parameters and thresholds for all four detection methods, using cross-validation and ROC-based analyses. Meanwhile the improvement of the automated methods for these type of EEG data, two methods can be used to improve the preliminary results of the spindle detection.

A first approach to improve the performances of automated detection would be to consider the consensus between different detection methods, as proposed by Warby et al (Warby et al. 2014b). The goal would be to use the four automated detections together and accept the spindle by comparing them to a threshold. For example, a spindle could be accepted if at least two methods have detected it at the same location. I created such a consensus (i.e. threshold = spindle accepted if detected by at least 2 methods) and the results were not significantly better than when considering FASST method only. By knowing the performance of the different methods, I allocated a weight to each detection. As Fasst and Mölle were providing the best performances, their spindle detections were automatically accepted (weight at one), whereas the detection of Nir and Wamsley were accepted if their detection was similar to another one (weight at 0.5). With this consensus, the sensitivity increased to 47.2%, the precision to 29%, for an FDR reduced at 70%. This combination provided a better sensitivity than the best method FASST and a similar precision and FDR, so the detection was overall more accurate. However, to calculate such a consensus detection, we would need to know the performance of the methods, i.e. the consensus should be calculated on other

datasets that were not considered to compute the weights, otherwise, this consensus detection would be biased. The conclusion of this evaluation was that by combining the best two methods (FASST and Mölle), one could improve the quality of spindle detection.

The second approach one should consider to improve the performance of these automatic detections is to consider a post review of the detection with an expert. An expert would carefully review the automated detection and decide to accept or reject every event. Such a semi-automatic approach is quite more robust and was considered in Schabus et al. 2007, ensuring an accurate spindle detection and therefore a more reliable BOLD response to those events. In our case, the expert carefully reviewed the spindles detected by the best two methods (i.e. FASST and Mölle) on two subjects.

	Pre-Review		Post-Review	
	Fasst	**Mölle**	**Fasst**	**Mölle**
SDEP01	250	349	214	184
SDEP02	411	527	345	357

Table 10: Post-review performance on two subjects

Table 10 shows the number of spindles accepted for each method after post-review by the expert. For FASST, 85% of the spindles were accepted which means the detection was pretty accurate and only 15% of the spindles detected were considered as false positives. For Mölle, 60% of the spindles were accepted, which indicates that even if we increase the sensitivity of the methods, Mölle will detect too much of FP spindles. Mölle was not accurate enough, due to its large amount of FP spindles detected. Therefore, one should not consider this method to evaluate the BOLD response to spindles, because of the very large false positive. This behavior of Mölle method was also suggested in the study of Warby et al. since the sensitivity was good (83%) but the FDR was quite large (90%). So to classify spindle detection methods as good and accurate, the sensitivity has to be high but with a low FDR. The post-review method seems to be the best compromise between the visual and automated detection as both methods have their limitations. The post-review method could still present some false negative events, but at least it allows considering only detected true spindles, therefore limiting the number of false positives.

To conclude, whatever was the spindle detection method we considered, spindle detection on noisy EEG data acquired in the scanner was not really accurate. However, we believe that the performance of some of these methods can be significantly improved by investigating what could

the optimal detection parameters (cross-validation and ROC study) and by adding a post-review. As the overall purpose of spindle detection in our context is to prepare the analysis of the associate BOLD response it is really important to ensure optimizing the detection methods in order to provide a large number of true positive events and low false positive events, since those performances will have a direct impact on the power of the statistical analysis of the BOLD response.

6.1.3. BOLD response to detected spindles

BOLD responses to detected spindles obtained for our study will be carefully reviewed in comparison with the results published by Schabus et al., 2007. We will first compare the BOLD response that we obtained when considering the expert visual detection or FASST automated spindle detection.

The brain regions exhibiting a BOLD response at the time of detected spindles were overall similar when considering the canonical HRF only in the model or when considering the canonical HRF + its variations, although statistical values were larger when considering the most complete model (HRF + variations). In some case, brain areas were found when considering the canonical HRF but not with its variations, which can be explained by the fact that these locations were not significant by taking the variations into account. For discussion purposes, I will consider significant BOLD response found when considering the canonical HRF + Variation, as the most complete model. Results obtained when considering the expert visual detection and the automated detections were first compared. Overall, BOLD responses were more significant when considering the automated detection than when considering the expert detection with an uncorrected p-value < 0.001. Actually, I had to increase the p-value threshold for in expert visual detection in order to obtain some significant BOLD responses. It can be explained by the fact that automated detection detected spindles with exactly the same criteria so more likely associated to the same generators in the brain, whereas events marked by the expert could be more variable. However, expert detected different spindles with different criteria and generated by different location, so it is possible that not enough spindles generated from the same location were taken into account to provide a significant BOLD response. However, the positive finding was that overall similar brain regions have been found when considering both detections methods, as summarized in table 11. One can conclude that the brain regions reported in Table 11 are more likely involved in spindles generation during a recovery nap following sleep deprivation.

Spindle contrasts	Activated areas
All spindles	Hippocampal Thalamus Lingual Gyrus
Fast spindles	Mid-Frontal Gyrus Inferior Parietal Lobe
Slow spindles	Thalamus Superior Temporal Gyrus Insula Postcentral Gyrus Mid-Cingulate Gyrus Cerebellum
Fast-Slow spindles	Superior Temporal Gyrus Frontal Lobe

Table 11: Brain areas for both methods

By comparing our results with the ones reported in Schabus et al, 2007, we found that similar areas were activated during spindles generation. To determine if the activation was similar, I compared the XYZ coordinates in the MNI template provided in their study with the results obtained on my study. When we found a significant BOLD response located within a sphere of 10 mm around the location reported in Schabus et al (Manuel Schabus et al. 2007), this brain region

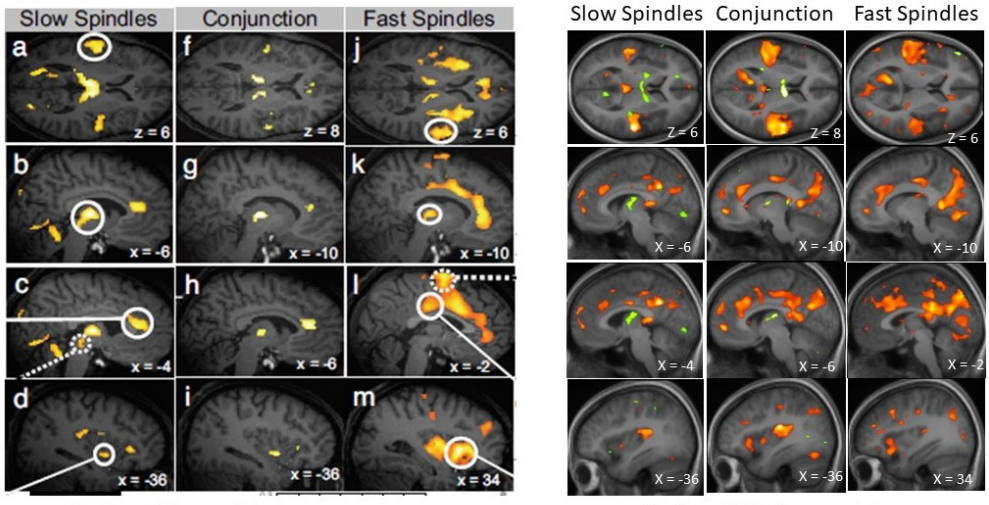

Brain activity on Schabus paper

Brain activity for our data

Figure 44: Comparison of brain activity with Schabus paper

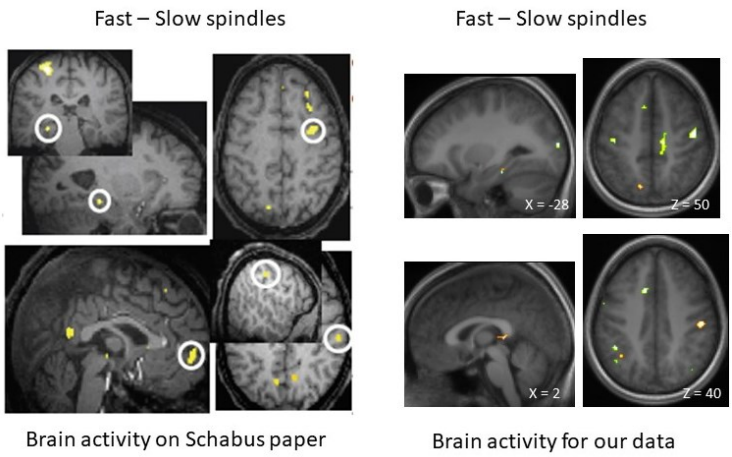

Figure 466: Comparison of the brain activity with Schabus et al (Manuel Schabus et al. 2007)

was considered as being reported by the two studies The results of this comparison are summarized in table 12.

Figure 45 and 46 are comparing brain regions showing a significant BOLD response to spindles reported in our study and from Schabus et al (Manuel Schabus et al. 2007). In figure 45, which represents the activation maps obtained for fast spindles, slow spindles, and the conjunction, similar brain regions were found by both studies. Results were less in agreement when comparing the brain regions involved when considering the Fast-Slow spindles contrast, as illustrated in Figure 46.

Table 12 reports that brain regions identified when using the automated method were more similar to the results reported in Schabus et al (Manuel Schabus et al. 2007) than when considering the expert visual detection method. This finding is coherent because the spindle detection in Schabus et al (Manuel Schabus et al. 2007) was done using the same automated detection method FASST, considered in our study. Finding similar brain regions involved in the two studies is encouraging and reports some reproducibility. Moreover, it is important to keep in mind few important difference. A post-review of detected spindle was performed after FASST in the study reported by Schabus et al (Manuel Schabus et al. 2007). Finally, their study is reporting brain regions involved in spindle generation during a normal night, whereas we might expect the involvement of different brain regions when considering spindles generation after a sleep deprivation night.

Contrasts	Automated (Fasst)	Visual (Expert)
All spindles	Anterior Cingulate Cortex Superior Temporal Gyrus	Thalamus
Fast spindles	Insula (Left and Posterior) Middle Frontal Gyrus Postcentral Gyrus Anterior Cingulate Cortex Mid-Cingulate Cortex Superior Temporal Gyrus Thalamus	
Slow spindles	Midbrain tegmentum Thalamus Anterior Cingulate Cortex Posterior Insula Superior Temporal Gyrus	Thalamus Hypothalamus/Basal forebrain
Fast-Slow spindles	Orbito-Frontal Cortex Postcentral Gyrus Hippocampus	Middle Frontal Gyrus Precentral Sulcus Hippocampus

Table 12: Comparison of brain activity with Schabus paper

To conclude, the BOLD responses of the spindles found in my projects are interested because brain map coming from automated and visual detection have similarities. Moreover, they are confirmed by Schabus paper, but they have to be more carefully studied to assess their link with the sleep deprivation night.

Chapter 7

Conclusion

The sleep deprivation study was a complex study requiring considerable time to prepare the protocol and to collect the amount of data necessary to obtain significant results. Once the data were collected, analyzing EEG/fMRI data was challenging due to the overall quality of the EEG data. EEG data acquired inside the scanner are complicated data because a preprocessing has to be performed before allowing further analysis. The preprocessing that mainly consisted in the removal of MR related artifact was an important step, but the user has to be careful when applying these correction methods. Actually, some of the artifact removal procedures considered in my project, and especially the ICA, could also remove some important physiological information and significantly impact our spindle detection notably. So, the user had to find a compromise to get correct data quality instead of poor data quality. Whereas such an evaluation is highly qualitative and difficult to formalize, quality of the data was actually one of the main factors to obtain a good spindle detection. The two spindle detection methods considered in my project have their limitations. On the one hand, the expert neurologist who marked the events was not trained to read low-quality EEG data acquired in the scanner, and visual spindle detection might have been influenced by the presence of residual artifacts. Considering expert visual detection as the gold standard was therefore questionable in our context. The involvement of more than one expert for visual marking might overcome this issue. On the other hand, automated spindle detection methods have been developed and evaluated when considering EEG data of good quality from data acquired outside the scanner. So, it is more than likely that their performances on our data were not as efficient as they should be. To overcome this issue, the parameters and the calculation thresholds should be further investigated and adapted to those data. On the other hand, since the quality of spindle detection will directly impact the reliability of BOLD analysis, it seems important to identify those optimal parameters and to improve the overall quality of spindle detection. The first approach one can consider would be to use all the automated detection and calculate a consensus by taking spindles detected by at least half of the methods. The second approach would be to perform with the expert a careful a post-review of the automated method by accepting only events evaluated as true spindles by the expert. Once the spindle detection was approved, we then performed the statistical analysis of the BOLD response to spindles. Our preliminary results for

this section are actually quite encouraging because they are in agreement with the results reported in a similar study.

In order to improve the reliability of our preliminary results, three main perspectives will be implemented in a next future. We will first consider visual spindle detection made by multiple experts, involving notably an expert neurologist trained to read EEG data acquired inside MRI scanner. The gold standard should then be a consensus between the two different visual detections. The second objective will consist in investigating the best parameters and the best way to calculate the thresholds for every spindle detection automated methods, thus ensure to obtain better detection performance on low-quality EEG data acquired in the scanner. The third objective is to perform a post-review on each subject for each spindle detection method. Post-review could be the best compromise between visual and automated spindle detection.

The sleep deprivation study was a complex study, from which I acquired many skills and knowledge. It taught me how to write protocol to get ethic approbation, and how to perform different types of neuroimaging data acquisition. It allowed me to improve my knowledge of preprocessing analyses and mathematical tools to analyze EEG data and detect specific events. Doing these two years and half of my Master allowed me to be involved in research and I appreciated it.

References:

Abdallah, Chifaou, Louis G. Maillard, Estelle Rikir, Jacques Jonas, Anne Thiriaux, Martine Gavaret, Fabrice Bartolomei, Sophie Colnat-Coulbois, Jean-Pierre Vignal, and Laurent Koessler. 2017. "Localizing Value of Electrical Source Imaging: Frontal Lobe, Malformations of Cortical Development and Negative MRI Related Epilepsies Are the Best Candidates." *NeuroImage: Clinical* 16: 319–29. https://doi.org/10.1016/j.nicl.2017.08.009.

Alhola, Paula, and Päivi Polo-Kantola. 2007. "Sleep Deprivation: Impact on Cognitive Performance." *Neuropsychiatric Disease and Treatment* 3 (5): 553–67.

Allen, Philip J., Giovanni Polizzi, Karsten Krakow, David R. Fish, and Louis Lemieux. 1998a. "Identification of EEG Events in the MR Scanner: The Problem of Pulse Artifact and a Method for Its Subtraction." *Neuroimage* 8 (3): 229–239.

———. 1998b. "Identification of EEG Events in the MR Scanner: The Problem of Pulse Artifact and a Method for Its Subtraction." *NeuroImage* 8 (3): 229–39. https://doi.org/10.1006/nimg.1998.0361.

Anderer, P., G. Klösch, G. Gruber, E. Trenker, R. D. Pascual-Marqui, J. Zeitlhofer, M. J. Barbanoj, P. Rappelsberger, and B. Saletu. 2001. "Low-Resolution Brain Electromagnetic Tomography Revealed Simultaneously Active Frontal and Parietal Sleep Spindle Sources in the Human Cortex." *Neuroscience* 103 (3): 581–92.

Babkoff, Harvey, Tamir Caspy, Mario Mikulincer, and Helen C. Sing. 1991. *Monotonic and Rhythmic Influences: A Challenge for Sleep Deprivation Research*. Vol. 109. https://doi.org/10.1037//0033-2909.109.3.411.

Bergmann, Til O., Matthias Mölle, Jens Diedrichs, Jan Born, and Hartwig R. Siebner. 2012. "Sleep Spindle-Related Reactivation of Category-Specific Cortical Regions after Learning Face-Scene Associations." *NeuroImage* 59 (3): 2733–42. https://doi.org/10.1016/j.neuroimage.2011.10.036.

Bhopal, Nishi, and Umakanth Khatwa. 2014. "Sleep Deprivation and Human Development." In *Sleep Deprivation and Disease*, edited by Matt T. Bianchi, 91–99. New York, NY: Springer New York. https://doi.org/10.1007/978-1-4614-9087-6_8.

Bódizs, Róbert, János Körmendi, Péter Rigó, and Alpár Sándor Lázár. 2009. "The Individual Adjustment Method of Sleep Spindle Analysis: Methodological Improvements and Roots in the Fingerprint Paradigm." *Journal of Neuroscience Methods* 178 (1): 205–13. https://doi.org/10.1016/j.jneumeth.2008.11.006.

Chavhan, Govind B., Paul S. Babyn, Bejoy Thomas, Manohar M. Shroff, and E. Mark Haacke. 2009. "Principles, Techniques, and Applications of T2*-Based MR Imaging and Its Special Applications." *Radiographics* 29 (5): 1433–49. https://doi.org/10.1148/rg.295095034.

Chee, Michael W. L., and Wei Chieh Choo. 2004. "Functional Imaging of Working Memory after 24 Hr of Total Sleep Deprivation." *The Journal of Neuroscience* 24 (19): 4560–67. https://doi.org/10.1523/JNEUROSCI.0007-04.2004.

Collins, DL, P Neelin, TM Peters, and Alan C. Evans. 1994. "Automatic 3D Intersubject Registration of MR Volumetric Data in Standardized Talairach Space." *J Comput Assist Tomogr* 18 (2): 192–205.

Dang-Vu, Thien Thanh. 2014. "Imaging Sleep and Sleep Deprivation." In *Sleep Deprivation and Disease*, edited by Matt T. Bianchi, 33–43. New York, NY: Springer New York. http://link.springer.com/10.1007/978-1-4614-9087-6_4.

Dang-Vu, Thien Thanh, Scott M. McKinney, Orfeu M. Buxton, Jo M. Solet, and Jeffrey M. Ellenbogen. 2010. "Spontaneous Brain Rhythms Predict Sleep Stability in the Face of Noise." *Current Biology* 20 (15): R626–27. https://doi.org/10.1016/j.cub.2010.06.032.

Dang-Vu, Thien Thanh, Manuel Schabus, Martin Desseilles, Virginie Sterpenich, Maxime Bonjean, and Pierre Maquet. 2010a. “Functional Neuroimaging Insights into the Physiology of Human Sleep.” *Sleep* 33 (12): 1589–1603.

———. 2010b. “Functional Neuroimaging Insights into the Physiology of Human Sleep.” *Sleep* 33 (12): 1589–1603.

Daunizeau, Jean, Christophe Grova, Guillaume Marrelec, Jérémie Mattout, Saad Jbabdi, Mélanie Pélégrini-Issac, Jean-Marc Lina, and Habib Benali. 2007. “Symmetrical Event-Related EEG/FMRI Information Fusion in a Variational Bayesian Framework.” *NeuroImage* 36 (1): 69–87. https://doi.org/10.1016/j.neuroimage.2007.01.044.

Dawson, Drew, and Kathryn Reid. 1997. “Fatigue, Alcohol and Performance Impairment.” *Nature* 388 (6639): 235. https://doi.org/10.1038/40775.

De Gennaro, Luigi, and Michele Ferrara. 2003a. “Sleep Spindles: An Overview.” *Sleep Medicine Reviews* 7 (5): 423–40.

———. 2003b. “Sleep Spindles: An Overview.” *Sleep Medicine Reviews* 7 (5): 423–40. https://doi.org/10.1053/smrv.2002.0252.

Debener, Stefan, Karen J. Mullinger, Rami K. Niazy, and Richard W. Bowtell. 2008. “Properties of the Ballistocardiogram Artefact as Revealed by EEG Recordings at 1.5, 3 and 7 T Static Magnetic Field Strength.” *International Journal of Psychophysiology*, Integration of EEG and fMRI, 67 (3): 189–99. https://doi.org/10.1016/j.ijpsycho.2007.05.015.

Diekelmann, Susanne, and Jan Born. 2010. “The Memory Function of Sleep.” *Nature Reviews Neuroscience* 11 (2): 114. https://doi.org/10.1038/nrn2762.

Dijk, D. J., and C. A. Czeisler. 1995. “Contribution of the Circadian Pacemaker and the Sleep Homeostat to Sleep Propensity, Sleep Structure, Electroencephalographic Slow Waves, and Sleep Spindle Activity in Humans.” *The Journal of Neuroscience: The Official Journal of the Society for Neuroscience* 15 (5 Pt 1): 3526–38.

Dijk, Derk-Jan, Boyd Hayes, and Charles A. Czeisler. 1993. “Dynamics of Electroencephalographic Sleep Spindles and Slow Wave Activity in Men: Effect of Sleep Deprivation.” *Brain Research* 626 (1–2): 190–199.

Doran, S. M., H. P. A. Van Dongen, and D. F. Dinges. 2001. “Sustained Attention Performance during Sleep Deprivation: Evidence of State Instability.” *Archives Italiennes de Biologie* 139 (3): 253–67. https://doi.org/10.4449/aib.v139i3.503.

Driver, H. S., D. J. Dijk, E. Werth, K. Biedermann, and A. A. Borbély. 1996. “Sleep and the Sleep Electroencephalogram across the Menstrual Cycle in Young Healthy Women.” *The Journal of Clinical Endocrinology and Metabolism* 81 (2): 728–35. https://doi.org/10.1210/jcem.81.2.8636295.

Drummond, Sean PA, and Gregory G. Brown. 2001. “The Effects of Total Sleep Deprivation on Cerebral Responses to Cognitive Performance.” *Neuropsychopharmacology* 25 (5): S68–S73.

Drummond, Sean PA, Gregory G. Brown, J. Christian Gillin, John L. Stricker, Eric C. Wong, and Richard B. Buxton. 2000. “Altered Brain Response to Verbal Learning Following Sleep Deprivation.” *Nature* 403 (6770): 655–657.

Fan, J, B Mccandliss, J Fossella, J Flombaum, and M Posner. 2005. “The Activation of Attentional Networks.” *NeuroImage* 26 (2): 471–79. https://doi.org/10.1016/j.neuroimage.2005.02.004.

Fan, Jin, Bruce D. McCandliss, Tobias Sommer, Amir Raz, and Michael I. Posner. 2002. “Testing the Efficiency and Independence of Attentional Networks.” *Journal of Cognitive Neuroscience* 14 (3): 340–47. https://doi.org/10.1162/089892902317361886.

Ferrarelli, Fabio, Reto Huber, Michael J. Peterson, Marcello Massimini, Michael Murphy, Brady A. Riedner, Adam Watson, Pietro Bria, and Giulio Tononi. 2007. “Reduced Sleep Spindle Activity in Schizophrenia Patients.” *American Journal of Psychiatry* 164 (3): 483–492.

Ferreira, Jose L., Ronald M. Aarts, and Pierre JM Cluitmans. 2014. “Optimized Moving-Average Filtering for Gradient Artefact Correction during Simultaneous EEG-FMRI.” In *Biosignals and Biorobotics Conference (2014): Biosignals and Robotics for Better and Safer Living (BRC), 5th ISSNIP-IEEE*, 1–6. IEEE. http://ieeexplore.ieee.org/xpls/abs_all.jsp?arnumber=6880955.

Ferreira, José L., Pierre JM Cluitmans, and Ronald M. Aarts. 2012. “Gradient Artefact Correction in the EEG Signal Recorded within the FMRI Scanner.” In *BIOSIGNALS*, 110–117. Citeseer.

Fogel, Stuart M., and Carlyle T. Smith. 2011. “The Function of the Sleep Spindle: A Physiological Index of Intelligence and a Mechanism for Sleep-Dependent Memory Consolidation.” *Neuroscience & Biobehavioral Reviews* 35 (5): 1154–65. https://doi.org/10.1016/j.neubiorev.2010.12.003.

Friston, Karl J., P. Fletcher, Oliver Josephs, ANDREW Holmes, M. D. Rugg, and Robert Turner. 1998. “Event-Related fMRI: Characterizing Differential Responses.” *Neuroimage* 7 (1): 30–40.

Friston, K.J, C.D Frith, R.S.J Frackowiak, and R Turner. 1995. “Characterizing Dynamic Brain Responses with fMRI: A Multivariate Approach - ScienceDirect.” *NeuroImage 2*, April, 166–72.

Gibbs, Erna L., and Frederic A. Gibbs. 1962. “Extreme Spindles: Correlation of Electroencephalographic Sleep Pattern with Mental Retardation.” *Science* 138 (3545): 1106–7. https://doi.org/10.1126/science.138.3545.1106.

Gotman, Jean, and Francesca Pittau. 2011. “Combining EEG and fMRI in the Study of Epileptic Discharges.” *Epilepsia* 52 (Suppl 4): 38–42. https://doi.org/10.1111/j.1528-1167.2011.03151.x.

Herrmann, Christoph S., and Stefan Debener. 2008. “Simultaneous Recording of EEG and BOLD Responses: A Historical Perspective.” *International Journal of Psychophysiology*, Integration of EEG and fMRI, 67 (3): 161–68. https://doi.org/10.1016/j.ijpsycho.2007.06.006.

Huster, René J., Stefan Debener, Tom Eichele, and Christoph S. Herrmann. 2012. “Methods for Simultaneous EEG-fMRI: An Introductory Review.” *Journal of Neuroscience* 32 (18): 6053–60. https://doi.org/10.1523/JNEUROSCI.0447-12.2012.

Ives, J. R., S. Warach, F. Schmitt, R. R. Edelman, and D. L. Schomer. 1993. “Monitoring the Patient’s EEG during Echo Planar MRI.” *Electroencephalography and Clinical Neurophysiology* 87 (6): 417–20.

Kaufmann, C., R. Wehrle, T. C. Wetter, F. Holsboer, D. P. Auer, T. Pollmächer, and M. Czisch. 2006. “Brain Activation and Hypothalamic Functional Connectivity during Human Non-Rapid Eye Movement Sleep: An EEG/fMRI Study.” *Brain* 129 (3): 655–67. https://doi.org/10.1093/brain/awh686.

Killgore, William D. S., and Mareen Weber. 2014. “Sleep Deprivation and Cognitive Performance.” In *Sleep Deprivation and Disease*, 209–29. Springer, New York, NY. https://doi.org/10.1007/978-1-4614-9087-6_16.

Knoblauch, Vera, Wim L. J Martens, Anna Wirz-Justice, and Christian Cajochen. 2003. “Human Sleep Spindle Characteristics after Sleep Deprivation.” *Clinical Neurophysiology* 114 (12): 2258–67. https://doi.org/10.1016/S1388-2457(03)00238-4.

Landolt, H. P., D. J. Dijk, P. Achermann, and A. A. Borbély. 1996. “Effect of Age on the Sleep EEG: Slow-Wave Activity and Spindle Frequency Activity in Young and Middle-Aged Men.” *Brain Research* 738 (2): 205–12.

Langlois, Dominic, Sylvain Chartier, and Dominique Gosselin. 2010. “An Introduction to Independent Component Analysis: InfoMax and FastICA Algorithms.” *Tutorials in Quantitative Methods for Psychology* 6 (1): 31–38.

Lichstein, Kenneth L., Brant W. Riedel, and Stephanie L. Richman. 2000. “The Mackworth Clock Test: A Computerized Version.” *The Journal of Psychology* 134 (2): 153–61. https://doi.org/10.1080/00223980009600858.

Lindquist, Martin A., Ji Meng Loh, Lauren Y. Atlas, and Tor D. Wager. 2009. “Modeling the Hemodynamic Response Function in FMRI: Efficiency, Bias, and Mis-Modeling.” *NeuroImage* 45 (1): S187–98. https://doi.org/10.1016/j.neuroimage.2008.10.065.

Loomis, A.L, E.N Harvey, and G Hobart. 1935. “Potential Rythms of the Cerebral Cortex during Sleep.” *Science* 81: 597–98.

Mantini, D., M.G. Perrucci, S. Cugini, A. Ferretti, G.L. Romani, and C. Del Gratta. 2007. “Complete Artifact Removal for EEG Recorded during Continuous FMRI Using Independent Component Analysis.” *NeuroImage* 34 (2): 598–607. https://doi.org/10.1016/j.neuroimage.2006.09.037.

Maquet, P., D. Dive, E. Salmon, B. Sadzot, G. Franco, R. Poirrier, R. von Frenckell, and G. Franck. 1990. “Cerebral Glucose Utilization during Sleep-Wake Cycle in Man Determined by Positron Emission Tomography and [18F]2-Fluoro-2-Deoxy-D-Glucose Method.” *Brain Research* 513 (1): 136–43.

MARIA, THOMAS. 2000. “Neural Basis of Alertness and Cognitive Performance Impairments during Sleepiness. I. E Ects of 24 h of Sleep Deprivation on Waking Human Regional Brain Activity.” *J. Sleep Res* 9: 335–352.

Martin, Nicolas, Marjolaine Lafortune, Jonathan Godbout, Marc Barakat, Rebecca Robillard, Gaétan Poirier, Célyne Bastien, and Julie Carrier. 2013. “Topography of Age-Related Changes in Sleep Spindles.” *Neurobiology of Aging* 34 (2): 468–76. https://doi.org/10.1016/j.neurobiolaging.2012.05.020.

Massimini, M. 2004. “The Sleep Slow Oscillation as a Traveling Wave.” *Journal of Neuroscience* 24 (31): 6862–70. https://doi.org/10.1523/JNEUROSCI.1318-04.2004.

Mölle, Matthias, Til O. Bergmann, Lisa Marshall, and Jan Born. 2011. “Fast and Slow Spindles during the Sleep Slow Oscillation: Disparate Coalescence and Engagement in Memory Processing.” *Sleep* 34 (10): 1411–21. https://doi.org/10.5665/SLEEP.1290.

Mölle, Matthias, Lisa Marshall, Steffen Gais, and Jan Born. 2002. “Grouping of Spindle Activity during Slow Oscillations in Human Non-Rapid Eye Movement Sleep.” *The Journal of Neuroscience* 22 (24): 10941–10947.

Mulert Christoph, and Lemieux Louis. 2010. *EEG - fMRI - Physiological Basis, Technique, and | Christoph Mulert | Springer*. //www.springer.com/us/book/9783540879183.

Niazy, R.K., C.F. Beckmann, G.D. Iannetti, J.M. Brady, and S.M. Smith. 2005. “Removal of FMRI Environment Artifacts from EEG Data Using Optimal Basis Sets.” *NeuroImage* 28 (3): 720–37. https://doi.org/10.1016/j.neuroimage.2005.06.067.

Nicolas, A, D Petit, S Rompré, and J Montplaisir. 2001. “Sleep Spindle Characteristics in Healthy Subjects of Different Age Groups.” *Clinical Neurophysiology* 112 (3): 521–27. https://doi.org/10.1016/S1388-2457(00)00556-3.

Nir, Yuval, Richard J. Staba, Thomas Andrillon, Vladyslav V. Vyazovskiy, Chiara Cirelli, Itzhak Fried, and Giulio Tononi. 2011. “Regional Slow Waves and Spindles in Human Sleep.” *Neuron* 70 (1): 153–69. https://doi.org/10.1016/j.neuron.2011.02.043.

Owen, Adrian M., Kathryn M. McMillan, Angela R. Laird, and Ed Bullmore. 2005. “N-Back Working Memory Paradigm: A Meta-Analysis of Normative Functional Neuroimaging Studies.” *Human Brain Mapping* 25 (1): 46–59. https://doi.org/10.1002/hbm.20131.

Penny, William, Karl J. Friston, John Ashburner, Stefan Kiebel, and Thomas Nichols. 2006. *Statistical Parametric Mapping: The Analysis of Functional Brain Images*. Academic Press.

Rechtschaffen, Allan, and Anthony Kales. 1968. “A Manual of Standardized Terminology, Techniques and Scoring System for Sleep Stages of Human Subjects.” *Bethesda, Md., U. S. National Institute of Neurological Diseases and Blindness, Neurological Information Network*, 57.

Schabus, M., T. T. Dang-Vu, G. Albouy, E. Balteau, M. Boly, J. Carrier, A. Darsaud, et al. 2007. “Hemodynamic Cerebral Correlates of Sleep Spindles during Human Non-Rapid Eye Movement Sleep.” *Proceedings of the National Academy of Sciences of the United States of America* 104 (32): 13164–69. https://doi.org/10.1073/pnas.0703084104.

Schabus, Manuel, Thien Thanh Dang-Vu, Geneviève Albouy, Evelyne Balteau, Mélanie Boly, J. Carrier, Annabelle Darsaud, Christian Degueldre, Martin Desseilles, and S. Gais. 2007. “Hemodynamic

Cerebral Correlates of Sleep Spindles during Human Non-Rapid Eye Movement Sleep." *Proceedings of the National Academy of Sciences* 104 (32): 13164–13169.
Schimicek, P., J. Zeitlhofer, P. Anderer, and B. Saletu. 1994. "Automatic Sleep-Spindle Detection Procedure: Aspects of Reliability and Validity." *Clinical Electroencephalography* 25 (1): 26–29.
Schmidt, Heike, Jigar Jogia, Kristina Fast, Tessa Christodoulou, Morgan Haldane, Veena Kumari, and Sophia Frangou. 2009. "No Gender Differences in Brain Activation during the N-Back Task: An fMRI Study in Healthy Individuals." *Human Brain Mapping* 30 (11): 3609–15. https://doi.org/10.1002/hbm.20783.
Schrouff, Jessica, Dorothée Coppieters, Remy Lehembre, Yves Leclercq, Pierre Maquet, Quentin Noirhomme, Christian Degueldre, and Christophe Phillips. 2013. "FASST Developpers at the Cyclotron Research Centre."
Sejnowski, Terrence J., and Alain Destexhe. 2000. "Why Do We Sleep?11Published on the World Wide Web on 7 November 2000." *Brain Research*, Towards 2010, A brain Odyssey, The 3rd Brain Research Interactive, 886 (1): 208–23. https://doi.org/10.1016/S0006-8993(00)03007-9.
Shibagaki, M., and S. Kiyono. 1983. "Duration of Spindle Bursts during Nocturnal Sleep in Mentally Retarded Children." *Electroencephalography and Clinical Neurophysiology* 55 (6): 645–51. https://doi.org/10.1016/0013-4694(83)90274-2.
Short, Michelle A., and Siobhan Banks. 2014. "The Functional Impact of Sleep Deprivation, Sleep Restriction, and Sleep Fragmentation." In *Sleep Deprivation and Disease*, 13–26. Springer, New York, NY. https://doi.org/10.1007/978-1-4614-9087-6_2.
Steriade, Mircea, David A. McCormick, and Terrence J. Sejnowski. 1993. "Thalamocortical Oscillations in the Sleeping and Aroused Brain." *Science* 262 (5134): 679–85.
Sun, Limin, and Hermann Hinrichs. 2009. "Simultaneously Recorded EEG-fMRI: Removal of Gradient Artifacts by Subtraction of Head Movement Related Average Artifact Waveforms." *Human Brain Mapping* 30 (10): 3361–77. https://doi.org/10.1002/hbm.20758.
Tyvaert, Louise, Pierre LeVan, Christophe Grova, François Dubeau, and Jean Gotman. 2008. "Effects of Fluctuating Physiological Rhythms during Prolonged EEG-fMRI Studies." *Clinical Neurophysiology* 119 (12): 2762–74. https://doi.org/10.1016/j.clinph.2008.07.284.
Ueda, Kazutaka, Hiroshi Nittono, Mitsuo Hayashi, and Tadao Hori. 2001a. "Spatiotemporal Changes of Slow Wave Activities before and after 14 Hz/12 Hz Sleep Spindles during Stage 2 Sleep." *Psychiatry and Clinical Neurosciences* 55 (3): 183–184.
———. 2001b. "Spatiotemporal Changes of Slow Wave Activities before and after 14 Hz/12 Hz Sleep Spindles during Stage 2 Sleep." *Psychiatry and Clinical Neurosciences* 55 (3): 183–84. https://doi.org/10.1046/j.1440-1819.2001.00817.x.
Vanderwal, Tamara, Clare Kelly, Jeffrey Eilbott, Linda C. Mayes, and F. Xavier Castellanos. 2015. "Inscapes : A Movie Paradigm to Improve Compliance in Functional Magnetic Resonance Imaging." *NeuroImage* 122 (November): 222–32. https://doi.org/10.1016/j.neuroimage.2015.07.069.
Walker, Matthew P. 2008. "Sleep-Dependent Memory Processing." *Harvard Review of Psychiatry* 16 (5): 287–98. https://doi.org/10.1080/10673220802432517.
Wamsley, Erin J., Matthew A. Tucker, Ann K. Shinn, Kim E. Ono, Sophia K. McKinley, Alice V. Ely, Donald C. Goff, Robert Stickgold, and Dara S. Manoach. 2012. "Reduced Sleep Spindles and Spindle Coherence in Schizophrenia: Mechanisms of Impaired Memory Consolidation?" *Biological Psychiatry*, Functional Consequences of Altered Cortical Development in Schizophrenia, 71 (2): 154–61. https://doi.org/10.1016/j.biopsych.2011.08.008.
Warby, Simon C., Sabrina L. Wendt, Peter Welinder, Emil G. S. Munk, Oscar Carrillo, Helge B. D. Sorensen, Poul Jennum, Paul E. Peppard, Pietro Perona, and Emmanuel Mignot. 2014a. "Sleep-Spindle

Detection: Crowdsourcing and Evaluating Performance of Experts, Non-Experts, and Automated Methods." *Nature Methods* 11 (4): nmeth.2855. https://doi.org/10.1038/nmeth.2855.

Warby, Simon C, Sabrina L Wendt, Peter Welinder, Emil G S Munk, Oscar Carrillo, Helge B D Sorensen, Poul Jennum, Paul E Peppard, Pietro Perona, and Emmanuel Mignot. 2014b. "Sleep-Spindle Detection: Crowdsourcing and Evaluating Performance of Experts, Non-Experts, and Automated Methods." *Nature Methods* 11 (4): 385–92. https://doi.org/10.1038/nmeth.2855.

Wendt, Sabrina L., Julie A. E. Christensen, Jacob Kempfner, Helle L. Leonthin, Poul Jennum, and Helge B. D. Sorensen. 2012. "Validation of a Novel Automatic Sleep Spindle Detector with High Performance during Sleep in Middle Aged Subjects." *Conference Proceedings: ... Annual International Conference of the IEEE Engineering in Medicine and Biology Society. IEEE Engineering in Medicine and Biology Society. Annual Conference* 2012: 4250–53. https://doi.org/10.1109/EMBC.2012.6346905.

Yoo, Seung-Schik, Peter T. Hu, Ninad Gujar, Ferenc A. Jolesz, and Matthew P. Walker. 2007. "A Deficit in the Ability to Form New Human Memories without Sleep." *Nature Neuroscience* 10 (3): 385. https://doi.org/10.1038/nn1851.

Zerouali, Younes, Jean-Marc Lina, Zoran Sekerovic, Jonathan Godbout, Jonathan Dube, Pierre Jolicoeur, and Julie Carrier. 2014. "A Time-Frequency Analysis of the Dynamics of Cortical Networks of Sleep Spindles from MEG-EEG Recordings." *Frontiers in Neuroscience* 8. https://doi.org/10.3389/fnins.2014.00310.

Appendix

A - Set-up of equipment for EEG/fMRI acquisition

The installation of the EEG/fMRI requires a lot of different tools that I will explain you thanks to a picture.

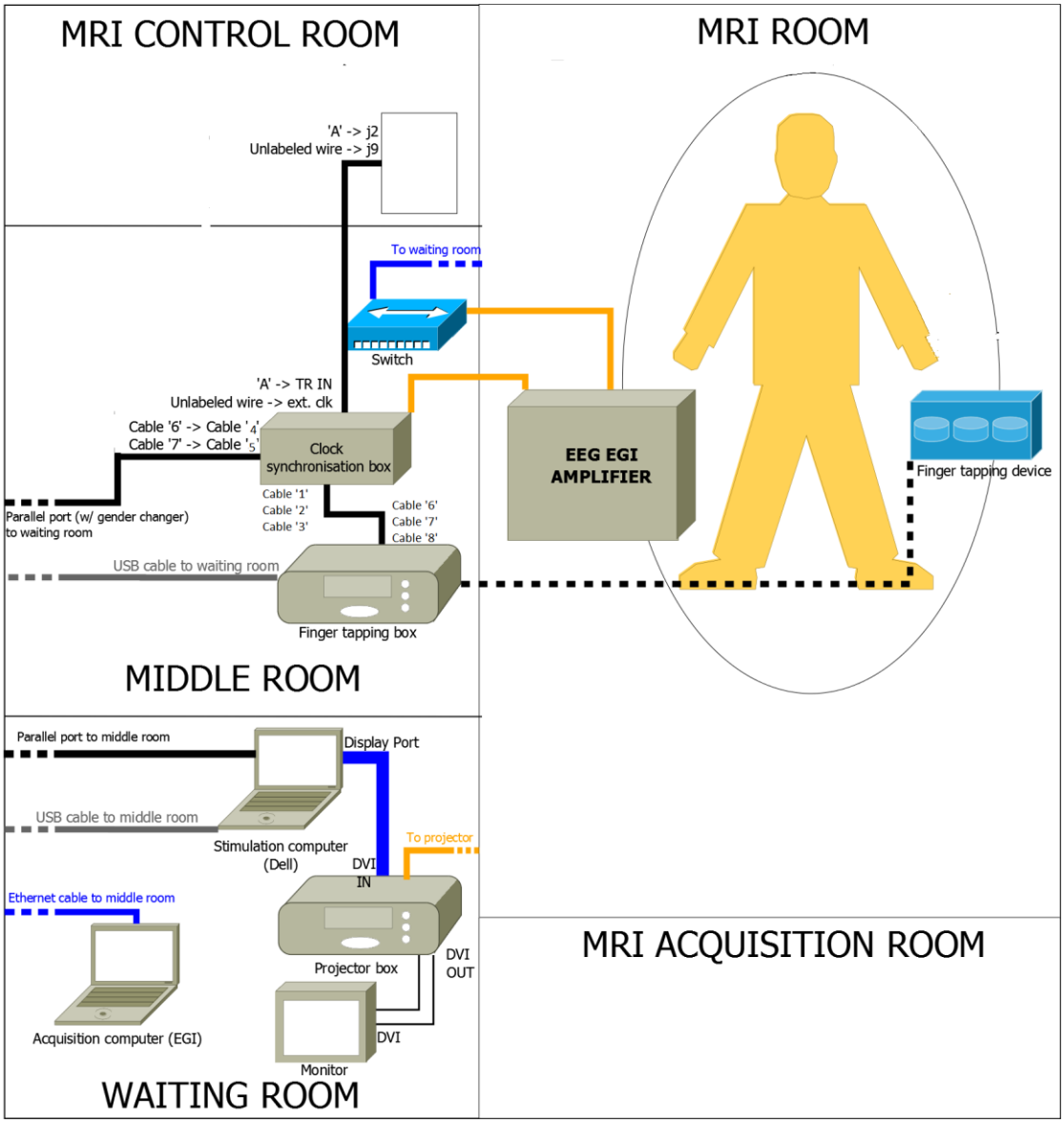

Figure 47: Equipment setup (By Tanguy Hedrich)

The MRI room is the room with the machine, and where the participant is installed with the EEG cap. Under his hand, there is a finger tapping device to allow him to answer to the different task appearing on the screen behind the machine. A mirror allows him to watch the screen when is lying down. The EEG cap is plugged to the EGI amplifier which amplifies the EEG signal and

transmits it to the other devices. Thanks to a hole in the wall, the cable connected to the amplifier and tapping device can be transmitted to the other devices in the other room. EGI amplifier transmits the EEG data by fiber optical to the acquisition laptop in the waiting room through the switch. In the middle room, there is an important component which is connected to several devices, the Clock synchronization box. This box allows to synchronize the triggers of different devices and to synchronize the clock between MRI and EGI system. A coaxial cable connecting the MRI and the clock box allows to get the trigger sends at each scan (TR) and to display it on the EEG through the fiber optical connection to the amplifier. Another coaxial cable is connected to finger tapping device to get the answers of the participant and give it to the task laptop and the EGI laptop. A parallel port is plugged to the clock and the laptop generating the tasks to get the triggers on the EEG. In our case, triggers sending by the laptop depend on the tasks. For example, for the N-Back task, 2 different triggers are sent. One is when the displaying letter is the target and the other is when the displaying letter is not the target. So, all the trigger are seen on the EEG laptop.

The installation of this system including the EEG cap takes around 45 min. Then, the participant is installed comfortably in the MRI. Participant is lying down inside the MRI with a small pillow under his head and his arms; moreover, his legs are raised to avoid pain in the back. Avoiding the pain during acquisition is the most important point. Participants were allowed to go out before or after the nap to stretch his legs or use the bathroom.